FUNCTIONALIZED MESOPOROUS SILICA FOR HEAVY METAL AND PHOSPHATE CAPTURE IN GI TRACT

By

Thanapon Sangvanich

A DISSERTATION

Presented to the Department of Biomedical Engineering
and the Oregon Health & Science University
School of Medicine
in partial fulfillment of
the requirements for the degree of

Doctor of Philosophy
In Biomedical Engineering

August 2016

School of Medicine

Oregon Health & Science University

CERTIFICATE OF APPROVAL

This is to certify that the Ph.D. dissertation of

Thanapon Sangvanich

has been approved

Wassana Yantasee, Ph.D., M.B.A.
Associate Professor, Dissertation Advisor

Leslie Muldoon, Ph.D.
Associate Professor, Chair

Hiroyuki Nakai, M.D., Ph.D.
Associate Professor

Summer Gibbs, Ph.D.
Assistant Professor

Andras Gruber, M.D.
Professor

TABLE OF CONTENTS

LIST OF TABLES

LIST OF FIGURES

LIST OF ABBREVIATIONS

µg	Microgram
µL	Microliter
µm	Micron
µM	Micromolar
µmol	Micromole
Å	Angstrom
ACS	American Chemical Society
As	Arsenic
ATCC	American Type Culture Collection
BAL	Dimercaprol
BCA	Bicinchoninic acid
BET	Brunauer–Emmett–Teller
Ca	Calcium
Cd	Cadmium
$CdCl_2$	Cadmium chloride
CDC	Center for Disease Control and Prevention
CH_3CN	Acetonitrile
CKD	Chronic kidney disease
CrO_4^{2-}	Chromate
CTAC	Cetyltrimethylammonium chloride
Cu	Copper

CysH	Cysteine
DI	Deionized
DLS	Dynamic light scattering
DMEM	Dulbecco's modified Eagle's medium
DMPS	Dimercapto propane succinic acid
DMSA	Dimercaptosuccinic acid
DMSO	Dimethyl sulfoxide
DPBS	Dulbecco's phosphate buffered saline
DPCN	D-penicillamine
DSP	Dithiobis(succinimidyl propionate)
E. coli	Escherichia coli
EDA	Ethylene diamine
EDTA	Ethylene diamine tetraacetic acid
EtHg	Ethylmercury
EXAFS	Extended X-ray absorption fine structure
FBS	Fetal bovine serum
FDA	US Food and Drug Administration
Fe	Iron
Fe-EDA	Iron-diamine
$FeCl_3$	Ferric chloride
g	Gram
GI	Gastrointestinal
GSH	Glutathione

h	Hour
H_2O	Water
$H_2AsO_4^-$	Dihydrogen arsenate ion
$H_2PO_4^-$	Dihydrogen phosphate ion
H_3PO_4	Phosphoric acid
HCl	Hydrochloric acid
HER2	Receptor tyrosine-protein kinase erbB-2
Hg	Mercury
$HgCl_2$	Mercuric chloride
HNO_3	Nitric acid
HPO_4^{2-}	Hydrogen phosphate ion
IACUC	Institutional Animal Care and Use Committee
ICP-MS	Inductively-coupled plasma mass spectrometer
IMD	Intestinal Metals Detox™
IND	Investigational new drug
K	Potassium
K_2HPO_4	Potassium phosphate dibasic
KCl	Potassium chloride
kDa	Kilo dalton
kg	Kilogram
KH_2PO_4	Potassium phosphate monobasic
L	Liter
LD50	Lethal dose, 50%

LPA	Lyoprotectant agent
m	Meter
M	Molar
MCM-41	Mobil Composite of Matter no. 41
MCM-48	Mobil Composite of Matter no. 48
MeHg	Methylmercury
MeHgCl	Methylmercury chloride
mg	Milligram
Mg	Magnesium
min	Minute
mL	Milliliter
mM	Millimolar
mmol	Millimole
MSNP	Mesoporous silica nanoparticle
MW	Molecular weight
Na_2HPO_4	Sodium phosphate dibasic
Na_2SO_4	Sodium sulfate
$Na_3C_6H_5O_7$	Sodium citrate
NAC	N-acetylcysteine
$NaC_2H_3O_2$	Sodium acetate
NaCl	Sodium chloride
NaH_2PO_4	Sodium phosphate monobasic
$NaHCO_3$	Sodium bicarbonate

$NaNO_3$	Sodium nitrate
NaOH	Sodium hydroxide
ng	Nanogram
NHNES	National Health and Nutrition Examination Survey
NHS	N-Hydroxysuccinimide
nm	Nanometer
nM	Nanomolar
NP	Nanoparticle
OD	Optical density
OH	Hydroxyl group
OHSU	Oregon Health & Science University
p	Probability
P	Phosphorus
P/S	Penicillin/streptomycin
Pb	Lead
$Pb(CH_3COO)_2$	Lead acetate
PBS	Phosphate buffered saline
PCL	Polycaprolactone
PEG	Polyethyleneglycol
PEI	Polyethylenimine
PLGA	Poly(lactic-co-glycolic acid)
PNNL	Pacific Northwest National Laboratory
PO_4^{3-}	Phosphate ion

ppb	Parts per billion
ppm	Parts per million
PTH	Parathyroid hormone
PVDF	Polyvinylidene fluoride
Rb	Rubidium
RCT	Randomized controlled trial
rpm	Round per minute
S	Sulfur
S.D.	Standard deviation
SAMMS	Self-assembled monolayers on mesoporous supports
SBA-15	Santa Barbara Amorphous type material no. 15
Se	Selenium
SGF	Simulated gastric fluid
SH	Thiol
Si	Silicon
SIF	Simulated intestinal fluid
siHER2	HER2 siRNA
siLUC	Luciferase siRNA
siRNA	Small interfering ribonucleic acid
siSCR	Scrambled siRNA
Sr	Strontium
T	Trastuzumab
T-NP	Trastuzumab-modified nanoparticle

TEA	Triethanolamine
TEER	Trans-epithelial electrical resistance
TEM	Transmission electron microscope
TEOS	Tetraethyl orthosilicate
TL	Trehalose
US-EPA	US Environmental Protection Agency
WHO	World Health Organization
Zn	Zinc
Zr	Zirconium

LIST OF SYMBOLS

C_0	Initial concentration
C_e	Equilibrium concentration
L/S	Liquid-to-solid ratio
Q_e	Equilibrium uptake
Q_{max}	Maximum adsorption capacity
K_L	Langmuir isotherm constant

ACKNOWLEDGEMENTS

I extend my thanks to all individuals who made this dissertation and graduate studies successful.

Dr. Wassana Yantasee, Ph.D., M.B.A. (W.Y.), my mentor

Dissertation Advisory and Oral Examination Committee:

Dr. Leslie Muldoon, Ph.D.

Dr. Hiroyuki Nakai, M.D., Ph.D.

Dr. Summer Gibbs, Ph.D.

Dr. Andras Gruber, M.D.

Friends and Colleagues:

Dr. Glen E. Fryxell, Ph.D. (G.E.F.)

Dr. Anne O. Summers, Ph.D. (A.O.S.)

Dr. Shaun M. Goodyear, Ph.D. (S.M.G.)

Dr. David J. Castro, Ph.D. (D.J.C.)

Dr. Worapol Ngamcherdtrakul, Ph.D. (W.N.)

Dr. Xinran Li, Ph.D. (X.L.)

Jingga Morry (J.M.)

Shenda Gu (S.G.)

Moataz M. Reda (M.M.R.)

Samuel A. Mihelic (S.A.M.)

Brandon L. Beckman (B.L.B.)

Cade Fox (C.F.)

Richard Lee (R.L.)

Elizabeth Rick (E.R.)

Specific contributions are listed below:

Dissertation writing: Thanapon Sangvanich (T.S.), self

Figure and table preparation: T.S.

Dissertation oversight: W.Y.

Dissertation editing: D.J.C., W.Y.

Chapter 2: SH-SAMMS for heavy metal chelation (*published in ACS Applied Material and Interfaces*)

Concept and design: W.Y., T.S.

Analysis, interpretation, and revision: W.Y., T.S., G.E.F., A.O.S., J.M.

Figure and table preparation: T.S.

Writing the article: T.S., W.Y.

In vitro experiment: T.S.

Bacteria experiment: C.F., T.S.

Cytotoxicity experiment: T.S, D.J.C.

Heavy metal animal experiment: J.M., E.R., T.S., W.N.

Chapter 3: Fe-EDA-SAMMS as oral phosphate binder (*published in Journal of Nanomedicine and Nanotechnology*)

Concept and design: T.S., W.Y.

Analysis, interpretation, and revision: T.S., W.Y., G.E.F.,

SAMMS synthesis and in vitro experiment: T.S.

Cytotoxicity experiment: T.S, D.J.C., S.M.G.

Writing the article: T.S., W.Y.

Chapter 4: Future directions

Concept and design: T.S., W.Y.

Chronic Hg exposure animal experiment: T.S, D.J.C., S.M.G., S.G.

Fe-EDA-SAMMS in vivo and in vitro experiment: T.S., D.J.C.

Appendix: Lyophilization of cationic polymer modified mesoporous nanoparticle

Concept and design: T.S., W.Y.

Nanoparticle synthesis: W.N., M.M.R., S.A.M.

Tissue culture: S.G., B.L.B.

Conduction experiments: T.S.

The work presented in Chapter 2 was published in ACS Applied Material and Interfaces. The Chapter 2 figures/tables have been slightly modified from our published work for use in this dissertation. According to the ACS AuthorChoice License Agreement, an original work may be reused, adapted, translated, texted and data mined for non-commercial research and education purposes.

Parts of the works presented in Chapter 3 and Chapter 4 were published in Journal of Nanomedicine and Nanotechnology. The works have been slightly modified from its published form for use in this dissertation. According to the OMICS International Open Access Policy and Creative Commons Attribution license, an original work may be copied, distributed, transmitted and adapted as long as the original work and source is appropriately cited.

Funding:

Works in this dissertation were supported by awards to W.Y. from the National Institute of General Medical Sciences (NIGMS; R01GM089918), the National Institute of Diabetes and Digestive and Kidney Diseases (NIDDK; R41DK094571), the National Institute of Environmental Health Sciences (NIEHS; R21ES015620), the Prospect Creek Foundation, OHSU's KCI pilot award, and OHSU's VPR fund.

ABSTRACT

Well-ordered mesoporous silica has emerged in the past decade as a promising platform in nanomedicine and biomedical applications due to its unique characteristics such as ease of synthesis and surface modification, large surface area and pore volume, controllable pore size and particle size, and bio-compatibility. Synthesis conditions can be adjusted to produce particles with sizes ranging from nanoscale to microscale suitable for diverse applications. Herein, I apply micron-sized particles for targeted delivery of metal chelating ligands in the gastrointestinal tract. Specifically, 20 – 250 micron mesoporous silica functionalized with thiol (SH-SAMMS) was investigated as an orally administered drug for the capture of heavy metals (e.g., mercury, cadmium, and lead) in the gastrointestinal (GI) tract. The three metals have been identified by the World Health Organization (WHO) to be among the top ten chemicals of major public health concern. Dimercaprol (BAL), dimercaptosuccinic acid (DMSA), and dimercaptopropanesulfonic acid (DMPS) were developed decades ago for treating acute, high level toxic metal poisoning. Their use must be closely monitored by medical personnel due to potential renal and liver toxicity, and essential mineral depletion. To date, there is no well-established material to treat chronic, low level heavy metal exposure. I found that SH-SAMMS, given together with the toxic metals or post hoc, reduced dietary methyl mercury and cadmium in organs of rats and helped the rats' recover from weight loss. It also reduced the blood lead levels of the rats. Due to its non-absorbable nature and high selectivity for the target metals, SH-SAMMS did not alter the essential mineral levels. Thus, data suggest that it has high potential to be used for an extended period of time to treat chronic metal exposure. In another project, I optimize iron-ethylenediamine (Fe-

EDA)-SAMMS as a potential phosphate binder. It is aimed for treating hyperphosphatemia, common in end-stage chronic kidney disease and dialysis patients. I improved the Fe deposition method on SAMMS, resulting in a 4-fold increase in binding capacity over the previous report. I also found Fe-EDA-SAMMS to have excellent selectivity for phosphate over other GI tract anions and able to capture phosphate from pH 3 – 11, suitable for GI tract application. Both applications are excellent examples of how nanostructured materials may improve efficacy, safety, and delivery of conventional compounds.

CHAPTER 1: INTRODUCTION

1.1 Toxic Heavy Metal Poisoning

1.1.1 Background

Toxic heavy metal exposure, especially mercury (Hg), lead (Pb), and cadmium (Cd) is a growing health problem worldwide. They have been listed among the top ten chemicals of public health concern by the World Health Organization (WHO). People can be exposed to Hg, Cd, and Pb trough different routes such as ingestion, inhalation, and dermal absorption. The exposure to these heavy metals, both acute and chronic, can cause diverse and severe toxicities to multiple organ systems.

Mercury (Hg). Hg exposure even at low levels may cause serious health problems, especially to the development of the child in utero and early in life [1]. WHO lists the toxic effects of Hg to nervous, digestive and immune systems, and in lungs, kidneys, skin and eyes. People are mainly exposed to methylmercury (MeHg) from fish and shellfish. Elemental mercury (Hg(0)) (from dental amalgam or mercury spill) easily vaporizes; once inhaled, it is oxidized in blood to reactive inorganic Hg(II) [2] which spontaneously combines with thiols such as cysteine and glutathione [3]. Once in circulation Hg(II)-thiol conjugates partition into all tissues. Those which go to the liver then pass into the gastrointestinal (GI) tract where Hg(II) are converted by Hg-resistant bacteria into volatile, membrane permeant Hg vapor (Hg(0)) [4], and highly absorbable methyl mercury [5,6]. The growing health impact of mercury exposure has resulted in the new global treaty agreed in January of 2013 to phase out all mercury use by 2020. Even as Hg use declines, existing deposits from old waste sites to dental amalgams already in place, will extend significant Hg exposure for decades beyond 2020.

Cadmium (Cd) Cd is very harmful to the respiratory system, kidneys, prostate, and blood, and has been identified as a human carcinogen for prostrate and lung cancer [7]. Oral route is common for Cd exposure. Tobacco accumulates Cd from soil and smokers have twice the blood Cd compared to non-smokers [8]. Food contaminated with Cd, such as seafood and wildlife, is a major source of Cd exposure in non-smokers, and is linked to increased use of phosphate fertilizers or sewage sludge to farm fields [9]. Roughly 6 – 9% of ingested Cd absorb from the GI tract [10]. Cd is an accumulative toxin in humans, mainly in the liver and kidney, since humans do not have effective pathways to eliminate it [10].

Lead (Pb). Pb is the most prevalently used metal throughout a number of industries. Old Pb based paints is a common source of Pb poisoning in children. Pb-contaminated water from old water pipes along with gasoline and emissions from industrials also contribute to Pb exposure issue. The Center for Disease Control and Prevention (CDC) reported that children in at least 4 million US households are exposed to high levels of lead, and about 0.5 million children ages 1-5 have blood lead levels above an action level of 50 ppb [11]. Children absorb Pb better than adults (30-50% vs. 10% [12]) and Pb toxicity may cause permanent damage to their health and learning ability [13]. The majority of oral Pb exposure is of the inorganic form, Pb(II), while organic Pb exposure is rarer following the elimination of lead additive in gasoline. Inhaled Pb (e.g., lead oxide) can be absorbed directly through the lung, but may be excreted via mucociliary clearance, become soluble Pb(II), and absorb back to the body in the GI tract [14,15]. Absorbed lead is primarily excreted in urine via kidneys or via

bile to the GI tract [16]. All these facts suggest that removing inorganic Pb(II) in GI tract may have beneficial effects.

1.1.2 Current treatments for toxic heavy metal poisoning

Chelation therapy is the standard of care for patients showing symptoms of heavy metal poisoning. Chelating agents developed decades ago (Dimercaprol (British anti-lewisite or BAL)), 2,3-dimercapto-1-propanesulfonic acid (DMPS), and 2,3-dimercaptosuccinic acid (DMSA or succimer) remain the primary therapies for heavy metal detoxification. These molecules contain thiol functional groups which have high affinity to heavy metals such as Hg, Cd, Pb and arsenic (As).

Dimercaprol (BAL) was developed in 1940s as an antidote first for arsenical nerve gas and later for other heavy metals. The formulation is an oil-based and administered intramuscularly. BAL is typically formulated with peanut oil which can lead to further allergic reaction [17]. It was later found to be toxic and to increase metal deposition in the brain [18,19].

Dithiol molecules, DMSA and DMPS, were later developed as replacement chelators to BAL [20]. These molecules are water soluble and can be administered orally, intravenously, or by transdermal preparation. Twenty percent of orally-administered DMSA is absorbed to the body and mostly binds to proteins. Only a small portion of absorbed DMSA remains as free drug [20]. Up to 25% of absorbed DMSA is cleared via urinary excretion, while the majority excreted in feces [21,22]. DMSA can cause rare side effects such as mucocutaneous eruptions and toxic epidermal necrosis [17]. Oral absorption of DMPS is higher than DMSA at approximately 39% [23]. Due to relatively

higher stability in solution, DMPS is more commonly administered intravenously than DMSA. The majority of intravenously-administered DMPS is excreted in urine with half-life of 20 hours [23]. Both DMSA and DMPS were shown to increase urinary excretion of As, Cd, Pb, and both organic and inorganic Hg. However, DMPS also increases the excretion of essential minerals such as copper (Cu), zinc (Zn), selenium (Se) and magnesium (Mg) [24]. In comparison, DMSA was more effective at removing MeHg from brain, while DMPS was better at removing MeHg in kidney (observation from animal studies) [20]. DMSA was also superior for Cd removal in mice [25].

Both DMSA and DMPS have a better therapeutic index [26], and lower side effects than BAL due to rapid clearance and limited systemic accumulation [27,28]. However, because they are rapidly cleared, both require high, frequent dosing to achieve efficacy and are often taken with a multivitamins to avoid loss of essential minerals. They require close monitoring of liver and kidney functions [29]. In spite of their enhanced efficacy, only DMSA (succimer or CHEMET®) has gained US Food and Drug Administration (FDA) approval for the treatment of lead poisoning in children, yet it has compliance issue due to gastrointestinal side effects [30]. DMPS (Dimaval®), while not approved by FDA, has been used in Europe to treat mercury poisoning without prescription required [31]. Although initially beneficial, toxic metal blood levels can rebound when the chelator is discontinued [32]. Furthermore, excretory pathways can become overwhelmed upon mobilizing large amounts of metal with DMPS and DMSA treatment, thus leading to redistribution of the metals among the organs, including the brain. This is particularly of concern, considering Hg has a very long half-life [33,34] and known chelators cannot cross the blood brain barrier [35]. Lastly, DMSA use in young

children is complicated by its unpleasant ‘‘rotten egg’’ odor when it must be sprinkled onto food three times a day [36].

1.1.3 Unmet medical needs

Current standard of treatment for heavy metal poisoning were developed decades ago. All of them were based on small chelator molecules. The toxicities of these drugs are related to the absorbable nature and not highly specific to the target metals only. Apart from treating acute metal exposure, there is no formally accepted treatment for sub-acute, chronic metal exposure. Thus, persons who consider themselves to suffer chronic metal exposure often use commercial naturopathic or homeopathic remedies advertised for removal of harmful metals. These supplements include N-acetylcysteine (NAC), glutathione (GSH), selenocysteine, taurine, methionine, zinc, charcoal, zeolite, and alginate. These natural supplements are believed to act as chelators for toxic metals. Some can be orally administered, while other, such as GSH, need to be injected intravenously due to the issue of degradation in GI tract [17].

Beside the conventional chelators and natural supplements, two silica-based materials with thiol functionality are lately available over the counter, Intestinal Metals Detox™ (IMD), and MetalSweep™. Both are advertised as dietary supplement with oral administration together with vitamin E. Neither of these materials has been approved by FDA and there is limited or no peer-reviewed scientific evidence to validate marketing claims in terms of efficacy and safety.

1.2 Hyperphosphatemia in Chronic Kidney Disease Patients

1.2.1 Background

Hyperphosphatemia is universal to end stage chronic kidney disease (CKD) patients and dialysis patients. Normal kidneys regulate serum inorganic phosphate level by filtering and reabsorbing phosphate in renal tubule [37]. As the kidney conditions deteriorate, the regulated mechanism fails and leads to elevated serum phosphorus levels. Hyperphosphatemia can lead to secondary hyperthyroidism by promoting parathyroid gland hyperplasia and parathyroid hormone (PTH) synthesis and secretion [38]. Since hyperphosphatemia and hyperparathyroidism have clinical consequences of increased risk of cardiovascular disease, bone disease, and calcification of soft tissues and eventual morbidity and mortality [39,40], management of hyperphosphatemia is believed to be critical for the care of end stage chronic kidney disease patients which total ~ 400,000 in the US, and 2 million worldwide [41]. Elevated serum phosphate can be managed by dietary restriction, dialysis, and drug treatment using oral phosphate binders. Dietary restriction is not practical for many patients due to limitation cooking skill and the risk of protein malnutrition [42]. Both conventional hemodialysis and peritoneal dialysis do not remove sufficient amount of phosphate to maintain the level within recommended target [43,44]. While daily slow nocturnal hemodialysis is more effective in phosphate removal, it is neither cost-effective nor convenient which results in limit utilization [45]. Hence; dietary restriction of phosphate and dialysis do not adequately control the serum phosphorus level. The majority of hyperphosphatemia patients are required to take oral phosphate binders.

1.2.2 Current treatment for hyperphosphatemia

Current prescribed oral phosphate binders are calcium salts, magnesium salts, Sevelamer, and lanthanum carbonate. Each drug has both advantages and disadvantages, and, based on interventional randomized controlled trials (RCTs), does not have superiority over each other [37].

Calcium salts (carbonate and acetate) bind to phosphate ionically and are moderately effective and inexpensive which lead to them being prescribed as first line treatment [46]. They have a moderate to large pill burden and some gastrointestinal side effects. However, calcium salts have been linked to hypercalcemia [47], oversuppression of PTH [46] and ectopic calcification [48].

Magnesium salts (carbonate and hydroxide) can be used as alternatives to calcium salts. They work similarly to the calcium-based binders but are general less effective [37]. The advantage of magnesium salts over calcium salts is that they do not contain calcium and do not cause hypercalcemia and eventually ectopic calcification [46]. They are less widely used for long term due to the toxicity related to magnesium and increased serum magnesium levels (hypermagnesemia) [43].

Sevelamer hydrochloride (Renagel®), a non-absorbed poly (allyamine hydrochloride) ion-exchange resin, was the first calcium-free synthetic phosphate binder commercially available [37]. The abundant amine functional groups become partially protonated in intestinal environment and bind to negative-charged phosphate ions through ionic and hydrogen bond interactions [49]. Several open-label studies showed Sevelamer hydrochloride to be as effective as calcium salts and does not lead to hypercalcemia [37]. However, Sevelamer hydrochloride has several drawbacks such as metabolic acidosis,

pH-dependent efficacy, high pill burden and high price, and low affinity and selectivity to phosphate ions [37,43,49]. *Sevelamer carbonate (Renvela®)* was later developed as a buffered formulation to reduce the risk of metabolic acidosis [49]. Sevelamer binders have the largest market share of all phosphate binders contributing by their high costs.

Lanthanum carbonate is one of the newer phosphate binder developed in the past decades. It binds to phosphate ionically similar to other inorganic binders. It has a more favorable safety profile than aluminum or calcium-based binders due to low systemic absorption [37]. It is shown to be as effective as calcium carbonate in clinical trials [50] with a small pill burden since it is chewable. It is however expensive, has severe GI side effects, dialysis graft complication, and possible accumulation of lanthanum in bone and liver [51]. Lanthanum carbonate is available in the US under the tradename of Fosrenol® since 2005 [37].

Sucroferric oxyhydroxide is an iron-based phosphate binder approved by FDA for CKD patients receiving dialysis in 2013 [52]. It consists of polynuclear iron(III) oxyhydroxide core which is stabilized by carbohydrate shell of sucrose and starch [53]. Phosphate in GI tract binds to insoluble iron oxyhydroxide in both stomach and intestine and excrete in feces [53]. In a phase III clinical study, the efficacy of this binder was comparable to Sevelamer carbonate (Renvela®); however, more patients withdrew due to GI tract adverse effects [54]. The advantage of iron oxyhydroxide over other phosphate binders is low pill burden at 3 pills of 500 mg each per day [55].

Ferric citrate, under tradename Auryxia®, is the latest compound approved by the FDA for hyperphosphatemia treatment in 2014. The mechanism of this binder is similar to other inorganic binders which bind to phosphate ionically in GI tract,

precipitate, and eliminate through fecal excretion [56]. There was no significant difference in both efficacy and safety profiles between ferric citrate and Sevelamer hydrochloride in a recent clinical trial on dialysis patients [57]. Main adverse effects of ferric citrate are GI tract related issues [58] and iron overload [56]. Ferric citrate has high pill burden (1-g tablet, two tablets each, 3 times daily) [58]. Monthly cost of ferric citrate is estimated to be similar to both Sevelamer and lanthanum carbonate [58]. Currently, ferric citrate is approved in the US for only treating dialysis patients.

1.2.3 Unmet medical needs of current approved phosphate binders

Current oral phosphate binders have many drawbacks, including high risk of calcification for calcium based pills, high costs ($11,000 – $15,000 per patient a year for non-calcium oral phosphate binders [58]), low-to-moderate efficacy, common gastrointestinal adverse effects, high pill burdens (500 – 1,000 mg tablet, 3 – 6 tablets a day [58]), and other adverse effects (e.g., hypercalcemia, diarrhea, and nausea [43]). All these factors result in low pill compliance, which is a major reason why patients fail to manage their serum phosphorus levels. A new oral phosphate binder that is calcium-free and much improved in terms of efficacy and safety beyond simple anion exchange resins or inorganic metal salts are needed.

1.3 Microscale functionalized ordered mesoporous silica

Self-assembled monolayers on mesoporous supports (SAMMS) were originally developed as sorbent materials for nuclear and environmental waste cleanup at Pacific Northwest National Laboratory (PNNL), Richland, WA. The framework of these materials is based on MCM-41, a hexagonal mesoporous silica framework with particle sizes in the range of 5 – 500 microns and pore sizes of 1 – 20 nm. MCM-41 (Mobile Composition of Matter no. 41) is a mesoporous template first introduced by Kresge in 1992 [59]. It has widespread applications such as catalysts in chemical reactions, adsorbents in waste water treatment and environmental cleanup, and drug delivery systems. Since entering the biomedical application landscape back in 2001, it has garnered increasing attention due to its unique characteristics (e.g., ease of synthesis and surface modification, large surface area and pore volume, controllable pore size and particle size, and relatively inert compositions) [60].

Built on MCM-41, SAMMS are highly efficient sorbents with superior properties over conventional sorbents. Their multi-ligand chelation ability enhances their binding affinity and stability. The high surface area of the porous silica substrate (~500-1,000 m^2/g) and the monolayer self-assembly technique achieves functional group density up to 10-fold higher than simpler methods [61-63] and consequent high metal loading capacity. SAMMS' rigid, open channel structure is ideal for mass transport of metal ions (fast binding kinetics).

SAMMS are hybrid materials generated by covalently functionalized organic groups onto mesoporous silica framework, **Figure 1.1**. Functional groups on the silica surface can be tailored to capture a wide range of metals in periodic table (see **Figure**

1.1C): toxic heavy metals [61-64], oxomatallate anions [65,66], lanthanides and actinides [67-71], transition metals [72,73], and cesium and thallium [71,74]. Due to rigid open pores of SAMMS, they possess fast binding kinetics to their target metals [61,66]. With these advantages (non-absorbable micron size, high metal loading and fast binding kinetics), SAMMS have a very high potential in becoming new orally-administrated non-absorbable drugs with target delivery in gastrointestinal (GI) tract.

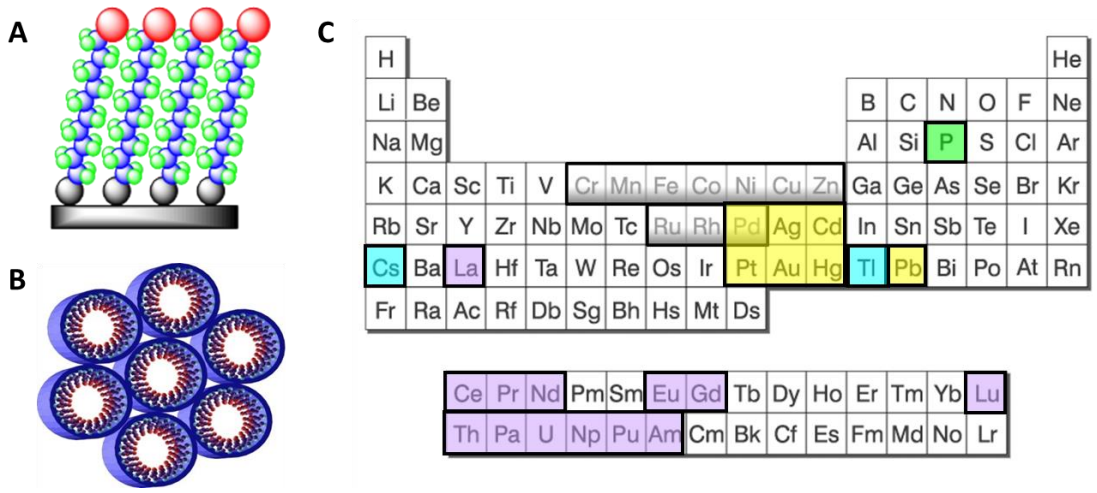

Figure 1.1 Schematic illustrations of SAMMS (A) self-assembled monolayer, (B) monolayers lining walls of channels, (C) SAMMS's ligands are tailored to selectively bind various classes of metals in the Periodic Table: thiol for soft heavy metals (yellow), iron-diamine for oxometallate anions (e.g., phosphate, green), diamine for transition metals (gray), copper ferrocyanide for cesium and thallium (blue), phosphonic acid and hydroxypyridinone for lanthanides and actinides (purple).

1.4 Advantages of functionalized mesoporous silica over current treatment of toxic heavy metal poisoning and hyperphosphatemia

Treatments for both metal poisoning and hyperphosphatemia have common drawbacks due to the nature of current drugs. Chelating drugs for heavy metal and inorganic salts for phosphate binding are absorbable in GI tract. The absorbed drugs/ions can increase serum levels of drug components and can lead to multiple adverse effects. Low affinity and low specificity to target ions are also an issue.

Microscale ordered mesoporous silica, which are traditionally used in catalytic and environmental applications [62,63,75,76], dose not transport across most physiological membranes due to the larger particle size. This characteristic can be exploited for targeted drug delivery to the gastrointestinal tract (GI tract) to alleviate the absorption issue of current technology. Recently, Yantasee et al reported micron-scale functionalized ordered mesoporous silica to have properties suitable for oral heavy metal detoxification [61]. The robust silica template was shown to be stable over a wide pH range found within the GI tract. When tested in vitro, the material did not get taken up by cells mimicking enterocytes lining the small intestine (Caco-2).

Two types of SAMMS have been designed to selectively capture heavy metals and phosphate; thiol-functionalized (SH) SAMMS for heavy metal chelation and iron-diamine (Fe-EDA) SAMMS for phosphate binding. Both SAMMS materials demonstrate high affinity and high specify for their target molecules. I have studied these two SAMMS as potential oral drugs for treating heavy metal poisoning and hyperphosphatemia. The work will be discussed in the Chapter 2 and 3, respectively.

1.5 Dissertation's goals, hypotheses and organization

The overall goal of this dissertation is to optimize and evaluate functionalized ordered mesoporous silica (SAMMS) as oral drugs to treat heavy metal poisoning and hypophosphatemia.

In Chapter 2, I will focus on utilizing thiol-modified SAMMS (SH-SAMMS) as a potential oral drug for heavy metal poisoning, especially for mercury (Hg), cadmium (Cd), and lead (Pb). SH-SAMMS was previously reported to effectively capture these metals in biological fluids (blood, urine, and GI fluid simulants) [61]. I hypothesize that SH-SAMMS will work effectively in a rodent model of heavy metal exposure and have low toxicity due to non-absorbable nature of micron-size particles. In this chapter, I will assess SH-SAMMS for (1) heavy metal binding capacities in simulation intestinal fluids, (2) capture of mercury (as MeHg and Hg(II)) in the present of competitive molecules, (3) capture of MeHg in fish digestate, (4) interaction of bacteria and Hg-bound SH-SAMMS, (5) toxicity of SH-SAMMS vs. DMSA and DMPS on intestinal endothelial cell model (Caco-2), and (6) in vivo efficacy and toxicity of SH-SAMMS in rodent model.

In Chapter 3, I will focus on optimization and evaluation of iron-diamine functionalized SAMMS (Fe-EDA-SAMMS) as potential oral drug for treating hyperphosphatemia. Fe-EDA-SAMMS was previously reported for capture of phosphate in simple deionized water with some challenging anions [66]. Although selectivity for phosphate over anions (e.g., chloride, nitrate, bicarbonate) is outstanding, low phosphate binding capacity of the original Fe-EDA-SAMMS makes it less competitive than Sevelamer. Therefore, I will optimize several parameters in material synthesis (e.g., solvent used during Fe incorporation, substrates, amine functional groups, reaction time

and temperature) to improve phosphate binding capacity. I hypothesize that replacing water with aprotic organic solvent will lead to improved Fe deposition and ultimately higher phosphate binding capacity. In this chapter, I will also investigate phosphate binding characteristics of optimized material in simulated gastrointestinal fluids and other challenging environment. Lastly, I will evaluate the potential toxicity of the material to intestinal endothelial cell model against gold standard oral phosphate binders.

In Chapter 4, I will summarize my work on developing SH-SAMMS and Fe-EDA-SAMMS as potential oral drugs. I will also discuss and propose future directions based on what I have learned. Lastly, in the Appendix, I have included my recent work focusing on lyophilization optimization of nano-size mesoporous silica nanoparticle previously developed and reported by other lab members for siRNA delivery to treat breast cancer [77] and skin fibrosis [78].

CHAPTER 2: THIOL FUNCTIONALIZED MESOPOROUS SILICA

AS NOVEL ORAL DETOXIFICATION OF MERCURY, CADMIUM AND LEAD

2.1 Introduction

Heavy metal exposure, especially mercury (Hg), is a growing health problem worldwide. Hg and its organometallic compounds are among the most toxic substances in environment. Hg exists in different forms; elemental mercury (Hg(0)), inorganic divalent mercury (Hg(II)) or organic mercury in the form of methylmercury (MeHg) and ethylmercury (EtHg). Hg poisoning is a major health concern around the world. In the US, blood and urine Hg level have been shown to increase with age and time within the same population (data from National Health and Nutrition Examination Survey (NHNES) during 2003-2004 with over 8,000 participants). Similarly, Laks [79] have reported a sharp increase of blood Hg levels from 2% in 1999 – 2000 to 30% in 2005-2006 with over 6,000 female participants. Hg vapor and Hg residual wastes released from industrial production will accumulate in bodies of water. The elemental Hg and inorganic Hg are then converted to MeHg by aquatic microbiotic organisms which are then consumed by predator fishes [80]. According to US Environmental Protection Agency (US-EPA), the most common way people in the US are exposed to mercury is by consuming food, especially fish or shellfish, containing MeHg. One to two percent of the US population eats enough fish daily to potentially exceed EPA advisory level. Of this number, 4 million are women of child-bearing age and 3 million are children between ages 3 to 6. The US-EPA estimated that each year over 300,000 newborns may have increased risks of learning disabilities from in-utero MeHg exposure via maternal consumption of fish. Chronic exposure to MeHg can impair neurological development and reproductive systems, especially in fetuses, infants and children. Mercury exposure to pregnant mothers from consumption of fish with high mercury level (e.g., kingfish, swordfish and

shark) can adversely affect the baby's growing brain and nervous system. Impacts on cognitive thinking, memory, attention, language, and fine motor and visual spatial skills have been reported in children exposed to methylmercury in the womb. 'Silver' dental amalgam fillings, which consists of 50% metaling Hg by weight, was reported as another major source of chronic Hg exposure [81]. Hg contents in feces, urine, blood and various tissues and organs were found to increase with amalgam doses. Dental amalgam filling is banned in Europe; however, it is still actively used in the US. Other means of exposure are industrial and mining generating volatile elemental mercury and inorganic mercury as by-products (e.g., steel production, pesticides and gold and silver mining). Elemental Hg vapor is readily released and enters human body by inhalation. High exposure to elemental mercury and inorganic mercury may result in damage to the GI tract, nervous system and kidneys. Chronic, low level Hg exposure can be slow to show any symptoms as the body detoxification systems are effective in limiting the body burden of Hg. However, these mechanisms are less effective with aging when the symptoms manifest. The health concern from Hg exposure is recognized and the global treaty was put in place in January 2013 to eliminate the use of Hg in several product s such as batteries, soaps, cosmetics and thermometers [3]. However, it will take years for Hg exposure rate to drop.

Currently, chelation therapy is the standard of care for a patient showing symptoms of Hg poisoning. Chelation therapy for Hg poisoning can be accommodated with dimercaptosuccinic acid (DMSA), dimercapto propane succinic acid (DMPS), D-penicillamine (DPCN), or dimercaprol (BAL). BAL, a general chelating agent in 1940s, was later found to be toxic and increase metal accumulation in the brain [18,19]. Oral chelating agents, DMSA and DMPS, are found to be the most effective and have least

side effects among the current chelating drugs for Hg chelation due to rapid clearance and limited accumulation [26-28]. However, these chelating drugs form complexes with Hg. The complexes are cleared mostly via kidney and bile, thus increasing burden on the kidney and liver [29]. Most of these drugs have been reported to have adverse effects such as nausea, vomiting, stomach pain, elevated liver enzymes, drowsiness, rash and flu-like symptoms. Only DMSA has been FDA-approved to treat acute Hg poisoning in children. None of these chelation drugs have been approved by FDA for chronic Hg exposure. These findings justify the development of a novel chelating drug to minimize the body burden of Hg from fish consumption. Upon entering the body, 95% of MeHg is absorbed in the GI tract and distributed to all tissues within 30 hours [3]. Fecal excretion is a major elimination route for MeHg. The idea of using non-absorbable chelating drugs to capture ingested Hg in the GI tract to reduce the GI absorption of Hg and enhance Hg excretion is a promising alternative.

Recent study of thiol functionalized SAMMS (SH-SAMMS) suggests that it possesses many desired characteristics for oral mercury detoxification. The linear rigid channels of the mesoporous silica make the thiol sites readily available to metal ions. Over 99% of Hg(II) in simulated gastric fluid (SGF, pH 1.1) was removed in 3 minutes. Similarly other toxic heavy metals, Cd(II) and Pb(II) were also removed within a couple of minutes in simulated intestinal fluid (SIF, pH 6.8) [61] and natural waters [82], respectively. Fast binding kinetics is advantageous for rapid capture of toxic metals in the GI tract to minimize re-absorption back to the body. The extent of Hg capture on SH-SAMMS was stable over a 24-h exposure period tested, indicating no significant leaching of Hg from the sorbent nor degradation of the SH-SAMMS in SGF. The affinity of SH-

SAMMS for Cd(II), Pb(II) and Hg(II) in simulated gastrointestinal fluids with a pH range of 1 – 8, chosen to cover physiological pH's along the gastrointestinal tract, has been reported [61]. When exposing SH-SAMMS bound with Cd(II), Pb(II) and Hg(II) to Caco-2 cells (possessing many properties of the small intestinal epithelium), there was no leachate of the three metal ions from SH-SAMMS across the Caco-2 monolayer and no decrease in trans-epithelial electrical resistance (TEER) across the exposed cell monolayers, thus SH-SAMMS did not damage the cell monolayer. There was no cellular uptake of SH-SAMMS having particle size greater than 5 micron [61]. SH-SAMMS was also found to have 100-fold higher Hg capacity than other conventional sorbents such as sulfur-impregnated activated carbon [61,83].

In this section, the work was extended to include other essential in vitro and in vivo studies to show the great potential of SH-SAMMS for detoxification of heavy metals in humans. I hypothesize that SH-SAMMS would retain ability to capture heavy metal in heavily complex environment of gastrointestinal tract and have low toxicity due to non-absorbable nature of micron-size particles both in vitro and in vivo. This work resulted in parts of *Novel oral detoxification of mercury, cadmium, and lead with thiol modified nanoporous silica*, published in ACS Applied Materials and Interfaces, 2014, 6 (8), 5483-5493.

2.2 Materials and Methods

2.2.1 *Sorbent Material*

SH-SAMMS was synthesized as described elsewhere from MCM-41 [63,84] with a pore size of 5.0 nm and a Brunauer–Emmett–Teller (BET) surface area of 870 m^2/g.

After thiol functionalization, the material had a pore size of 3.8 nm, a BET surface area of 438 m^2/g, and a silane population of 3.9 thiol silanes/nm^2.

2.2.2 *Hg Sorption Isotherms*

The adsorption isotherm of Hg (as Hg(II) and MeHg(I)) is a measure of sorption capacity (in mg Hg/g SH-SAMMS) as a function of the equilibrium concentration of Hg in solution (in mg Hg/L). The adsorption isotherm was measured in deionized water spiked with mercury (final pH 4.0) at room temperature. The Hg concentrations were increased until the thiol binding sites were saturated (e.g., 0 – 2,000 mg Hg/L). The sorbent material was added to the solution to obtain a solid per liquid ratio (S/L) of 0.2 g/L. The control was performed in the same fashion but without solid sorbent. The sample was then shaken for 2 h at 200 rpm on an orbital shaker. After 2 h, the solid was removed by centrifugation at 16,100×g for 5 min and the supernatant was kept in 1 wt% HNO_3 and 1 ppm Au to stabilize Hg species prior to the metal analysis. The metal concentrations in the control (no sorbent) and the test solutions (after being contacted with a sorbent material) were analyzed using an inductively coupled plasma-mass spectrometer (ICP-MS, Agilent 7700X, Agilent Technologies, CA).

2.2.3 *Competition by GSH*

SH-SAMMS was incubated with an excess (7.5 mM) of either Hg(II) or MeHg(I) on an orbital shaker at 200 rpm and room temperature for 2 h to achieve loading of 350 mg Hg as Hg(II) or 250 mg Hg (as MeHg(I)) per gram of SH-SAMMS. The amount of Hg loaded on SH-SAMMS was determined by ICP-MS in the same fashion as the

sorption isotherms experiment. The Hg-loaded SH-SAMMS (Hg-S-SAMMS) were then washed three times with deionized water (500 mL/g of SH-SAMMS for each wash) to remove the unbound Hg species and finally re-suspended at 5 mg/mL. The Hg-S-SAMMS was incubated by stirring at 200 rpm with 10 mM glutathione (GSH) for 4 hours at 37 °C. The amount of Hg leached from the Hg-S-SAMMS was measured in the supernatant fluid by ICP-MS.

2.2.4 *In vitro Capture of Hg from Fish*

Various predator fish (kingfish, shark, Chilean seabass, red tuna, and white tuna) were purchased from a supermarket in Portland, OR, and quantified for total Hg content. Kingfish muscle containing 1.29 ± 0.03 mg total Hg/kg (wet weight), higher than FDA action level of 1.0 mg/kg, was selected for the study. Prior to mixing with SH-SAMMS, the fish was digested using a process shown in **Figure 2.1**. Briefly, gastric digestion was simulated by incubating 8 g of fish muscle on an orbital shaker at 150 rpm in 80 mL of 0.075 M HCl and 0.3% pepsin (pH 1.6) for 3 h at 37 °C. This was followed by 1 h of intestinal digestion simulation by adjusting the suspension's pH to 5.0 with 1.0 M $NaHCO_3$ and adding pancreatin (a hog pancreas extract containing amylase, lipase, and protease activities) and bile extract to 0.0025 wt% and 0.015 wt%, respectively. SH-SAMMS were added to the fish tissue suspension at 0.5 – 2.5 g/L after 2 h of gastric digestion and remained in the suspension during the intestinal digestion. After the gastric and intestinal digestions, the suspensions were centrifuged at 16,100×g for 15 min to pellet the SH-SAMMS and the mineral content of the supernatant was determined by

ICP-MS. A control fish tissue was digested without SH-SAMMS. The wt% Hg removed and wt% change of other minerals by SH-SAMMS were compared with the control.

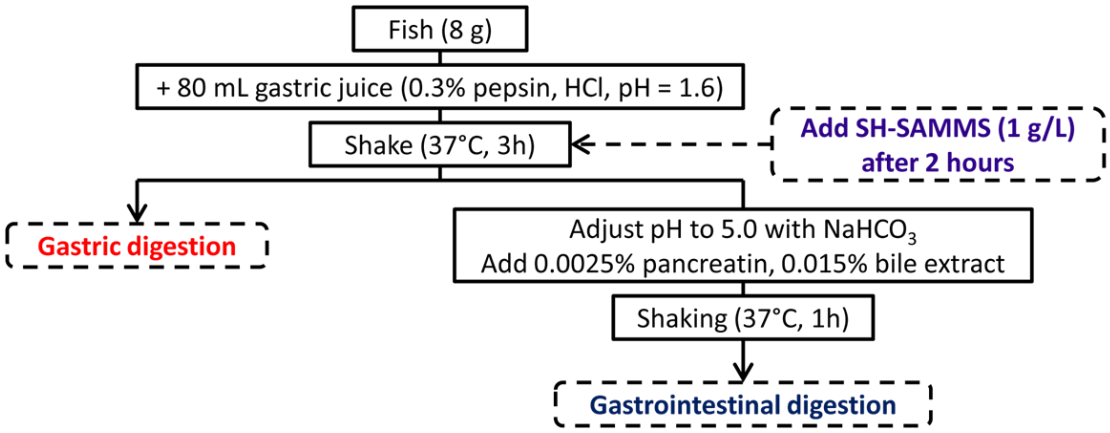

Figure 2.1 Schematic of in vitro fish digestion and SH-SAMMS treatment processes.

2.2.5 *Bacterial Conversion of Hg(II) Bound SH-SAMMS*

The Escherichia coli MG1655 strains with or without the NR1 plasmid conferring mercury resistance via mercuric reductase expression [85,86] were cultured in Luria-Bertani Broth (10 g/L tryptone, 5 g/L yeast extract, 5 g/L NaCl, and 1 mM NaOH) at 37 °C (with shaking at 200 rpm). Overnight cultures were diluted 100-fold into fresh broth and incubated at 200 rpm for 3.5 h to reach their exponential growth stage (absorbance at 600 nm, OD600, of 0.24), at which time $HgCl_2$ (0, 10, or 50 µM), SH-SAMMS (100 µg/mL), or Hg-S-SAMMS (100 µg/mL SH-SAMMS with 1.2 mmol Hg(II)/g loaded) were added to replicate 10 mL aliquots of the Hg-sensitive and Hg-resistant bacterial cultures. Growth of the cultures was measured using OD600 at 0, 0.5, 1, 2, 4, 6, 10, 20, and 25 h after addition of $HgCl_2$, SH-SAMMS or Hg-S-SAMMS.

2.2.6 *Cell Culture and Cytotoxicity Studies*

Immortal human colon epithelial cells, Caco-2, were grown in Dulbecco's Modified Eagle's Medium (DMEM, Corning/Cellgro, VA) supplemented with 10% fetal bovine serum (GIBCO, Life Technologies, NY) and 1X penicillin/streptomycin (Corning/Cellgro, VA). Cells were maintained at 37 °C in 5% CO_2 air atmosphere and were passaged weekly by trypsinization (TrypLE, Life Technologies, NY). For cytotoxicity assays, cells were sub-cultured and seeded at 3000 cells/well in 96-well flat plates and grown to optimal confluency in 5 days. Cells were then directly exposed to SH-SAMMS, DMSA, DMPS (0 – 10,000 µg/mL), $HgCl_2$ (0 – 0.32 mM), MeHgCl (0 – 0.04 mM) or Hg-S-SAMMS for 24 h. The Hg-S-SAMMS used had 0.16 mmol Hg(II) or MeHg(I) per gram of SH-SAMMS and were added to the Caco-2 culture media to obtain Hg concentrations in the well volume equivalent to those of soluble Hg counterparts above (e.g., Hg(II)-S-SAMMS was added at a dose of 2 mg/mL in cell culture well to achieve the equivalent dose of 0.32 mM Hg(II)). After 24 h, cell viability was quantified with the CellTiter-Glo® Luminescent Cell Viability Assay (Promega, Madison, WI) and normalized to an untreated control (e.g., no mercury compounds or soluble chelators added).

2.2.7 *Evaluation of Metals in Tissues and Blood Samples of Rats*

Methylmercury chloride (CH_3HgCl), cadmium chloride ($CdCl_2$) and lead acetate ($Pb(CH_3COO)_2$) were purchased from Sigma Aldrich, USA. The rodent diet was Purina 5001 Rodent Chow (St. Louis, MO). The metal rich diet was prepared by mixing powdered Purina 5001 with the aforementioned metal salts to achieve 0.01% by weight

of each metal per weight of the food (inherently having insignificant amount of mercury (in ng/kg) [87], compared to what was added). The SH-SAMMS-containing diet was prepared in the same manner but with 1.0% by weight of SH-SAMMS per weight of the food. All mixing was performed daily on dry material to avoid pre-binding of metals to SH-SAMMS prior to administering to the rats. The diet was fed to rats as dried powder and consumption (in gram) was record daily.

Male Wistar rats weighing an average of 250 ± 10 g were purchased from Charles River Laboratory (Wilmington, MA). They were placed individually in metabolic cages (Tecniplast, Italy) during the entire period of the study. All animals were maintained on a 12-h light cycle (6 a.m. to 6 p.m.) and given water ad libitum. All animal experiments were approved by OHSU's IACUC and were carried out under the auspices of the OHSU Department of Comparative Medicine.

Two groups of 8 week old rats (6 rats per group; based on reported in vivo chelation studies [88,89]) were fed rodent diets containing either: (1) metal-rich diet (prepared as above); (2) a diet with 1.0 wt% of SH-SAMMS; or (3) a diet mixed with metals as stated above and 1.0 wt% of SH-SAMMS. The rats were fed for 2 weeks and then the metal-rich diet was removed and the rats were regrouped (3/group) with half receiving normal diet and the other half receiving 1.0 wt% SH-SAMMS diet for an additional 2 weeks. Blood samples were collected from each animal twice weekly for monitoring heavy metal concentration in the blood. Rat body weight was measured daily except weekends. Then the rats were sacrificed, and blood, liver, kidneys, brain, bone, and muscles were collected. Blood and tissue samples were digested in concentrated

nitric acid until fully digested. Then the samples were diluted 50-fold in deionized water prior to metal analysis by ICP-MS.

2.2.8 *Statistical Analysis*

Experimental data was presented as mean ± S.D. To compare between the 2 groups, pairwise statistical comparisons were performed using unpaired, two-tailed Student's t test. Statistical significance was established at $p < 0.05$. Statistical power for the animal studies was calculated using "Power and Sample Size Calculation Ver. 3.0, 2009" based on the within-group standard deviation (S.D.) and mean difference of experimental groups. Power analysis with a power of 0.9 and Type I error (α) of 0.05 was performed to validate the number of animals used in section 2.2.7 to be sufficient to detect difference between the SAMMS treated group and the untreated group.

2.3 Results and Discussion

2.3.1 *Hg Binding Capacity of SH-SAMMS*

The adsorption isotherms of Hg(II) and MeHg(I) on SH-SAMMS, are well fitted by a Langmuir model ($R^2 > 0.98$) consistent with monolayer adsorption without precipitation of the metals (**Figure 2.2**). It was previously reported this standard SH-SAMMS to contain 3.9 SH/nm^2 or 2.8 mmol SH/g [61]. Here (**Figure 2.2**) the maximum mercury binding capacities were found to be 385 mg/g for Hg(II) (1.9 mmol/g) and 250 mg for MeHg(II) (1.2 mmol/g). The molar ratio of S and Hg(II) of 1.47 is in agreement with our previous reports based on Extended X-ray Absorption Fine Structure (EXAFS) approach indicating that Hg(II) binds to SH-SAMMS as a mixture of S-Hg-O-Hg-S

(S/Hg = 1) and S-Hg-S (S/Hg = 2) [90]. The SH-SAMMS loading capacity for Hg(II) in water was the same as in SGF (380 mg/g) [61]. The metal binding capacity of SH-SAMMS was not affected by temperature from 24 °C to 37 °C as expected for covalent bonding [61]. Lastly, there was no evidence that binding Hg induces any agglomeration of the silica particles.

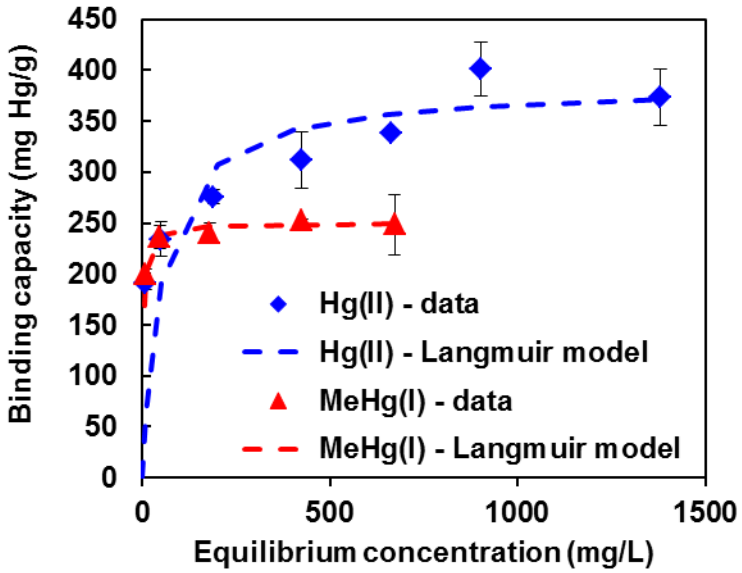

Figure 2.2 Binding capacity of SH-SAMMS for inorganic Hg(II) and MeHg(I) in deionized water (pH 4.0); data (symbols) modeled with Langmuir adsorption isotherm (dash lines). All with SH-SAMMS at 0.2 g/L. Error bars represent S.D. from triplicates.

2.3.2 *Impact of other Thiol Compounds on SH-SAMMS Performance*

Reduced glutathione (GSH) and cysteine (CysH) are abundant in the GI tract and may compete with SH-SAMMS for Hg. Since SH-SAMMS has a strong affinity for Hg even at low pH [91], it should capture Hg in the stomach where levels of GSH and CysH are negligible [92], while the thiol concentrations measured in human small intestines were higher (e.g., 3 – 8 mM) [93]. After SH-SAMMS loaded with Hg equivalent to 0.34 mM Hg(II) or 0.25 mM MeHg(I) in solution were incubated with 10 mM GSH for 4 h at 37 °C, I found that only 28 ± 0.1% of Hg(II) and 33 ± 1.7% of MeHg(I) was released into the solution. Thus, SH-SAMMS retains ~70% of its Hg(II) or MeHg(I) load even when in equilibrium with small monothiols capable of entering its interior channels.

2.3.3 *SH-SAMMS Captured Hg from Fish Digestate without Removing Most Essential Metals*

SH-SAMMS effectively captured Hg(II) and MeHg(I) in simulated gastric and intestinal fluids [91], so I asked if they can capture Hg from digested fish. Kingfish contained 1.29 ± 0.03 mg total Hg/kg-wet weight and over 90% of total Hg in predator fish is methyl mercury [94,95]. The fish was digested by simulating gastric and intestinal processes. After gastric digestion, soluble Hg was 85% of total Hg and remained the same after simulated intestinal digestion. I found 1.0 g/L of SH-SAMMS (added directly to the fish digestion without removing fish particulates) captured 62 ± 1.4% (n = 3) of soluble Hg (**Table 2.1**) after gastric digestion (pH 1.6) and 65 ± 0.7% (n = 3) after gastrointestinal digestion (pH 5.0). Thus, Hg capture could largely occur in the stomach and the Hg would remain bound at higher pH with competing thiols in the large intestine

(measured to be 1.5 mM by Ellman's assay from the same digested fish). In contrast, 1.0 g/L of high surface area activated carbon (Darco KB-B) only removed ~16% and 24% of Hg after gastric and gastric+intestinal digestion, respectively, consistent with lower K_d values than for SH-SAMMS [91]. Hg capture by SH-SAMMS was dose-dependent with 25%, 62%, and 84% of fish Hg being captured by 0.5, 1.0, and 2.5 g/L of SH-SAMMS, respectively. The fish also contained a small amount of Pb, of which 49% was removed by SH-SAMMS in the simulated digestate. Importantly, SH-SAMMS did not deplete some Group I and II nutritional minerals from the fish tissue (i.e., Mg, K, Ca, Se, Rb, and Sr). In this in vitro test on the fish digestate, SH-SAMMS did remove some trace nutritional transition metals Fe, Zn, and Cu (**Table 1**), which could be soluble or bound to biomolecules smaller than the pore size of SH-SAMMS (to be accessible to thiol groups on the inner walls of SH-SAMMS). Removal of essential minerals is common with systemically administered metal chelators, DMSA, DMPS, or EDTA, but because SH-SAMMS acts only in the GI tract such mineral-depleting side effects on the host organism could be milder. I investigated this hypothesis in the animal studies described below.

Table 2.1 SH-SAMMS (1.0 g/L) capture of metals from in vitro fish digestate following simulated gastrointestinal digestion. Data represents mean ± S.D. from triplicates.

Digestion stage	System	Metal content (mg/kg fish-wet weight)										
		Mg	**K**	**Ca**	**Fe**	**Cu**	**Zn**	**Se**	**Rb**	**Sr**	**Hg**	**Pb**
Gastric	Untreat I	341 ± 3	4550 ± 31	57 ± 0	1.32 ± 0.32	0.31 ± 0.00	8.34 ± 0.09	3.74 ± 0.04	0.81 ± 0.01	0.32 ± 0.00	1.09 ± 0.02	0.005 ± 0.002
	SH-SAMMS	340 ± 1	4540 ± 28	57 ± 0	1.12 ± 0.01	0.22 ± 0.01	8.34 ± 0.04	3.81 ± 0.04	0.81 ± 0.00	0.32 ± 0.00	0.41 ± 0.01	0.005 ± 0.000
	% Removal	0	0	0	16	30	0	0	0	0	62	0
Gastric + Intestinal	Untreat II	378 ± 14	5520 ± 300	70 ± 1	1.93 ± 0.05	0.27 ± 0.01	8.31 ± 1.49	3.34 ± 0.02	0.90 ± 0.00	0.37 ± 0.01	1.01 ± 0.09	0.004 ± 0.003
	SH-SAMMS	363 ± 13	5090 ± 330	64 ± 3	1.42 ± 0.03	0.02 ± 0.00	6.93 ± 0.31	3.47 ± 0.11	0.88 ± 0.05	0.36 ± 0.02	0.35 ± 0.01	0.002 ± 0.000
	% Removal	4	8	9	26	94	17	0	2	2	65	49

2.3.4 *Bacterial Access to SH-SAMMS-bound Hg*

In the environment, bacterial methylation of Hg(II) is an established component of Hg cycling; e.g., Hg(II) is converted by bacteria in natural sediments to MeHg(I), which bio-accumulates in fish and the higher food chain [4,96]. However, bacterial biotransformation of Hg compounds is not limited to the external environment. Summers et al. observed enrichment of Hg(II)-reducing bacteria in the primate GI tract in response to Hg exposure from dental mercury fillings [97]. The ability to reduce Hg(II) makes the bacteria resistant to Hg(II) but the resulting monatomic Hg(0) vapor may be absorbed back into circulation instead of being excreted with feces [3,98,99]. More recently, Summers' group has also observed MeHg(I) formation in the feces of monkeys fitted with amalgam restorations. Bacteria are typically spherical or rod-shape with the dimension between 0.5 – 3 micron [100]. The small pores of SH-SAMMS, from 3.8 – 6.5 nm [61], would prevent bacterial access to Hg(II) bound in SH-SAMMS' interior channels and hence could limit bacterial reduction and methylation of Hg(II) in the GI tract. I tested whether Hg bound to SAMMS is accessible to bacteria by exposing cultures of Hg(II)-reducing (aka 'resistant') E. coli and Hg(II)-non-reducing E. coli (aka 'sensitive') [101] to soluble Hg(II) (as $HgCl_2$) or to Hg-S-SAMMS. Two control cultures were conducted; those exposed to SH-SAMMS and untreated. The culture growth was measured by absorbance at 600 nm for Hg-sensitive E. coli (**Figure 2.3A**) and for Hg-resistant E. coli (**Figure 2.3B**). Addition of 10 μM $HgCl_2$ to early exponential phase cultures had little effect on the growth of either E. coli strain but 50 μM $HgCl_2$ initially inhibited growth of both strains. However, as expected the Hg-resistant strain recovered at 6 h after Hg addition and eventually reached a turbidity similar to its growth in

medium without $HgCl_2$; the lag period reflects the induction of the expression of the genes for mercury transformation. In contrast, the Hg-sensitive strain never recovered from 50 μM $HgCl_2$ exposure since it cannot convert Hg(II) to less reactive, volatile Hg(0). The addition of SH-SAMMS alone to the E. coli cultures did not affect growth of either strain, indicating the material does not harm nor promote growth of this typical intestinal bacterium. Addition of Hg(II)-S-SAMMS (with the equivalent Hg(II) of 120 μM) initially slowed growth of the Hg-sensitive strain, but it fully recovered by 20 h. Addition of Hg-S-SAMMS to Hg-resistant E. coli had no effect on its growth. The brief dip in growth rate of the Hg-sensitive strain and the unchanged growth of the Hg-resistant strain indicated minimal Hg exposures, perhaps due to the release of surface bound Hg(II) by micromolar monothiols naturally secreted by bacteria during growth or possibly due to the presence of Hg bound to thiols external to the pores. Clearly most of the Hg(II) bound on SH-SAMMS was not accessible to the bacteria. SH-SAMMS's effective sequestration of Hg(II) from intestinal bacteria will thus prevent enrichment of bacteria with genes for Hg(II) resistance and their genetically linked, transmissible antibiotic resistance genes [97,102-104] and will also limit availability of Hg(II) for methylation by intestinal methanogens and sulfate reducing bacteria.

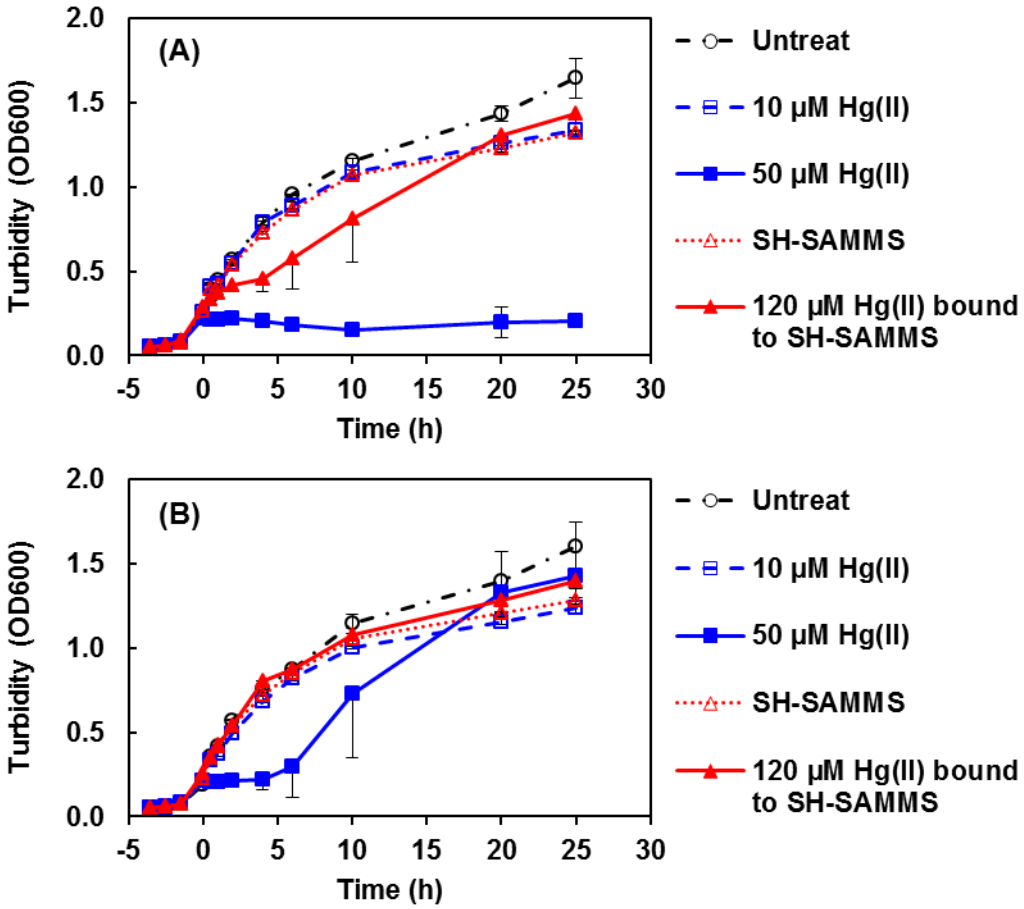

Figure 2.3 Cell density (OD600) of **(A)** Hg-sensitive *E. coli* and **(B)** Hg-resistant *E. coli* after exposure to 10 – 50 μM $HgCl_2$, 120 μM Hg bound to SH-SAMMS (0.1 g/L), SH-SAMMS (0.1 g/L), or untreated. Overnight *E. coli* cultures were diluted 100x into fresh Luria-Bertani Broth and treated 3.5 h later. Error bars represent S.D. from triplicates.

2.3.5 *Low Cytotoxicity of SH-SAMMS and Hg-bound SH-SAMMS to Intestinal Tissue Culture Cells*

The Caco-2 cell line morphologically and functionally resembles the epithelial cells (enterocytes) lining the small intestine. I sought to establish a safety profile of the SAMMS material in this relevant in vitro cell model. I found SH-SAMMS to have low cytotoxicity for Caco-2 cells after 24-h exposure at doses from 0 to 10,000 µg/mL, whereas detectable toxicity of DMSA and DMPS was observed at 1,000 µg/mL and became severe at 5,000 µg/mL and above (**Figure 2.4A**). Although SH-SAMMS is not bioequivalent of soluble and absorbable DMSA and DMPS, they all are given orally and the cells of the GI tract will be exposed to the drugs. The Caco-2 cell represents the best qualitative prediction because it is closest to the site of action. The low cytotoxicity of SH-SAMMS is due to the fact that SH-SAMMS is not water soluble and not taken up by the cells. It was demonstrated previously that SH-SAMMS > 5 micron in particle size was not taken up by Caco-2 cells and kept the cell monolayer integrity intact [61]. It is worth noting that I compare the material safety on a per mass basis rather than molar basis of active components to mimic the prescribed dose of oral DMSA and DMPS (in mg/day). In addition, safety of SH-SAMMS should be considered as whole material (include the inactive silica substrate) and not just for active thiol groups. Nevertheless, when comparing active ingredients by molar basis, 10,000 µg/mL of SH-SAMMS contains 28 µmol/mL of thiol which is on par with 5,000 µg/mL of DMSA (27 µmol/mL) or DMPS (22 µmol/mL). At this same molar concentration, SH-SAMMS is still the safest to Caco-2 cells.

In **Figure 2.4B**, soluble Hg species, in the range of 0.04 – 0.32 mM for Hg(II) or 0.01 – 0.04 mM for MeHg(I), were highly toxic to Caco-2 cells exhibiting a Lethal Dose, 50% (LD50) of 0.17 mM for Hg(II) and 0.035 mM for MeHg(I). In contrast, equivalent doses of both Hg species (Hg(II) and MeHg(I)) were not toxic when bound to SH-SAMMS. This protection against mercury toxicity was maintained even when using 4-fold less SH-SAMMS for loading the maximum Hg studied, 0.32 mM Hg(II) or 0.04 mM MeHg(I) (data not shown).

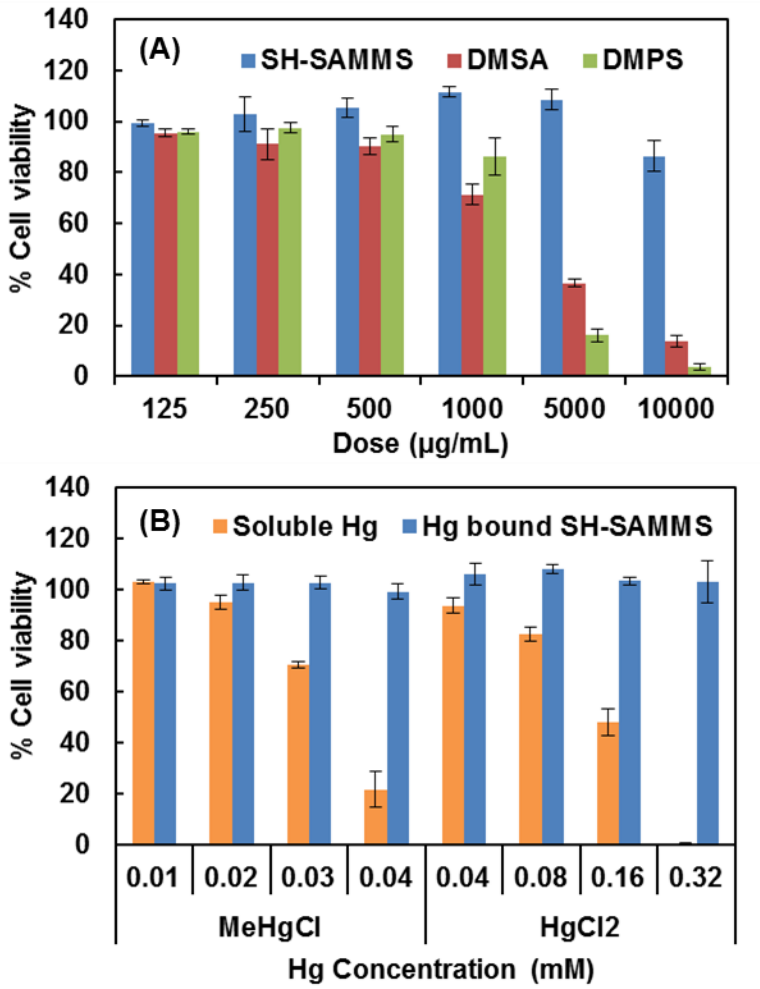

Figure 2.4 Cell viability of Caco-2 cells after 24-h exposure to individual agents; SH-SAMMS, DMSA, or DMPS at indicated dose range **(A)** and the cell viability after 24-h exposure to MeHg(I) and Hg(II) as soluble species and as SH-SAMMS bound **(B)**. Error bars represents S.D. from triplicates.

2.3.6 *SH-SAMMS for Oral Mercury Detoxification: In Vivo Studies*

Because of its encouraging in vitro performance, SH-SAMMS was evaluated in rats for detoxification of MeHg(I) while in concurrent metal stress. Rats on a metal-rich diet + SH-SAMMS had blood Hg levels much lower than rats fed the metal-rich diet alone (**Figure 2.5B**). When the metal-rich diet was stopped after 2 weeks, blood Hg levels in rats subsequently fed with the SH-SAMMS diet decreased faster and to a greater extent than in rats on the normal diet follow-on regime. SH-SAMMS use also prevented the weight loss typically associated with heavy metal toxicity (MS vs. M, **Figure 2.5A**). Indeed, when the metal-rich diet was stopped, rats subsequently fed with SH-SAMMS gained weight, whereas rats switched to the normal diet continued to lose weight (see S vs. N, **Figure 2.5A**). Thus, enhanced removal of previously accumulated mercury by SH-SAMMS assists recovery of the rats from prior toxic effects of heavy metals. Rats fed the SH-SAMMS diet alone gained weight normally (**Figure 2.5A**, (I) S), supporting the safety and bio-compatibility of the material when administered orally.

The Hg contents per gram of wet tissue at sacrifice (**Figure 2.6**) revealed Hg accumulated in kidneys > liver > muscle ~ bone ~ brain. Rats fed the SH-SAMMS diet throughout the study had the lowest Hg accumulation, compared to those fed partially with SH-SAMMS, and those fed without SH-SAMMS. Thus, SH-SAMMS not only reduced the absorption of MeHg(I) when given concurrently, but also accelerated clearance of Hg deposited in the target organs.

Power analysis was performed on blood Hg level of the animals (Figure2.5B) at the end of initial phase (day 16) the end of second phase (day 30) between the SH-SAMMS treated animals and the no-SAMMS counterparts. By applying a statistical

power analysis with power of 0.9 and Type I error of 0.05, two animals per group are needed to detect difference between the SAMMS treated group and the untreated group at the end of both initial phase and second phase. Six and three animals per group were used during the initial phase and second phase, respectively, in this in vivo efficacy study. Hence, the number of animals used in the study is sufficient to validate the hypothesis.

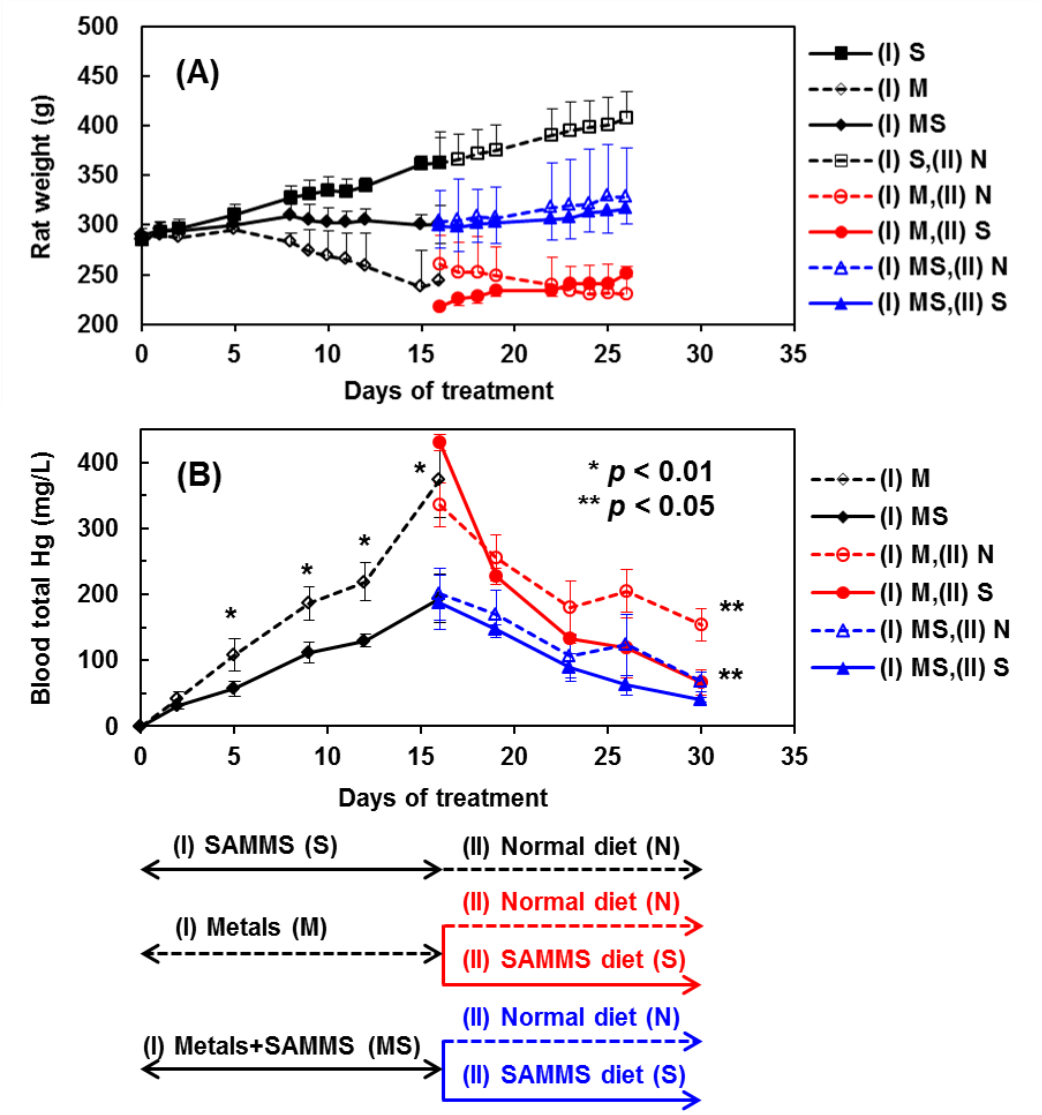

Figure 2.5 Body weights **(A)** and blood Hg contents **(B)** of male Wistar rats after the following dietary treatment exposures: the initial phase (denoted I; n = 6) consisted of 2 weeks of diet containing 0.01 wt% metals (Cd(II), Pb(II), and MeHg(I) (denoted M), 1.0 wt% SH-SAMMS (denoted S), or both (denoted MS) and then the second phase (denoted II; n = 3) after regroupings to compare SH-SAMMS intervention (denoted S) to normal diet (denoted N) for another 2 weeks. *p* values compared to no-SAMMS counterparts for (B).

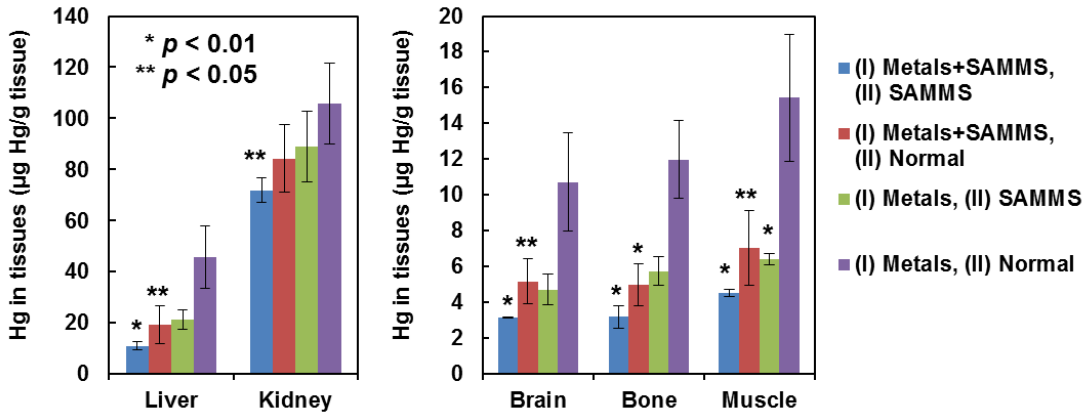

Figure 2.6 Hg contents in organs of rats (n = 3) after the dietary treatment exposures (inset protocol flow chart in Figure 2.5): the initial phase (denoted I) consisted of 2 weeks of diet containing 0.01 wt% metals (Cd(II), Pb(II), and MeHg(I) (denoted M), 1.0 wt% SH-SAMMS (denoted Metals), or both (denoted Metals+SAMMS) and then the second phase (denoted II) after regroupings to compare SH-SAMMS intervention (denoted SAMMS) to normal diet (denoted Normal) for another 2 weeks. *p* values compared to "(I) Metals, (II) Normal" group (purple bars).

2.3.7 *Capture of Dietary Cd(II) and Pb(II) in rats*

In addition to MeHg(I), SH-SAMMS effectively captured Cd(II) and Pb(II) from the diet as shown in **Figure 2.7**. Inorganic Cd(II) and Pb(II) are typically absorbed more poorly than mercurial and were detected in blood at much lower levels than MeHg(I). Pb was below detection in most tissues except bones (~1 – 2 µg Pb/g of bone). However, the lower blood Pb with SH-SAMMS treatment compared to the no SH-SAMMS group was significant as shown in **Figure 2.7A**. Cd accumulated in liver ~ kidney > bone > brain ~ muscle, but the levels were 10- to 100-fold lower than Hg loading in the same organs (**Figure 2.6**). SH-SAMMS consistently lowered Cd in these tissues as shown in **Figure 2.7B**.

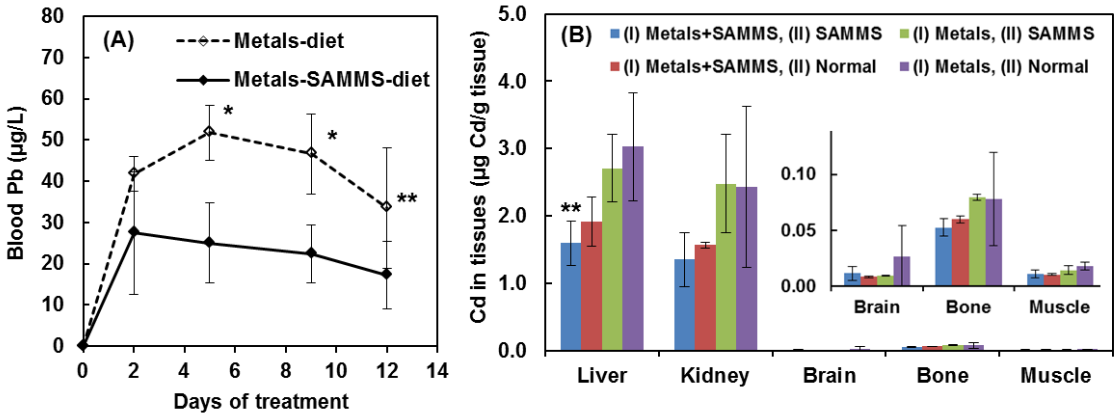

Figure 2.7 Blood Pb in rats (n = 6) after first 2 weeks of treatment **(A)** and tissue Cd levels in rats (n = 3) after 4 weeks of treatment **(B).** Exposure intervals to the metal diet and SH-SAMMS are in **Figure 2.5**. Graphical inset used to expand low scale for respective organs. *p* values compared to no-SAMMS counterparts for (A) and "(I) Metals, (II) Normal" group (purple bars) for (B). * $p < 0.01$ and ** $p < 0.05$

2.3.8 *Capture of Essential Minerals*

It is especially noteworthy that while largely preventing the accumulation of MeHg(I) by rat organs, SH-SAMMS did not diminish the blood contents of essential bulk and trace elements as shown in **Figure 2.8**. Unlike systemically administered chelating agents, SH-SAMMS exposure is restricted to the GI tract, and hence did not deplete most essential metal ions as measured in blood. Copper (Cu) could be captured by SH-SAMMS in vitro (**Table 2.1**), but its loss due to SH-SAMMS was much less dramatic when evaluated in animals. Blood Cu declined about 10% from pre-pretreatment levels after 2 days on SH-SAMMS, more importantly, levels did not decrease further after 5, 9, and 12 days of treatment. Interestingly, rats exposed to the heavy metals also had reduced blood Cu levels and the difference between the blood Cu levels of rats treated with SH-SAMMS or treated with heavy metals was not significant ($p > 0.5$) throughout the 12 days of treatment.

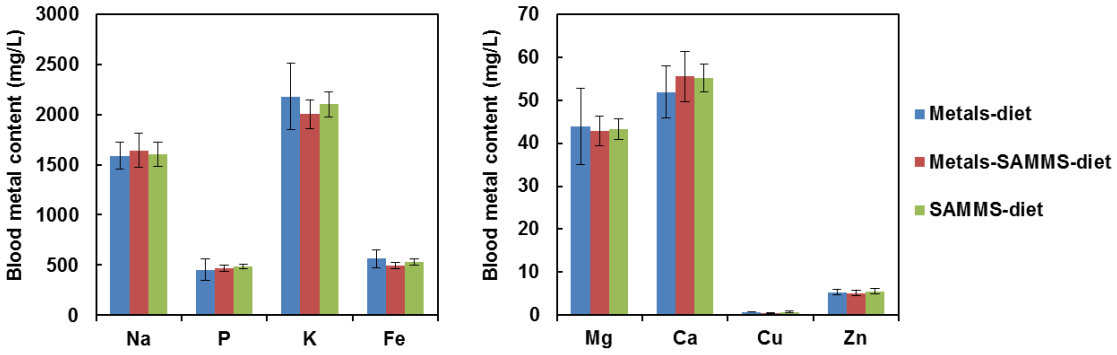

Figure 2.8 Blood contents of essential metals (Na, Mg, P, K, Ca, Fe, Cu and Zn) of rats (n = 6) after the first 2 weeks of treatment as in **Figure 2.5** (Metals, SAMMS and Metals-SAMMS diets).

2.4 Conclusions

SH-SAMMS has many favorable characteristics for oral Hg detoxification. SH-SAMMS demonstrated high binding capacity to both Hg(II) and MeHg(I) (section 2.3.1). SH-SAMMS bound stably to Hg even when challenged with other relevant thiol molecules (section 2.3.2). As fish consumption is one of the major routes of Hg exposure, SH-SAMMS effectively captured Hg from fish digestate from enzymatic digestion (section 2.3.3). The small pore sizes of SH-SAMMS effectively prevented bacteria to access Hg bound to SH groups inside the pore walls of SH-SAMMS. This avoided bacterial Hg biotransformation, which turned Hg into the forms that can circulate in enterohepatic pathway (section 2.3.4). SH-SAMMS demonstrated low toxicity in an intestinal epithelial cell model when compared to two of prescribed drugs for Hg poisoning, DMSA and DMPS. At equivalent Hg dose, Hg bound on SH-SAMMS showed lower toxicity to free Hg (section 2.3.5). Additionally, when administered to an in vivo rodent model, SH-SAMMS prevented Hg (MeHg) from absorbing to the body. SH-SAMMS also accelerated the excretion and reduced tissue retention of already accumulated Hg from the body (section 2.3.6). SH-SAMMS also captured and reduced the body burdens of dietary Cd(II) and Pb(II) (section 2.3.7) but did not affect other essential minerals (section 2.3.8).

CHAPTER 3: DEVELOPMENT OF FUNCTIONALIZED MESOPOROUS SILICA AS ORAL PHOSPHATE BINDER

3.1 Introduction

Hyperphosphatemia is universal to end stage chronic kidney disease patients and dialysis patients. It is indicated by elevated serum phosphorus levels. Hyperphosphatemia can lead to secondary hyperthyroidism by promoting parathyroid gland hyperplasia and parathyroid hormone (PTH) synthesis and secretion [38]. Since hyperphosphatemia and hyperparathyroidism have clinical consequences of increased risk of cardiovascular disease, bone disease, and calcification of soft tissues and eventual morbidity and mortality [39,40], management of hyperphosphatemia is believed to be critical for the care of end stage chronic kidney disease patients which total ~400,000 in the US, and 2 million worldwide [41]. Dietary restriction of phosphate and dialysis do not adequately control the serum phosphorus level and hence patients are required to take oral phosphate binders. The current prescribed phosphate binders in the market are calcium-based salts (acetate and carbonate), Sevelamer (hydrochloride and carbonate), lanthanum carbonate, aluminium salts and magnesium salts, which account for about $1 billion in global annual sales [105]. Yet they have several drawbacks including high risk of hypercalcemia and calcification [47,48], high costs, low-to-moderate efficacy, adverse gastrointestinal effects, and high pill burden [106]. A new oral phosphate binder with high efficacy, low adverse effects, low cost, and low pill burden is needed. Soluble iron based salts have recently been investigated as calcium-free oral phosphate binders. However, in clinical trials, they were linked to diarrhea, boating, and constipation [107].

Recently, iron-diamine on mesoporous silica support (Fe-EDA-SAMMS) had been developed for environmental phosphate removal [66]. Fe-EDA-SAMMS demonstrated moderate phosphate binding capacity, fast binding kinetics and

independence of pH and competing anions. With these characteristics, Fe-EDA-SAMMS has potential to be good phosphate binder; however, the moderate binding capacity can prevent it from competing with current commercially available high capacity phosphate. Several parameters in Fe-EDA-SAMMS synthesis (e.g., solvent used during Fe incorporation, silica and other substrate, and amine functional groups) can be optimized to improve phosphate binding capacity. I hypothesize that the change of solvent from water to aprotic organic solvent coupled with increasing temperature will lead to improved Fe deposition and ultimately higher phosphate binding capacity. The phosphate binding performance of optimized material in challenging environment and toxicity to intestinal endothelial cell model will be investigated. Parts of this work have been published as parts of *Nanoporous Sorbent Material as an Oral Phosphate Binder and for Aqueous Phosphate, Chromate, and Arsenate Removal*. J Nanomed Nanotechnol, 2014, 5:4.

3.2 Materials and Methods

3.2.1 *Chemicals and Reagents*

Potassium phosphate (KH_2PO_4 and K_2HPO_4), sodium chloride (NaCl), sodium nitrate ($NaNO_3$), sodium bicarbonate ($NaHCO_3$), sodium sulfate (Na_2SO_4), sodium citrate ($Na_3C_6H_5O_7 \cdot 2H_2O$), sodium acetate ($NaC_2H_3O_2$), potassium chloride (KCl), dimethoxyethane (glyme), [3-(2-aminoethylamino)propyl] trimethoxysilane, 25-kDa branched polyethylenimine (PEI), Cab-o-sil® M5 and StratoSpheres™ PL-EDA polystyrene resin were purchased from Sigma Aldrich (St. Louis, MO). Ferric chloride ($FeCl_3 \cdot 6H_2O$), acetonitrile (CH_3CN), methanol, 2-propanol, dimethyl sulfoxide (DMSO),

sodium hydroxide (NaOH), hydrochloric acid (HCl) and nitric acid (HNO_3) were purchased from Fisher Scientific (Waltham, MA). Ultrapure SiliaBond® Diamine functionalized silica gel was purchased from Silicycle® (Quebec City, QC). 3-isocyanatopropyl trimethoxysilane was purchased from Gelest (Morrisville, PA). Sevelamer HCl was purchased from Genzyme (Cambridge, MA) and AG® 1-X8 anion exchanger was purchased from BioRad (Hercules, CA). All common chemicals and reagents were of high purity grade.

3.2.2 *Material Synthesis*

Details for synthesis of EDA-SAMMS were described in previous works [65,66]. Briefly, pre-hydrated MCM-41 (with a surface area of 880 m^2/g and average pore size of 48 Å) was treated with [3-(2-aminoethylamino)propyl] trimethoxysilane in refluxing toluene for 6 h to obtain EDA-SAMMS. Fe(III) was incorporated onto the EDA-SAMMS by mixing Fe(III) solution with EDA-SAMMS. Fe(III) solution was prepared by dissolving $FeCl_3 \cdot 6H_2O$ in either de-ionized (DI) water or acetonitrile at a concentration of 5 wt%. Ten grams of EDA-SAMMS was mixed with 50 mL of Fe(III) solution resulting in Fe per EDA-SAMMS mass ratio of 0.52. The reaction was conducted at either room temperature or 65 °C for a duration of 1 h or 20 h. The resulting Fe-EDA-SAMMS was then washed extensively with DI water and 2-propanol to remove unbound Fe(III), air-dried and stored at room temperature until use.

For comparison, using the same conditions, Fe(III) was also incorporated into two other commercial ethylenediamine (EDA)-functionalized substrates: EDA-resin

(StratoSpheres™ PL-EDA polystyrene resin) and EDA-porous silica gel (SiliaBond® Diamine).

Lastly, as an alternative to EDA, polyethylenimine (PEI), having abundant amine groups, was grafted onto the surface of non-porous fumed silica (Cab-o-sil® M5). Briefly, 5.2 g of 25-kDa branched PEI was pre-treated with 60 mL of DMSO in 60 mL of warm glyme (40 – 50 °C) for 2 h. The warm mixture was treated with 120 µL of 3-isocyanatopropyl trimethoxysilane, then 3 g of the fumed silica was immediately added into the modified PEI mixture and stirred overnight under static nitrogen atmosphere. The material, PEI-fumed silica, was then washed with copious amount of methanol and air-dried. The Fe(III) incorporation was then conducted in the same manner as previously described.

3.2.3 *Batch Contact Experiments*

Sorbent materials developed in this work as well as commercially available materials, Sevelamer HCl and AG® 1-X8 anion exchanger, were tested in batch contact experiments as described in previous work [66]. Briefly, known weights of sorbent material were added into a phosphate solution prepared from KH_2PO_4 with a concentration range from 3 mg/L to 3,000 mg/L of phosphate in a polypropylene vial to achieve a liquid-to-solid ratio (L/S) of 200, 1,000 or 2,000 mL/g. Batch contact was carried out on an orbital shaker (200 rpm) for 2 h and then filtered prior to analysis. Phosphate concentration of the filtrates was analyzed with inductively-coupled plasma mass spectrometer (ICP-MS) Agilent 7700X (Agilent, Santa Clara, CA). All experiments were performed with control (same solutions without sorbents added) in parallel and in

triplicate. Sorbents' ability to capture phosphate was reported in terms of percentage of phosphate removal from the solution (Equation 3.1) or amount of phosphate adsorbed per gram of sorbent material (Equation 3.2):

$$Phosphate\ removal\ (\%) = 100 \times \frac{C_0 - C_e}{C_0} \qquad \text{(Equation 3.1)}$$

where C_0 and C_e are the initial and equilibrium concentrations of phosphate, respectively (in mg/L).

$$Phosphate\ adsorbed\ (\frac{mg\ phosphate}{g\ sorbent}) = (C_0 - C_e) \times L/S \qquad \text{(Equation 3.2)}$$

where L/S is the liquid-to-solid ratio (in mL/g).

Typical testing conditions were 3 mg/L of phosphate prepared from KH_2PO_4 in DI water and pH of 5.3. In anion competition study, test matrices included chloride, nitrate, bicarbonate, acetate, sulfate and citrate; all from sodium salts. In the pH-dependent phosphate capture study, 6 mg/L phosphate solution was prepared from K_2HPO_4; its pH was adjusted to 1.0 – 12.0 with 0.1 M HCl or 0.10 – 1.0 M NaOH.

Furthermore, for evaluating the materials as potential oral phosphate binders, simulated gastric fluid (SGF) and simulated intestinal fluid (SIF) were also used as the test matrices. Both SGF and SIF were prepared following the recommendations of the U.S. Pharmacopeia for drug dissolution studies in stomach and intestine [108,109]. The SGF (pH 1.1) contained 0.03 M NaCl and 0.085 M HCl. The SIF contained 0.14 M NaCl, 0.005 M KCl and 0.008 M $NaHCO_3$; its pH was adjusted to 4.0 and 6.5 with 0.1 M HCl. An additional SIF solution containing 0.08 M NaCl and 0.03 M $NaHCO_3$ with pH adjusted to 6.6 was also used [110].

3.2.4 *Phosphate Sorption Capacity*

The sorption capacity of Fe-EDA-SAMMS was measured in batch contact at room temperature. Phosphate solutions with varying concentrations from 0 to 500 mg/L were in contact with the sorbent at an L/S ratio of 2,000 mL/g for 2 h assuring equilibrium condition. Langmuir isotherm equation was used to fit sorption capacity data as shown in Equation 3.3.

$$Q_e = \frac{K_L Q_{max} C_e}{1 + K_L C_e} \qquad \text{(Equation 3.3)}$$

where C_e, Q_e, Q_{max} and K_L are equilibrium concentration (in mg/L), equilibrium uptake (in mg /g), maximum binding capacity (in mg/g) and Langmuir constant (in L/mg), respectively.

3.2.5 *Phosphate Sorption Kinetics*

The kinetics of phosphate capture was measured in a modified batch contact experiment. Briefly, a 50 mL solution of 3 mg/L phosphate was mixed with 0.5 g sorbent at an L/S ratio of 1,000 mL/g. At each designated time point; 1, 2.5, 5, 10, 30, 60, 120 and 240 min, 1.5 mL of mixture was collected, filtered, and subjected to phosphate analysis by ICP-MS. The sorption kinetics were measured in both DI water and SIF (0.14 M NaCl, 0.005 M KCl and 0.008 M $NaHCO_3$, pH 6.3).

3.2.6 *Cell Culture and Cytotoxicity Study*

Immortal human colon epithelial cells, Caco-2, were obtained from American Type Culture Collection (Manassas, VA). Cell stocks were cultured in DMEM (Corning/Cellgro, Manassas, VA) supplemented with 10% fetal bovine serum (GIBCO,

Life Technologies, Grand Island, NY) and 1X penicillin/streptomycin (Corning/Cellgro, Manassas, VA) at 37 °C in 5% CO_2 atmosphere. For cytotoxicity assays, cells were seeded at 3,000 cells/well in 96-well flat-bottomed plates and grown to optimal confluency in 5 days. Cells were then exposed to Fe-EDA-SAMMS, Sevelamer HCl (Renagel®, Genzyme, MA) or lanthanum carbonate (Fosrenol®, Shire Pharmaceuticals, Dublin) at a dose of 500, 1,000, 2,500 and 5,000 µg/mL for 24 h and 48 h. After the designated time, cell viability was quantified with the CellTiter-Glo® Luminescent Cell Viability Assay (Promega, Madison, WI) and normalized to an untreated control (without phosphate binder added).

3.3 Results and Discussion

3.3.1 *Optimization of Fe(III) Incorporation*

Varied conditions of Fe(III) incorporation onto EDA-SAMMS and the phosphate binding ability of the resulting materials are summarized in **Table 3.1**. In an attempt to increase the Fe loading on EDA-SAMMS, the amount of initial Fe(III) in the solution was increased by 20-fold compared to the earlier work (Iteration I) [66]. However, this did not result in increased Fe loading (0.83 mmol/g vs. 0.017 mmol/g). This is likely due to the fact that the pH of the loading solution dropped at the higher Fe(III) concentration (i.e., from pH 1.96 to 1.46), and the EDA-SAMMS are more likely to be protonated under the more acidic conditions. Accordingly, the phosphate capture did not improve under the SGF (pH 1.1) and SIF (pH 4.0) test matrices. To avoid fighting the pH issues associated with aqueous solutions of Fe(III) ion, I employed acetonitrile as our solvent for the Fe incorporation. As an anhydrous, polar aprotic solvent, acetonitrile does not

have any readily dissociable protons to increase the acidity of the reaction mixture upon dissolution of Fe(III) salts, resulting in no competing protonation of the EDA ligand. This solvent change led to a 7-fold increase in Fe loading after 1 h of contact time (Iteration III), which is associated with improved phosphate removal efficacy. Next I show that increasing the temperature of Fe(III) in acetonitrile from room temperature to 65 °C (Iteration IV) and contact time from 1 h to 20 h (Iteration V), I could substantially increase Fe loading to 0.140 and 0.224 mmol/g, respectively. The high reaction temperature and increased reaction time helped overcome kinetic barriers associated with charge accumulation (i.e., cation-cation repulsion) within the monolayer, thereby facilitating integration of Fe into the EDA monolayer inside the pores of SAMMS. The most optimal Fe-EDA-SAMMS (Iteration V) achieved 93 – 96% of phosphate removal in all three matrices. However, increasing the temperature of reaction to boiling point (82 °C) of acetonitrile did not further increase phosphate removal efficacy of the material (data not shown). It is worth noting that, although Fe loading of original material (Iteration I) was extremely high (0.83 mmol Fe/g) compared to others, it did not yield the best phosphate capture perhaps due to the iron oxide formation which did not attribute to the phosphate adsorption of the material. A control experiment (Iteration VI) was carried out similarly to Iteration V but without Fe(III) in the solution. The Iteration VI material likely contained protonated EDA as a functional group (occurring during material washing step with DI water), but had much lower phosphate removal in all matrices compared to Iteration V. This indicates the advantage of Fe(III)-EDA over protonated amine for phosphate binder in these three matrices. In summary, the incorporation of Fe(III) onto EDA-SAMMS was found to be optimum when carried out in acetonitrile

solvent, at 65 °C for 20 h using Fe(III) solution of 1 – 5 wt%. This protocol was hence used in all subsequent studies.

Table 3.1. Phosphate removal efficiency of Fe-EDA-SAMMS.[a] Data represents mean ± S.D. from triplicates.

Iteration	Fe Incorporation conditions				Fe content (mmol/g)	% Phosphate Removal		
	Fe:EDA SAMMS (mass)	Solvent	Temperature (°C)	Time (h)		SGF, pH 1.1[b]	SIF, pH 4.0[c]	SIF, pH 6.5[c]
I [66]	0.023	Water	25 °C	1	0.83	34 ± 5	63 ± 2	14 ± 4
II	0.52	Water	25 °C	1	0.017 ± 0.000	5 ± 2	58 ± 2	74 ± 1
III	0.52	Acetonitrile	25 °C	1	0.122 ± 0.003	51 ± 4	83 ± 1	61 ± 2
IV	0.52	Acetonitrile	65 °C	1	0.140 ± 0.013	75 ± 2	96 ± 1	98 ± 1
V	0.52	Acetonitrile	65 °C	20	0.224 ± 0.015	93 ± 0	96 ± 1	93 ± 1
VI	N/A	Acetonitrile	65 °C	20	N/A	0 ± 0	19 ± 2	8 ± 3

[a] Initial phosphate concentration of 3 mg phosphate/L (from KH_2PO_4), L/S ratio of 1000 mL/g

[b] SGF, pH 1.1, consists of 0.03 M NaCl and 0.085 M HCl

[c] SIF, pH 4.0 and 6.5, consist of 0.14 M NaCl, 0.005 M KCl, 0.008 M $NaHCO_3$, pH adjusted with 0.1 M HCl

3.3.2 *Optimization of Amine Functionalized Substrates*

To achieve the best overall sorbent for binding phosphate, it is important to optimize not only the interfacial binding chemistry, but also the substrates (supports) which can impact phosphate binding capacity and rate. In this regard, I compared four amine-functionalized substrates: EDA-resin (StratoSpheres™ PL-EDA), EDA-porous silica gel (SiliaBond® Diamine), PEI-fumed silica (on Cab-o-Sil® M5), and EDA-SAMMS (on MCM-41). All were incorporated with Fe(III) using the optimal incorporation conditions previously described. These materials varied in particle size, pore size, surface area, amine functional group (EDA or PEI) loading, and Fe loading as shown in Table 3. Their phosphate removal capabilities were measured in SIF (0.08 M NaCl, 0.03 M $NaHCO_3$, pH 6.6) with about 3.0 g phosphate/L at an L/S ratio of 200 mL/g and reported in **Table 3.2**.

Although the EDA-resin has higher EDA loading than our EDA-SAMMS (6.35 vs. 2.64 mmol/g), it exhibited lower Fe loading (0.053 vs. 0.224 mmol Fe/g), which in turn resulted in lower phosphate removal capacity (126 vs. 157 mg/g). This lower Fe loading may be due to limitations on the transport of the highly charged Fe(III) ion into the relatively nonpolar core of the polystyrene resin bead. The EDA-porous silica gel has comparable EDA loading with our SAMMS (1.98 vs. 2.64 mmol N/g), but could load only half the amount of Fe, resulting in 58% less phosphate removal capacity compared to our Fe-EDA-SAMMS. The synthesis process of this EDA-porous silica gel may result in a high level of self-reaction between the amine groups or the amine groups on the ligands could react with the hydroxyl groups (OH) on the silica surface resulting in less active EDA groups for Fe(III) to bind to, leading to lower phosphate binding capacity.

This was not the case with EDA-SAMMS since the amount of EDA ligands used was limited by design to only a monolayer deposition.

To increase phosphate binding capacity, branched PEI (25-kDa) was investigated as an alternate to EDA since it contains a high content of amines. 25-kDa PEI was too big to be loaded effectively inside the pores, and hence was loaded on fumed silica (Cab-o-sil® M5). The fumed silica is a non-porous material, thus the PEI was loaded on the external surface. I hypothesize that the lower surface area of fumed silica in comparison to SAMMS could be compensated by the considerably higher amount of amine groups of PEI than that of EDA. Despite the substantial surface area of fumed silica (200 m^2/g) and the high loading of PEI (6.97 mmol N/g), PEI-fumed silica had low Fe loading (0.047 mmol Fe/g) and the resulting material (Fe-PEI-fumed silica) yielded low phosphate binding capacity compared to Fe-EDA-SAMMS (45 vs. 157 mg/g). This is mostly due to PEI wrapping around fumed silica in thick layers, preventing the penetration of both Fe(III) and phosphate to the available amine groups in the inner layers. Only the outer layer amine groups remained active, resulting in low Fe loading and low phosphate binding capacity. Based on the finding in **Table 3.2**, SAMMS, produced from MCM-41, proved to be the best substrate for Fe-amine loading, yielding the highest phosphate binding capacity. It was therefore used in all subsequent experiments.

Table 3.2 Phosphate removal capacity of Fe-amine on various substrates.[a] Data represents mean ± S.D. from triplicates.

Material[b]	Capacity (mg/g)	N content (mmol/g)	Fe content (mmol/g)	Specific surface area[c] (m^2/g)	Pore size[c] (Å)	Particle size[c] (µm)
Fe-EDA-SAMMS	157 ± 6	2.64 ± 0.06	0.224 ± 0.015	880	48	20-75
Fe-EDA-resin	126 ± 3	6.35[d]	0.053 ± 0.005	N/A	N/A	194[d]
Fe-EDA-porous silica gel	66 ± 5	1.98 ± 0.02	0.113 ± 0.014	500[d]	60[d]	40-63[d]
Fe-PEI-fume silica	45 ± 5	6.97 ± 0.23	0.047 ± 0.001	200[e]	N/A	0.2-0.3[e]

[a] Initial phosphate concentration of 3.0 g phosphate/L (from KH_2PO_4) in SIF (0.08 M NaCl, 0.03 M $NaHCO_3$) pH 6.60, L/S ratio of 200 mL/g

[b] EDA-resin (StratoSpheres™ PL-EDA), EDA-porous silica gel (SiliaBond® Diamine), fumed silica (Cab-o-sil®)

[c] Specific surface area, pore size and particle size are of substrates.

[d] Data from manufacturer's certificate of analysis

[e] Data from manufacturer's product specification sheet

3.3.3 *Adsorption Isotherm*

The phosphate binding capacity of Fe-EDA-SAMMS was established with adsorption isotherm experiments conducted in DI water (pH 5.3) with an L/S ratio of 2,000 mL/g and room temperature. The phosphate uptake of Fe-EDA-SAMMS increased sharply with increasing initial concentrations of phosphate from 0 to 90 mg/L (or 22 mg/L of equilibrium concentration) and began to saturate thereafter. The adsorption data fitted the Langmuir adsorption model quite nicely, as shown in **Figure 3.1** ($R^2 > 0.999$). This confirmed that phosphate adsorption on the Fe-EDA-SAMMS followed a monolayer adsorption model similar to the original Fe-EDA-SAMMS previously reported [66]. However, the new Fe-EDA-SAMMS offered much higher phosphate binding capacity at 156 mg phosphate/g sorbent (1.65 mmol/g sorbent), which is almost 4 times higher than that of the older version (43.3 mg phosphate/g). This binding capacity measured in DI water was the same with that measured in SIF (see **Table 3.2**), indicating little dependency of matrix effect. The phosphate adsorption capacity is also significantly higher than other sorbents for phosphate capture reported by others, which are 47.8 mg/g for ammonium-functionalized MCM-48 [111], 63.4 mg/g for Fe-diamino-functionalized SBA-15 [112], 54.3 mg/g for lanthanum-diamino-functionalized MCM-41 [113], 51.8 mg/g for Fe-diamino-functionalized MCM-41 [114], 41.8 mg/g for magnetic Fe-Zr binary oxide [115], and 88.4 mg/g for chitosan hydrogel [116]. All phosphate binding capacities reported were measured in DI water.

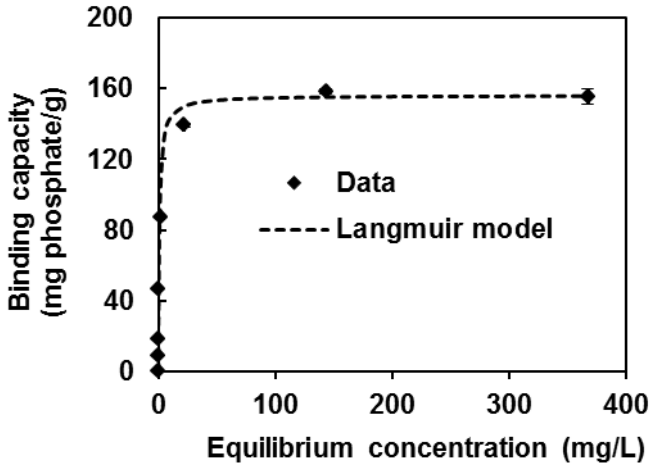

Figure 3.1 Adsorption isotherm of phosphate on Fe-EDA-SAMMS in DI water (pH 5.3), L/S of 2,000 mL/g, symbols represent data and dash-line represents Langmuir isotherm fitting. Error bars represent S.D. from triplicates.

3.3.4 *Adsorption Kinetics*

For oral phosphate binders, fast phosphate capture (onto the sorbent) reduces the degree of phosphate available to be absorbed into the body. The adsorption kinetics of Fe-EDA-SAMMS was measured in 3 mg phosphate/L in DI water (pH 5.3) with an L/S of 1,000 mL/g as shown in **Figure 3.2A**. I also benchmarked against two commercially available materials: Sevelamer HCl (the gold standard oral phosphate binder) and AG® 1-X8 resin (a commercial anion exchange resin). Both materials had slower phosphate binding kinetics than Fe-EDA-SAMMS. Specifically, while Fe-EDA-SAMMS removed over 98.7% of phosphate in 1 min, Sevelamer HCl and AG® 1-X8 only removed 79.2% and 31.7%, respectively. To remove more than 99% of phosphate, Fe-EDA-SAMMS took 5 min, while Sevelamer HCl took 10 min and AG® 1-X8 resin took 30 min. Similar to the previous reports on other types of SAMMS materials [67,69-71,73], fast kinetics is a signature of SAMMS performance, which is owed to the rigid and open pore structure, allowing easy access of metal ions to the binding sites inside the pores. These unique characteristics of SAMMS provides advantages over other recently developed phosphate removal materials, which require much longer time to reach equilibrium (e.g., more than 24 h for Fe-Zr binary oxide [115] or 7 h for chitosan hydrogel [116]). The binding kinetics on SAMMS was slightly affected by the coexisting anions (**Figure 3.2B**), to be described in subsequent section.

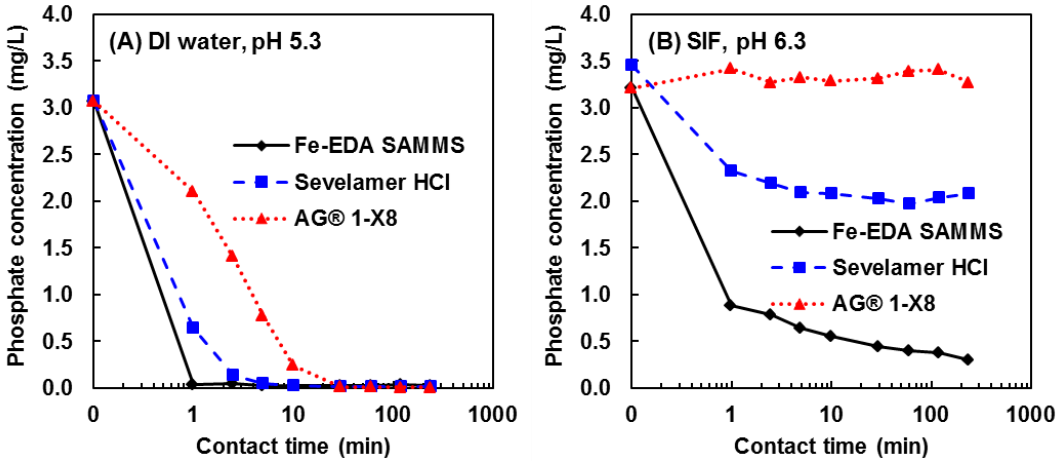

Figure 3.2 Phosphate adsorption kinetics on Fe-EDA-SAMMS, Sevelamer HCl and AG® 1-X8 in DI water (A) pH 5.3 and in SIF (B) pH 6.3, L/S ratio of 1,000 mL/g.

3.3.5 *Effect of Coexisting Anions*

The most common anion species in the gastrointestinal tract are chloride (0.10 – 0.13 M) and bicarbonate (0.006 – 0.040 M) [117]. These anions can compete with phosphate for Fe-EDA binding sites. The effect of coexisting anions was measured in 3 mg/L phosphate solution (0.00003 M) and 0.01 M coexisting anions, including chloride, nitrate, bicarbonate, sulfate and citrate, with an L/S ratio of 1,000 mL/g. All of the initial and final pH of the solution fell within 3.4 – 8.7. As shown in **Table 3.3**, there were no significant decreases in phosphate removal with chloride and nitrate even when the anions were 300 folds by mole in excess of phosphate. Only bicarbonate, sulfate, and citrate ions could hamper phosphate removal. This finding is in agreement with our earlier report on Cu-EDA-SAMMS that anion binding is a function of anion basicity [48]. However, as illustrated in **Table 3.3**, Fe-EDA-SAMMS was much less affected by the presence of coexisting anions than the commercial AG® 1-X8 resin, having simple quaternary ammonium as the binding site, which has little selectivity. Evidently, the addition of Fe(III) to the EDA group increases selectivity of the binding site for phosphate compared to simple ammonium which acts as an anion exchanger.

Table 3.3 Effect of coexisting anions on phosphate removal by Fe-EDA-SAMMS and AG® 1-X8 anion exchanger resin.[(a)] Data represents mean ± S.D. from triplicates.

Matrix	Initial pH	Fe-EDA-SAMMS		AG® 1-X8	
		Equilibrium pH	Phosphate removal (%)	Equilibrium pH	Phosphate removal (%)
0.00003 M phosphate	5.6	3.6	99.5 ± 0.0	9.6	99.8 ± 0.2
+ 0.01 M sodium chloride	5.5	3.8	97.7 ± 0.3	11.2	79.8 ± 9.6
+ 0.01 M sodium nitrate	5.7	3.9	93.8 ± 0.5	11.3	67.5 ± 10.6
+ 0.01 M sodium bicarbonate	8.7	7.7	28.7 ± 5.7	9.4	29.1 ± 1.0
+ 0.01 M sodium sulfate	5.7	5.8	24.2 ± 0.8	11.0	0.0 ± 0.6
+ 0.01 M sodium citrate	7.2	7.2	25.3 ± 3.2	10.7	1.3 ± 0.3

[(a)] Initial phosphate concentration of 3 mg phosphate/L (0.00003 M from KH_2PO_4), L/S ratio of 1,000 mL/g

Compared to Fe-EDA-SAMMS, simple anion exchangers were much more affected by increasing concentrations of the interfering anions. As shown in **Figure 3.2B**, when used to capture the same phosphate concentration (3 mg/L) but with higher anion content (i.e., SIF containing 0.145 M Cl^- and 0.008 M HCO_3^- (pH 6.3)), Fe-EDA-SAMMS could reach 80% removal within 5 min and 88% after 1 hour. On the contrary, both Sevelamer HCl and AG® 1-X8 resin were largely hindered by the anions such that only a total of 40% and 0% of phosphate could be removed by Sevelamer HCl and AG® 1-X8 resin, respectively. Compared to phosphate removal in DI water (**Figure 3.2A**), the Fe-EDA-SAMMS efficacy was reduced only by 10%, while that of Sevelamer HCl and AG® 1-X8 was reduced by 60% and 100%, respectively. In short, **Figure 3.2B** confirms that Fe-EDA-SAMMS with amine-chelated Fe(III) ion as the key functional group has better selectivity for phosphate (over Cl^- and HCO_3^-) than Sevelamer HCl and AG® 1-X8, with primary amine and quaternary ammonium as functional groups, respectively. This suggests a great potential of Fe-EDA-SAMMS over Sevelamer HCl as an oral phosphate binder.

3.3.6 *Effect of pH on Phosphate Capture*

The effect of pH on phosphate capture on Fe-EDA-SAMMS was measured in a 6 mg/L phosphate solution of varied pHs with an L/S ratio of 2,000 mL/g. **Figure 3.3** shows the phosphate removal by Fe-EDA-SAMMS as a function of initial pH (closed symbol) and equilibrium pH (open symbol). Fe-EDA-SAMMS showed >99% phosphate removal in large pH range of 3.0 to 11.0 (as initial pH). Phosphate removal by Fe-EDA-SAMMS resulted in a drop of solution pH (see initial pH vs. equilibrium pH), especially

when pH > 8.0. Based on equilibrium pH, >98% of phosphate was removed between pH of 3.0 and 7.0, and % removal decreased sharply outside of this pH range. Phosphate is a polyprotic acid and has 3 dissociation constants (pK_{a1} = 2.14, pK_{a2} = 7.20, pK_{a3} = 12.32) [118]. It can exist in 4 species in the system: H_3PO_4, $H_2PO_4^-$, HPO_4^{2-} and PO_4^{3-}. When the pH is lower than 2.1, the predominant species is neutral phosphoric acid (H_3PO_4). At pH between 2.1 and 7.2, the main species is $H_2PO_4^-$ monovalent, whereas pH between 7.2 and 12.3, the predominant species is HPO_4^{2-} divalent. These iron-amine-functionalized sorbent materials bind greater $H_2PO_4^-$ than HPO_4^{2-} based on stoichiometry [66,119], which agrees well with the data where the phosphate capture was best in the pH range of 3.0 – 7.0. In **Figure 3.3**, between equilibrium pH 7.0 and 9.0, Fe-EDA-SAMMS could capture some phosphate, which mostly are in the form of HPO_4^{2-}. When considering initial pH, Fe-EDA-SAMMS had a larger operating pH window (pH 2.0 – 11.0) than Fe-diamino-functionalized SBA-15 with an operating initial pH of 3.0 – 6.0 [112] and ammonium-functionalized MCM-48 with an operating initial pH of 4.0 – 6.0 [111].

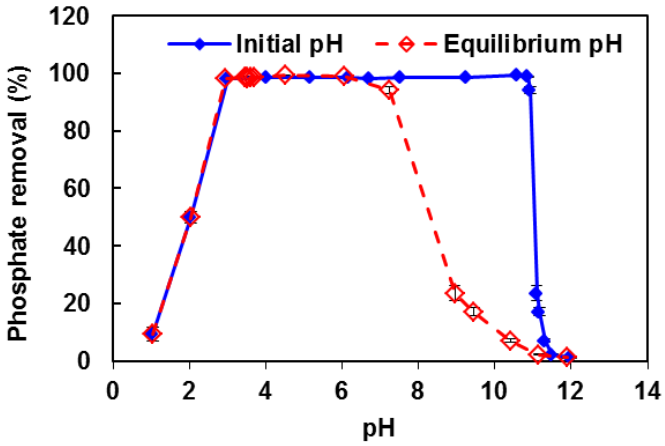

Figure 3.3 Effect of pH on phosphate removal efficiency of Fe-EDA-SAMMS. Initial phosphate concentration of 6 mg phosphate/L (from K_2HPO_4) and L/S ratio of 2,000 mL/g. Closed symbols and solid-line represent initial pH of phosphate solutions, while opened symbols and dash-line represent equilibrium pH. Error bars represent S.D. from triplicates.

3.3.7 *Cytotoxicity of Fe-EDA-SAMMS to Intestinal Tissue Culture Cells*

A safety profile for Fe-EDA-SAMMS in vitro was established. The Caco-2 cell line resembles the epithelial cells lining the small intestine both morphologically and functionally and has been previously used to establish drug safety profile of several oral drugs [91,120]. Fe-EDA-SAMMS was found to be well-tolerated by Caco-2 cells and did not cause significant toxicity up to 2,500 µg/mL both for 24 h and 48 h of contact time while Sevelamer HCl was tolerated up to 5,000 µg/mL (Figure 5). Fe-EDA-SAMMS was better tolerated than another prescribed oral phosphate binder, lanthanum carbonate, which started to show some toxicity at 1,000 µg/mL. Lanthanum carbonate is an inorganic salt which is dissociated in GI tract and is readily taken up by cells, making it more toxic to cells. On the other hand, the micron-scale particle sizes of Fe-EDA-SAMMS and Sevelamer HCl (both having similar zeta potential of 30-40 mV in water) made them not easily taken up by the cells, which limited cytotoxicity. This agrees with the previous work [61] that SAMMS (with thiol groups) having particle size of 1 – 2 µm could be taken up by Caco-2 cells after 3 h of contact time whereas particles of larger size (> 5 µm) were not. SAMMS with the size of 20 – 75 µm can be avoided uptake by the GI tract. Increases in dose and contact time might enhance the uptake, resulting in the increased cytotoxicity of SAMMS at high dose (e.g., 5,000 µg/mL at 24 – 48 h contact time, **Figure 3.4**). Preliminary clearance study of one SAMMS material (with thiol groups) of the same particle sizes (20 – 75 µm) after oral administration to rats (given as 0.1% by weight of food for 24 h, 4 animals) indicates that most of SAMMS administered was recovered (i.e., 91% within 2 days and 99% within 4 days, by silicon (Si) analysis of daily collected feces and urine using an ICP-MS). Out of the total Si excreted after 4

days, 0.98 fraction was found in feces, and 0.2 fraction was found in urine. Hence, the majority of SAMMS material does not absorb to the body and is cleared through fecal excretion.

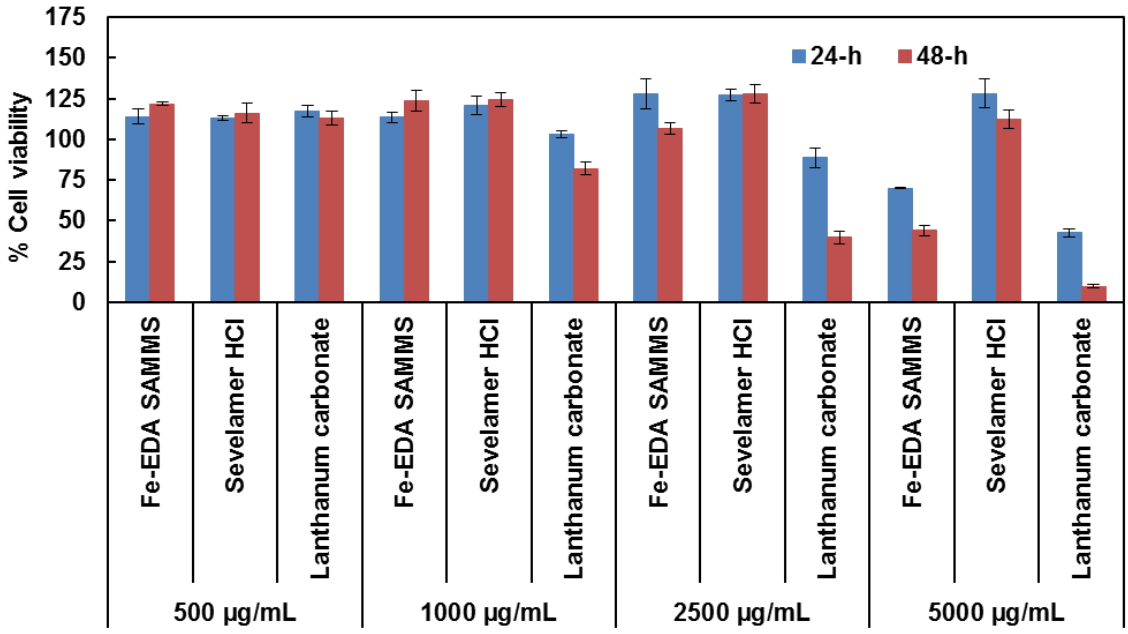

Figure 3.4 Cell viability of Caco-2 cells after 24 h (solid bar) and 48 h (striped bar) exposures to individual materials; Fe-EDA-SAMMS, Sevelamer HCl (Renagel®), or Lanthanum carbonate (Fosrenol®) at indicated dose range (500, 1,000, 2,500, 5,000 µg/mL). Error bars represent S.D. from triplicates.

3.4 Conclusions

Fe incorporation conditions were found to be optimum when switching of solvent from H_2O to aprotic solvent of acetonitrile and increasing reaction temperature to 65 °C and time to 20 h. Phosphate removal in simulated gastrointestinal fluids increased significantly over the original iteration (section 3.3.1). MCM-41 silica substrate was found to be the best substrate for Fe-EDA-incorporation compared to other polystyrene resin, porous silica or non-porous silica substrates (section 3.3.2). The optimum Fe-EDA-SAMMS (from improved Fe incorporation) had 4-fold increase in phosphate binding capacity over original iteration (section 3.3.3). Fe-EDA-SAMMS had faster phosphate binding kinetics than Sevelamer HCl (gold standard oral phosphate binder) or AG® 1-X8 (commercial anion exchanger) (section 3.3.4). In addition, the Fe-EDA also had higher specificity to phosphate over other coexisting anions than a ammonium based binding sites of Sevelamer HCl and AG® 1-X8 (section 3.3.5). Fe-EDA-SAMMS could remove >99% of phosphate in the pH range of 3-11, a much border working pH range than other similar materials (section 3.3.6). Fe-EDA-SAMMS was found to be well-tolerated in intestinal epithelial cell model and had lower toxicity than lanthanum carbonate, another oral phosphate binder in the market (section 3.3.7).

CHAPTER 4: SUMMARY, CONCLUSION, AND FUTURE DIRECTIONS

4.1 Summary and Conclusion

In this dissertation, I have evaluated two microscale functionalized ordered mesoporous silica as the potential oral drugs for treating heavy metal poisoning and hyperphosphatemia. As mentioned in Chapter 1, current treatments for both heavy metal exposure and hyperphosphatemia have several drawbacks. One of the common drawbacks is absorbable nature of the current drugs, leading to adverse side effects. For heavy metal chelators, DMSA and DMPS, the absorbed drugs need to be cleared by liver and kidney. This poses toxicity to the clearance organs especially once they bind to the toxic metals. They also capture essential minerals especially zinc and copper. Close monitoring of liver, kidney, and blood chemistry is required for patients under treatment. Thus, DMSA and DMPS are intended for short term treatment of acute metal poisoning and not for long term treatment of chronic metal exposure. For oral phosphate binders, most inorganic drugs (excluding Sevelamer) are soluble and can be absorbed to circulatory system. The absorbed components (i.e., calcium, magnesium and iron) can lead to unwanted conditions such as hypercalcemia (ectopic calcification), hypermagnesemia and iron overload. Sevelamer is not absorbed but has poor selectivity of simple protonated amines on the Sevelamer.

To address these short-comings, I proposed to develop a class of advanced sorbent material, the self-assembled monolayers on mesoporous supports (SAMMS) into oral drugs to capture heavy metals and phosphate in the GI tract. The outcomes of my research are summarized as below.

In **Chapter 2**, I showed that SH-SAMMS has extremely high binding capacity to both inorganic Hg and MeHg. When challenged with thiol-containing molecules such as

GSH and CysH that mimic the conditions in the GI tract, SH-SAMMS did not release Hg-bound on its surface. One of the major sources of Hg exposure in humans is from fish consumption. I simulated the gastrointestinal digestion of fish and discovered that SH-SAMMS effectively captured Hg from the fish digestate. The small pores of SH-SAMMS prevented bacterial access to the bound Hg inside the pores, avoiding the biotransformation of bound Hg into more mobile form. I demonstrated that SH-SAMMS has low toxicity to intestinal endothelial model (Caco-2) in comparison to DMSA and DMPS on the same mass basis. The Hg bound SH-SAMMS had lower toxicity to the Caco-2 cells than the free Hg counterpart likely because the cells were not exposed to the toxic metals residing inside the pores of the SAMMS. In a rodent model exposed to acute level of MeHg, SH-SAMMS reduced the absorption of dietary MeHg into the circulation, resulting to lower blood Hg levels. SH-SAMMS was also found to accelerate the clearance of already absorbed Hg. SH-SAMMS did not capture and remove essential minerals as indicated by unchanged blood levels of the minerals. Lastly, SH-SAMMS limited the absorption of inorganic Cd and Pb, as indicated by lower level of Cd in many organs especially liver, and lower blood and bone Pb compared to the rats receiving no SH-SAMMS.

In **Chapter 3**, I optimized and evaluated Fe-EDA-SAMMS as potential oral phosphate binders. Fe-EDA-SAMMS was synthesized, first by grafting diamine ligand (EDA) onto the mesoporous silica framework. Then ferric ion was incorporated onto the EDA-SAMMS to create Fe-EDA functional group. I optimized the Fe incorporation step by varying solvents, temperature and time. I found the optimum condition when switching the solvent from water to aprotic solvent of acetonitrile coupled with increasing

reaction temperature (65 °C) and time (20 h). MCM-41 silica substrate was found to be the best for Fe-EDA-incorporation compared to other substrates investigated (i.e. polystyrene resin, porous silica, and non-porous silica). The optimum Fe-EDA-SAMMS has 4-fold increase in phosphate binding capacity over the previously reported version. Fe-EDA-SAMMS had ~6 times faster binding kinetics than a current gold standard phosphate binder (Sevelamer HCl) and a commercial anion exchanger (AG® 1-X8). When tested in simulated intestinal fluid which contained high chloride and carbonate ions, the binding of phosphate by Fe-EDA-SAMMS was less affected than that by Sevelamer HCl and AG® 1-X8. The Fe-EDA had high specificity to phosphate over coexisting anions. Fe-EDA-SAMMS had a wide working pH range of 3 – 11, suggesting it should work well along the GI tract. Fe-EDA-SAMMS was found to have lower toxicity to intestinal epithelial cell model than lanthanum carbonate (Fosrenol®), another approved oral phosphate binder, which is soluble.

4.2 Future directions

By virtue of their high surface area and high selectivity of the ligands and ligand abducts, I have shown both in vitro and in vivo the excellent performance and favorable safety profile of two flavors of SAMMS, SH-SAMMS and Fe-EDA-SAMMS, warranting further future investigations.

4.2.1 *SH-SAMMS as oral treatment for chronic heavy metal exposure*

I demonstrated the capability of SH-SAMMS in treatment of acute heavy metal poisoning in **Chapter 2**. Acute poisoning was indicated by significant weight loss. Since

the ultimate goal is to develop SH-SAMMS into an oral drug for reducing the body burden of chronic Hg exposure, future work calls for further evaluation of efficacy and dose optimization of SH-SAMMS in a chronic heavy metal exposure animal model, which often takes a year to develop [121]. I did a preliminary study on subacute Hg exposure in rat model, which is intermediate between acute and chronic conditions. The amount of dietary MeHg dosing was reduced to 0.0003%, three times higher than permissible level in fish and seafood [122]. The SH-SAMMS treatment (0.5%, half of what used in acute exposure study) was delayed until the rats were on MeHg diet for one week. Blood Hg level decreased as soon as SH-SAMMS was administered and was reduced significantly within one week (**Figure 4.1A**). There was no significant GI absorption of SH-SAMMS, as indicated by normal blood level of Si (from silica substrate of SAMMS) (**Figure 4.1B**). Normal weight growth (**Figure 4.1C**) indicates that MeHg exposure was not acutely toxic.

Although the preliminary study showed promising result in preventing Hg absorption at low level, it was conducted at 2 week duration with still fairly high MeHg dosing. Although the level is only 3-fold higher than acceptable MeHg level in fish, giving it as MeHgCl, MeHg absorbed more than as fish MeHg [123]. Longer term and lower dose of MeHg are needed to establish the efficacy of SH-SAMMS in chronic Hg exposure management.

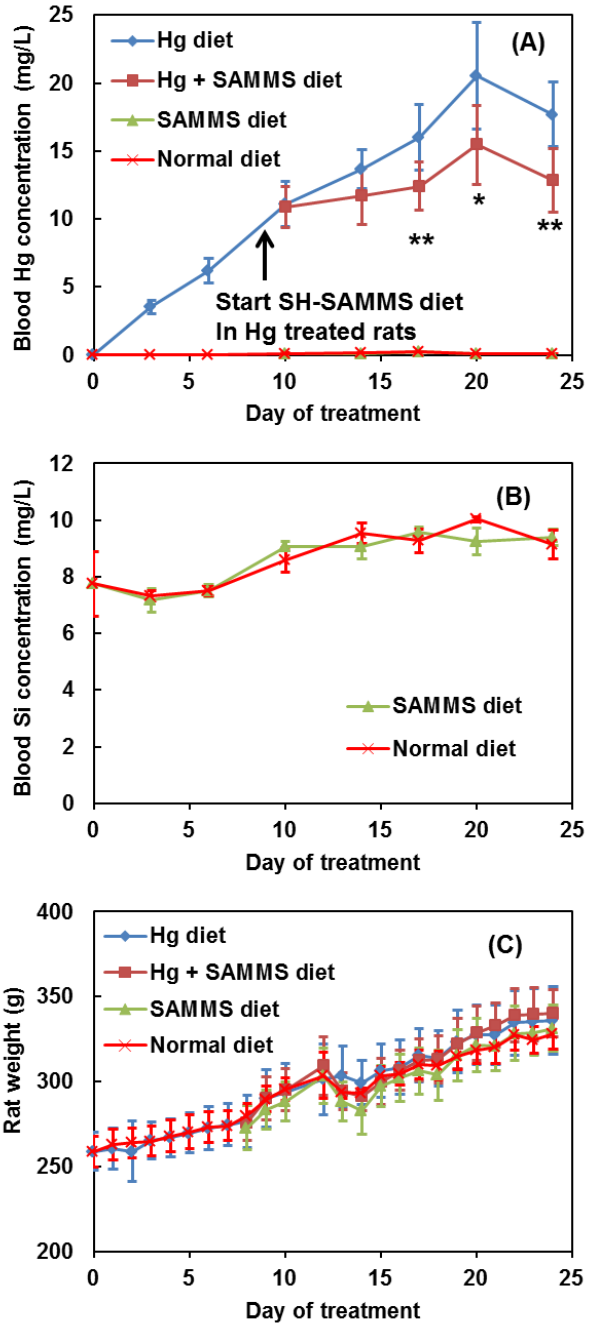

Figure 4.1 Oral SH-SAMMS treatment of chronic MeHg exposure from rats (n = 5) as monitored by (**A**) blood Hg level, (* $p < 0.02$, ** $p < 0.01$) (**B**) blood Si level, and (**C**) rat body weight. Rats were fed with powder diet containing 0.0003% Hg from MeHgCl. SH-SAMMS treatment started on day 8 (arrow in **Figure 4.1A**). All blood was collected from saphenous vein, except last data point, from cardiac puncture.

4.2.2 *Fe-EDA-SAMMS as oral phosphate binder in animal model*

In **Chapter 3**, I primarily focused on optimization of Fe-EDA-SAMMS synthesis and its evaluation in vitro. Results suggest that the material is promising for phosphate capture in the GI tract. However, the efficacy needs to be validated in vivo. I performed a pilot study in a rat model with normal kidney. The 6-week old male Wistar rats (5 rats per group) were fed with a customized rat chow with 0.4 wt% phosphorus (P) content. Note that normal diet has 0.1 wt% P content. The high P diet was mixed with 3 wt% of Fe-EDA-SAMMS, Sevelamer HCl, or calcium acetate. All three phosphate binders enhanced fecal excretion and decreased urinary excretion of P, indicating that the three materials limited dietary P absorption in the GI tract. Fe-EDA-SAMMS did not outperform the other two phosphate binders. The major drawback of this pilot study was the use of very high P diet in order to 'force' high phosphate in blood mimicking hyperphosphatemia conditions. High P was in favor of binding by both Sevelamer and calcium acetate. Sevelamer can bind to higher amount of phosphate due to higher capacity. Calcium acetate precipitates high P as calcium phosphate. Hence, both showed higher excretion of phosphorus in feces than Fe-EDA-SAMMS in the preliminary study. The Fe-EDA-SAMMS is shown in **Chapter 3** to have greater selectivity and faster kinetics than Sevelamer but not greater binding capacity. Nevertheless, Fe-EDA-SAMMS's capacity should be plenty at normal level of P. Therefore, future efficacy evaluation should be conducted in a rodent model with chronic kidney disease.

4.2.3 *Fe-EDA-SAMMS as an adsorbent to chromate and arsenate in water treatment*

Although not a main focus of this dissertation, I have found Fe-EDA-SAMMS to be very efficacious at capturing arsenate and chromate, two of the most hazardous oxometallate anions found in environmental water bodies [124]. Arsenate, As(V), is found in water with oxidizing conditions. In the reducing conditions of GI tract, it is converted to a more toxic form, As(III). Chromate, Cr(VI), has been used largely for plating of automobiles, equipment, and devices to prevent corrosion of underlying structural metals. The Fe-EDA-SAMMS offers a high capacity of 286 mg/g (1.89 mmol/g) for arsenate (pH 4.0) and 139 mg/g (1.12 mmol/g) for chromate (pH 7.5) in DI water (**Figures 4.2A-B**). The higher binding capacity for arsenate than chromate is likely due to differing speciation of the two anions at differing pH. At pH 4.0, arsenate exists primarily as monovalent $H_2AsO_4^-$ [125], while at pH 7.5, chromate has divalent CrO_4^{2-} as a predominant species [126]. Thus based on stoichiometry, Fe-EDA-SAMMS binds greater (per mole basis) with monovalent arsenate anion than divalent chromate anion, similar to phosphate binding as previously discussed in section 3.3.6.

SAMMS in large micron sizes can be packed into a cartridge format for drinking water treatment. Many surface water and ground water sources are contaminated with arsenate and chromate, especially in the developing countries, making water unsafe for consumption. Thus Fe-EDA-SAMMS may find its place in portable water treatment systems. The ability to regenerate and reuse sorbent materials is also highly desirable for cost-effectiveness. I did a flow experiment on phosphate adsorption and regeneration of Fe-EDA-SAMMS in a packed bed column. Phosphate solution was flow through at the rate of 2 mL/min to allow phosphate capture. Regeneration was performed with 0.2 M

HCl wash to strip the bound phosphate. The cycle was then repeated many times. I found that the % phosphate removal efficacy of Fe-EDA-SAMMS (**Figure 4.3**) was maintained after at least 10 cycles of adsorption and regeneration, indicating that most of the binding sites were preserved after the acid elution. Thus data to date suggests high feasibility of Fe-EDA-SAMMS for drinking water treatment that may be contaminated with phosphate, chromate, and arsenate, in addition to its potential use as oral phosphate binder.

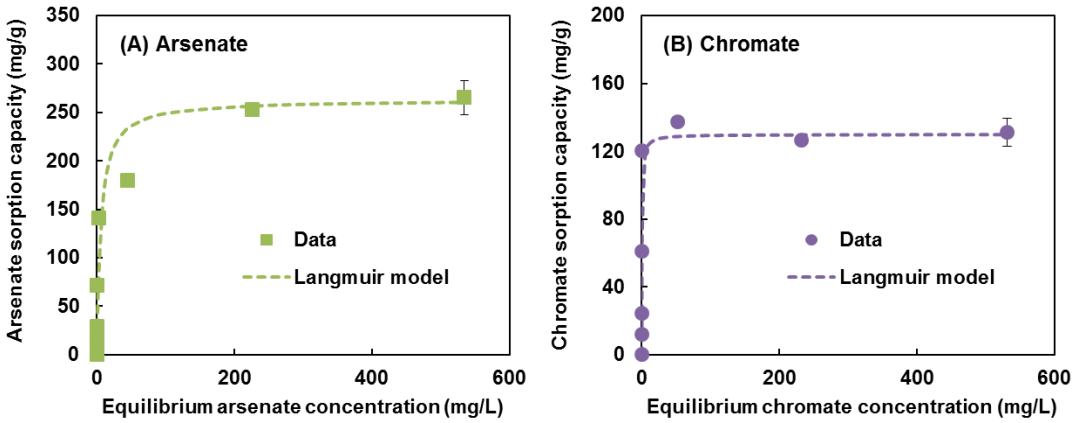

Figure 4.2 Adsorption isotherms of (**A**) arsenate (pH 4.0) and (**B**) chromate (pH 7.5) on Fe-EDA-SAMMS in DI water, L/S of 2,000 mL/g. Symbols represent data and dash-line represents Langmuir isotherm fitting. Fe-EDA-SAMMS has a capacity of 286 mg/g for arsenate and 139 mg/g for chromate. Error bars represent S.D. from triplicates.

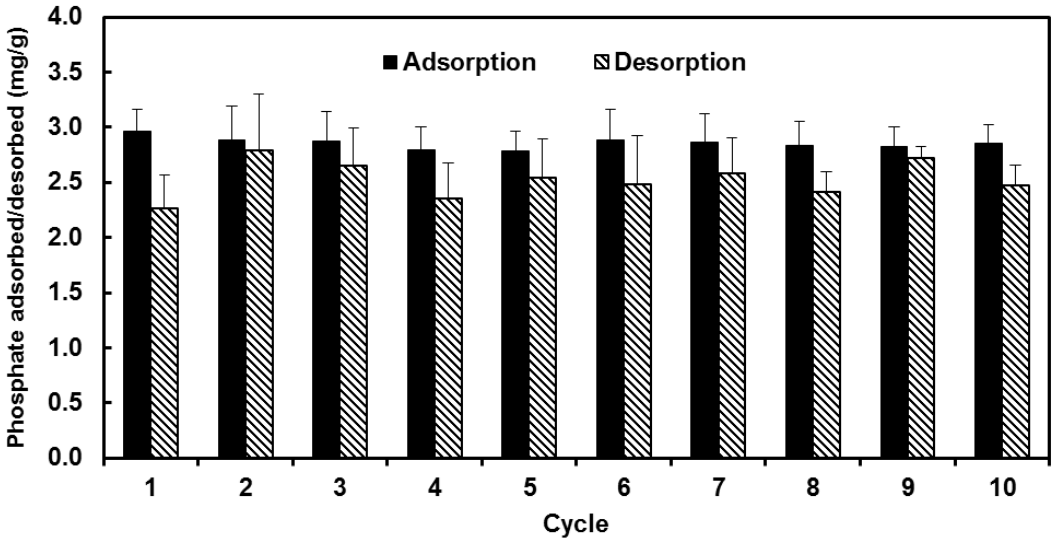

Figure 4.3 Adsorption and desorption of phosphate on Fe-EDA-SAMMS. During the adsorption process, 10 mL of 3 mg phosphate/L (from KH_2PO_4) pH 5.3 was pushed through a 0.01 g of Fe-EDA-SAMMS at a flow rate of 2 mL/min, followed by 10 mL of 0.2 M HCl at 2 mL/min for stripping off bound phosphate (desorption step). Error bars represent S.D. from triplicates.

REFERENCES

1. *Mercury and Health*. 2013; http://www.who.int/mediacentre/factsheets/fs361/en/.
2. Clarkson TW, Friberg L, Nordberg GF, Sager PR (2012) Biological Monitoring of Toxic Metals. Springer US.
3. Clarkson TW, Vyas JB, Ballatori N (2007) Mechanisms of mercury disposition in the body. Am J Ind Med 50: 757-764.
4. Barkay T, Wagner-Dobler I (2005) Microbial Transformations of Mercury: Potentials, Challenges, and Achievements in Controlling Mercury Toxicity in the Environment. Adv Appl Microbiol 57: 1-52.
5. Dutczak WJ, Ballatori N (1992) gamma-Glutamyltransferase-dependent biliary-hepatic recycling of methyl mercury in the guinea pig. J Pharmacol Exp Ther 262: 619-623.
6. Ballatori N, Clarkson TW (1985) Biliary secretion of glutathione and of glutathione-metal complexes. Fundam Appl Toxicol 5: 816-831.
7. Wang JP, Qi L, Moore MR, Ng JC (2002) A review of animal models for the study of arsenic carcinogenesis. Toxicol Lett 133: 17-31.
8. Schipper ML, Nakayama-Ratchford N, Davis CR, Kam NW, Chu P, et al. (2008) A pilot toxicology study of single-walled carbon nanotubes in a small sample of mice. Nat Nanotechnol 3: 216-221.
9. *Cadmium Compounds*. 2000; http://www.epa.gov/ttnatw01/hlthef/cadmium.html.
10. Tucker PG. *Cadmium Toxicity: What Is the Biological Fate of Cadmium in the Body?* ATSDR Case Studies in Environmental Medicine 2008; http://http://www.atsdr.cdc.gov/csem/cadmium/docs/cadmium.pdf.

11. *Lead*. 2015; http://www.cdc.gov/nceh/lead/.

12. McCabe EB (1979) Age and sensitivity to lead toxicity: a review. Environ Health Perspect 29: 29-33.

13. Bellinger DC (2008) Very low lead exposures and children's neurodevelopment. Curr Opin Pediatr 20: 172-177.

14. Cornelis R, *Handbook of Elemental Speciation, Handbook of Elemental Speciation II: Species in the Environment, Food, Medicine and Occupational Health*. 2005: Wiley.

15. Mushak P (1991) Gastro-Intestinal Absorption of Lead in Children and Adults: Overview of Biological and Biophysico-Chemical Aspects. Chem Spec Bioavailab 3: 87-104.

16. Tarragó O. *Lead Toxicity: What is the Biological Fate of Lead?* ATSDR Case Studies in Environmental Medicine 2010; http://www.atsdr.cdc.gov/csem/lead/docs/lead.pdf.

17. Sears ME (2013) Chelation: harnessing and enhancing heavy metal detoxification--a review. ScientificWorldJournal 2013: 219840.

18. Hoover TD, Aposhian HV (1983) BAL increases the arsenic-74 content of rabbit brain. Toxicol Appl Pharmacol 70: 160-162.

19. Berlin M, Ullrebg S (1963) Increased uptake of mercury in mouse brain caused by 2,3-dimercaptopropanol. Nature 197: 84-85.

20. Aposhian HV (1983) DMSA and DMPS--water soluble antidotes for heavy metal poisoning. Annu Rev Pharmacol Toxicol 23: 193-215.

21. Bradberry S, Vale A (2009) A comparison of sodium calcium edetate (edetate calcium disodium) and succimer (DMSA) in the treatment of inorganic lead poisoning. Clin Toxicol (Phila) 47: 841-858.

22. Bradberry S, Vale A (2009) Dimercaptosuccinic acid (succimer; DMSA) in inorganic lead poisoning. Clin Toxicol (Phila) 47: 617-631.

23. Hurlbut KM, Maiorino RM, Mayersohn M, Dart RC, Bruce DC, et al. (1994) Determination and metabolism of dithiol chelating agents. XVI: Pharmacokinetics of 2,3-dimercapto-1-propanesulfonate after intravenous administration to human volunteers. J Pharmacol Exp Ther 268: 662-668.

24. Torres-Alanis O, Garza-Ocanas L, Bernal MA, Pineyro-Lopez A (2000) Urinary excretion of trace elements in humans after sodium 2,3-dimercaptopropane-1-sulfonate challenge test. J Toxicol Clin Toxicol 38: 697-700.

25. Andersen O, Nielsen JB (1988) Oral cadmium chloride intoxication in mice: effects of penicillamine, dimercaptosuccinic acid and related compounds. Pharmacol Toxicol 63: 386-389.

26. Andersen O (2004) Chemical and biological considerations in the treatment of metal intoxications by chelating agents. Mini Rev Med Chem 4: 11-21.

27. Aposhian HV, Maiorino RM, Rivera M, Bruce DC, Dart RC, et al. (1992) Human studies with the chelating agents, DMPS and DMSA. J Toxicol Clin Toxicol 30: 505-528.

28. Maiorino RM, Dart RC, Carter DE, Aposhian HV (1991) Determination and metabolism of dithiol chelating agents. XII. Metabolism and pharmacokinetics of

sodium 2,3-dimercaptopropane-1-sulfonate in humans. J Pharmacol Exp Ther 259: 808-814.

29. Muran PJ (2006) Mercury elimination with oral DMPS, DMSA, vitamin C, and glutathione: an observational clinical review. Altern Ther Health Med 12: 70-75.

30. Lowry JA, *Oral Chelation Therapy for Patients with Lead Poisoning* 2010, World Health Organization (WHO).

31. Mercola J, Klinghardt D (2001) Mercury Toxicity and Systemic Elimination Agents. J Nutr Environ Med 11: 53-62.

32. Graziano JH, Lolacono NJ, Moulton T, Mitchell ME, Slavkovich V, et al. (1992) Controlled study of meso-2,3-dimercaptosuccinic acid for the management of childhood lead intoxication. J Pediatr 120: 133-139.

33. Opitz H, Schweinsberg F, Grossmann T, Wendt-Gallitelli MF, Meyermann R (1996) Demonstration of mercury in the human brain and other organs 17 years after metallic mercury exposure. Clin Neuropathol 15: 139-144.

34. Takeuchi T, Eto K, Tokunaga H (1989) Mercury level and histochemical distribution in a human brain with Minamata disease following a long-term clinical course of twenty-six years. Neurotoxicology 10: 651-657.

35. Buchet JP, Lauwerys RR (1989) Influence of 2,3-dimercaptopropane-1-sulfonate and dimercaptosuccinic acid on the mobilization of mercury from tissues of rats pretreated with mercuric chloride, phenylmercury acetate or mercury vapors. Toxicology 54: 323-333.

36. Cao Y, Chen A, Jones RL, Radcliffe J, Dietrich KN, et al. (2011) Efficacy of succimer chelation of mercury at background exposures in toddlers: a randomized trial. J Pediatr 158: 480-485 e481.

37. Hutchison AJ (2009) Oral phosphate binders. Kidney Int 75: 906-914.

38. Slatopolsky E (2003) New developments in hyperphosphatemia management. J Am Soc Nephrol 14: S297-299.

39. Block GA, Port FK (2000) Re-evaluation of risks associated with hyperphosphatemia and hyperparathyroidism in dialysis patients: recommendations for a change in management. Am J Kidney Dis 35: 1226-1237.

40. Malluche HH, Monier-Faugere MC (2000) Hyperphosphatemia: pharmacologic intervention yesterday, today and tomorrow. Clin Nephrol 54: 309-317.

41. Grassmann A, Gioberge S, Moeller S, Brown G (2005) ESRD Patients in 2004: Global Overview of Patient Numbers, Treatment Modalities and Associated Trends. Nephrol Dial Transplant 20: 2587-2593.

42. Kopple JD, Coburn JW (1973) Metabolic studies of low protein diets in uremia. I. Nitrogen and potassium. Medicine (Baltimore) 52: 583-595.

43. Mohammed I, Hutchison AJ (2009) Oral phosphate binders for the management of serum phosphate levels in dialysis patients. J Ren Care 35 Suppl 1: 65-70.

44. Delmez JA, Slatopolsky E, Martin KJ, Gearing BN, Harter HR (1982) Minerals, vitamin D, and parathyroid hormone in continuous ambulatory peritoneal dialysis. Kidney Int 21: 862-867.

45. Lowrie EG, Lew NL (1990) Death risk in hemodialysis patients: the predictive value of commonly measured variables and an evaluation of death rate differences between facilities. Am J Kidney Dis 15: 458-482.

46. Goldsmith D, Covic A (2014) Oral phosphate binders in CKD - is calcium the (only) answer? Clin Nephrol 81: 389-395.

47. Hutchison AJ, Whitehouse RW, Freemont AJ, Adams JE, Mawer EB, et al. (1994) Histological, Radiological, and Biochemical Features of the Adynamic Bone Lesion in Continuous Ambulatory Peritoneal Dialysis Patients. Am J Nephrol 14: 19-29.

48. Goodman WG, London G, Amann K, Block GA, Giachelli C, et al. (2004) Vascular Calcification in Chronic Kidney Disease. Am J Kidney Dis 43: 572-579.

49. Pai AB, Shepler BM (2009) Comparison of sevelamer hydrochloride and sevelamer carbonate: risk of metabolic acidosis and clinical implications. Pharmacotherapy 29: 554-561.

50. Hutchison AJ, Maes B, Vanwalleghem J, Asmus G, Mohamed E, et al. (2005) Efficacy, tolerability, and safety of lanthanum carbonate in hyperphosphatemia: a 6-month, randomized, comparative trial versus calcium carbonate. Nephron Clin Pract 100: c8-19.

51. de Freitas D, Donne RL, Hutchison AJ (2007) Lanthanum carbonate--a first line phosphate binder? Semin Dial 20: 325-328.

52. Shah HH, Hazzan AD, Fishbane S (2015) Novel iron-based phosphate binders in patients with chronic kidney disease. Curr Opin Nephrol Hypertens 24: 330-335.

53. Cernaro V, Santoro D, Lacquaniti A, Costantino G, Visconti L, et al. (2016) Phosphate binders for the treatment of chronic kidney disease: role of iron oxyhydroxide. Int J Nephrol Renovasc Dis 9: 11-19.

54. Floege J, Covic AC, Ketteler M, Rastogi A, Chong EM, et al. (2014) A phase III study of the efficacy and safety of a novel iron-based phosphate binder in dialysis patients. Kidney Int 86: 638-647.

55. Negri AL, Urena Torres PA (2015) Iron-based phosphate binders: do they offer advantages over currently available phosphate binders? Clin Kidney J 8: 161-167.

56. Rodby RA, Umanath K, Niecestro R, Bond TC, Sika M, et al. (2015) Ferric Citrate, an Iron-Based Phosphate Binder, Reduces Health Care Costs in Patients on Dialysis Based on Randomized Clinical Trial Data. Drugs R D 15: 271-279.

57. Yokoyama K, Akiba T, Fukagawa M, Nakayama M, Sawada K, et al. (2014) A randomized trial of JTT-751 versus sevelamer hydrochloride in patients on hemodialysis. Nephrol Dial Transplant 29: 1053-1060.

58. Pennoyer A, Bridgeman MB (2015) Ferric citrate (auryxia) for the treatment of hyperphosphatemia. P T 40: 329-339.

59. Kresge CT, Leonowicz ME, Roth WJ, Vartuli JC, Beck JS (1992) Ordered mesoporous molecular sieves synthesized by a liquid-crystal template mechanism. Nature 359: 710-712.

60. Wang Y, Zhao Q, Han N, Bai L, Li J, et al. (2015) Mesoporous silica nanoparticles in drug delivery and biomedical applications. Nanomedicine 11: 313-327.

61. Yantasee W, Rutledge RD, Chouyyok W, Sukwarotwat V, Orr G, et al. (2010) Functionalized nanoporous silica for the removal of heavy metals from biological systems: Adsorption and application. ACS Appl Mater Interfaces 2: 2749-2758.

62. Fryxell GE, Mattigod SV, Lin Y, Wu H, Fiskum S, et al. (2007) Design and synthesis of self-assembled monolayers on mesoporous supports (SAMMS): The importance of ligand posture in functional nanomaterials. J Mater Chem 17: 2863-2874.

63. Feng X, Fryxell GE, Wang LQ, Kim AY, Liu J, et al. (1997) Functionalized monolayers on ordered mesoporous supports. Science 276: 923-926.

64. Zemanian TS, Fryxell GE, Liu J, Mattigod S, Franz JA, et al. (2001) Deposition of self-assembled monolayers in mesoporous silica from supercritical fluids. Langmuir 17: 8172-8177.

65. Fryxell GE, Liu J, Hauser TA, Nie Z, Ferris KF, et al. (1999) Design and synthesis of selective mesoporous anion traps. Chem Mater 11: 2148-2154.

66. Chouyyok W, Wiacek RJ, Pattamakomsan K, Sangvanich T, Grudzien RM, et al. (2010) Phosphate removal by anion binding on functionalized nanoporous sorbents. Environ Sci Technol 44: 3073-3078.

67. Lin Y, Fiskum SK, Yantasee W, Wu H, Mattigod SV, et al. (2005) Incorporation of hydroxypyridinone ligands into self-assembled monolayers on mesoporous supports for selective actinide sequestration. Environ Sci Technol 39: 1332-1337.

68. Yantasee W, Fryxell GE, Lin Y, Wu H, Raymond KN, et al. (2005) Hydroxypyridinone functionalized self-assembled monolayers on nanoporous silica for sequestering lanthanide cations. J Nanosci Nanotechnol 5: 527-529.

69. Yantasee W, Fryxell GE, Addleman RS, Wiacek RJ, Koonsiripaiboon V, et al. (2009) Selective removal of lanthanides from natural waters, acidic streams and dialysate. J Hazard Mater 168: 1233-1238.

70. Yantasee W, Fryxell GE, Porter GA, Pattamakomsan K, Sukwarotwat V, et al. (2010) Novel sorbents for removal of gadolinium-based contrast agents in sorbent dialysis and hemoperfusion: preventive approaches to nephrogenic systemic fibrosis. Nanomed Nanotech Biol Med 6: e1-e8.

71. Sangvanich T, Sukwarotwat V, Wiacek RJ, Grudzien RM, Fryxell GE, et al. (2010) Selective capture of cesium and thallium from natural waters and simulated wastes with copper ferrocyanide functionalized mesoporous silica. J Hazard Mater 182: 225-231.

72. Busche B, Wiacek R, Davidson J, Koonsiripaiboon V, Yantasee W, et al. (2009) Synthesis of nanoporous iminodiacetic acid sorbents for binding transition metals. Inorg Chem Commun 12: 312-315.

73. Chouyyok W, Shin Y, Davidson J, Samuels WD, Lafemina NH, et al. (2010) Selective removal of copper(II) from natural waters by nanoporous sorbents functionalized with chelating diamines. Environ Sci Technol 44: 6390-6395.

74. Timchalk C, Creim JA, Sukwarotwat V, Wiacek R, Addleman RS, et al. (2010) In vitro and in vivo evaluation of a novel ferrocyanide functionalized nanopourous silica decorporation agent for cesium in rats. Health Phys 99: 420-429.

75. Ravikovitch PI, Wei D, Chueh WT, Haller GL, Neimark AV (1997) Evaluation of Pore Structure Parameters of MCM-41 Catalyst Supports and Catalysts by Means of Nitrogen and Argon Adsorption. J Phys Chem A 101: 3671-3679.

76. Climent MJ, Corma A, Iborra S, Navarro MC, Primo J (1996) Use of Mesoporous MCM-41 Aluminosilicates as Catalysts in the Production of Fine Chemicals: Preparation of Dimethylacetals. J Catal 161: 783-789.

77. Ngamcherdtrakul W, Morry J, Gu S, Castro DJ, Goodyear SM, et al. (2015) Cationic Polymer Modified Mesoporous Silica Nanoparticles for Targeted siRNA Delivery to HER2+ Breast Cancer. Adv Funct Mater 25: 2646-2659.

78. Morry J, Ngamcherdtrakul W, Gu S, Goodyear SM, Castro DJ, et al. (2015) Dermal delivery of HSP47 siRNA with NOX4-modulating mesoporous silica-based nanoparticles for treating fibrosis. Biomaterials 66: 41-52.

79. Laks DR (2009) Assessment of chronic mercury exposure within the U.S. population, National Health and Nutrition Examination Survey, 1999-2006. Biometals 22: 1103-1114.

80. Schaefer JK, Letowski J, Barkay T (2002) mer -Mediated Resistance and Volatilization of Hg(II) Under Anaerobic Conditions. Geomicrobiol J 19: 87-102.

81. Harris HH, Pickering IJ, George GN (2003) The chemical form of mercury in fish. Science 301: 1203.

82. Yantasee W, Warner CL, Sangvanich T, Addleman RS, Carter TG, et al. (2007) Removal of Heavy Metals from Aqueous Systems with Thiol Functionalized Superparamagnetic Nanoparticles. Environ Sci Technol 41: 5114-5119.

83. Hsi H, Rood M, Rostam-Abadi M, Chen S, Chang R (2002) Mercury Adsorption Properties of Sulfur-Impregnated Adsorbents. J Environ Eng 128: 1080-1089.

84. Chen X, Feng X, Liu J, Fryxell GE, Gong M (1999) Mercury Separation and Immobilization Using Self-assembled Monolayers on Mesoporous Supports (SAMMS). Sep Sci Technol 34 1121-1132.

85. Summers AO, Lewis E (1973) Volatilization of mercuric chloride by mercury-resistant plasmid-bearing strains of Escherichia coli, Staphylococcus aureus, and Pseudomonas aeruginosa. J Bacteriol 113: 1070-1072.

86. Summers AO, Silver S (1972) Mercury resistance in a plasmid-bearing strain of Escherichia coli. J Bacteriol 112: 1228-1236.

87. Weiss B, Stern S, Cernichiari E, Gelein R (2005) Methylmercury Contamination of Laboratory Animal Diets. Environ Health Perspect 113: 1120-1122.

88. Cherian MG, Miles EF, Clarkson TW, Cox C (1988) Estimation of mercury burdens in rats by chelation with dimercaptopropane sulfonate. J Pharmacol Exp Ther 245: 479-484.

89. Blanusa M, Prester L, Radic S, Kargacin B (1994) Inorganic mercury exposure, mercury-copper interaction, and DMPS treatment in rats. Environ Health Perspect 102 Suppl 3: 305-307.

90. Kemner KM, Feng X, Liu J, Fryxell GE, Wang LQ, et al. (1999) Investigation of the Local Chemical Interactions Between Hg and Self-assembled Monolayers on Mesoporous Supports. J Synchrotron Radiat 6: 633-635.

91. Sangvanich T, Morry J, Fox C, Ngamcherdtrakul W, Goodyear S, et al. (2014) Novel Oral Detoxification of Mercury, Cadmium, and Lead with Thiol-modified Nanoporous Silica. ACS Appl Mater Interfaces 6: 5483-5493.

92. Nalini S, Balasubramanian KA (1994) Studies on Acid Soluble Thiols in the Human Gastric Juice. Biochem Mol Biol Int 32: 449-454.

93. Busby RW, Kessler MM, Bartolini WP, Bryant AP, Hannig G, et al. (2013) Pharmacologic Properties, Metabolism, and Disposition of Linaclotide, a Novel Therapeutic Peptide Approved for the Treatment of Irritable Bowel Syndrome with Constipation and Chronic Idiopathic Constipation. J Pharmacol Exp Ther 344: 196-206.

94. Cabanero AI, Madrid Y, Camara C (2007) Mercury-selenium species ratio in representative fish samples and their bioaccessibility by an in vitro digestion method. Biol Trace Elem Res 119: 195-211.

95. Torres-Escribano S, Velez D, Montoro R (2010) Mercury and methylmercury bioaccessibility in swordfish. Food Addit Contam Part A Chem Anal Control Expo Risk Assess 27: 327-337.

96. Barkay T, Miller SM, Summers AO (2003) Bacterial Mercury Resistance from Atoms to Ecosystems. FEMS Microbiol Rev 27: 355-384.

97. Summers AO, Wireman J, Vimy MJ, Lorscheider FL, Marshall B, et al. (1993) Mercury released from dental "silver" fillings provokes an increase in mercury- and antibiotic-resistant bacteria in oral and intestinal floras of primates. Antimicrob Agents Chemother 37: 825-834.

98. Clarkson TW (2002) The three modern faces of mercury. Environ Health Perspect 110 Suppl 1: 11-23.

99. Magos L, Halbach S, Clarkson TW (1978) Role of Catalase in the Oxidation of Mercury Vapor. Biochem Pharmacol 27: 1373-1377.

100. Freitas RA (2005) Microbivores: Artificial Mechanical Phagocytes using Digest and Discharge Protocol. J Evol Technol 14: 55-106.

101. Womble DD, Rownd RH (1988) Genetic and Physical Map of Plasmid NR1: Comparison with other IncFII Antibiotic Resistance Plasmids. Microbiol Rev 52: 433-451.

102. Wireman J, Liebert CA, Smith T, Summers AO (1997) Association of Mercury Resistance with Antibiotic Resistance in the Gram-negative Fecal Bacteria of Primates. Appl Environ Microbiol 63: 4494-4503.

103. Liebert CA, Wireman J, Smith T, Summers AO (1997) Phylogeny of Mercury Resistance (mer) Operons of Gram-negative Bacteria Isolated from the Fecal Flora of Primates. Appl Environ Microbiol 63: 1066-1076.

104. Liebert CA, Wireman J, Smith T, Summers AO (1997) The impact of mercury released from dental "silver" fillings on antibiotic resistances in the primate oral and intestinal bacterial flora. Met Ions Biol Syst 34: 441-460.

105. Hutchison AJ, Smith CP, Brenchley PEC (2011) Pharmacology, Efficacy and Safety of Oral Phosphate Binders. Nat Rev Nephrol 7: 578-589.

106. Tonelli M, Pannu N, Manns B (2010) Oral Phosphate Binders in Patients with Kidney Failure. N Engl J Med 362: 1312-1324.

107. Yang WC, Yang CS, Hou CC, Wu TH, Young EW, et al. (2002) An Open-label, Crossover Study of a New Phosphate-binding Agent in Haemodialysis Patients: Ferric Citrate. Nephrol Dial Transplant 17: 265-270.

108. United States Pharmacopeial Convention Inc (2003) USPXXVI. (26thedn), Rockville, MD, USA.

109. United States Pharmacopeial Convention Inc (1990) USPXXII. (22ndedn), Rockville, MD, USA.

110. Rosenbaum DP, Holmes-Farley SR, Mandeville WH, Pitruzzello M, Goldberg DI (1997) Effect of RenaGel, a Non-absorbable, Cross-linked, Polymeric Phosphate Binder, on Urinary Phosphorus Excretion in Rats. Nephrol Dial Transplant 12: 961-964.

111. Hamoudi S, Saad R, Belkacemi K (2007) Adsorptive Removal of Phosphate and Nitrate Anions from Aqueous Solutions Using Ammonium-Functionalized Mesoporous Silica. Ind Eng Chem Res 46: 8806-8812.

112. Huang WY, Li D, Yang J, Liu ZQ, Zhu Y, et al. (2013) One-pot Synthesis of Fe(III)-coordinated Diamino-functionalized Mesoporous Silica: Effect of Functionalization Degrees on Structures and Phosphate Adsorption. Microporous Mesoporous Mater 170: 200-210.

113. Zhang J, Shen Z, Shan W, Mei Z, Wang W (2011) Adsorption Behavior of Phosphate on Lanthanum(III)-coordinated Diamino-functionalized 3D Hybrid Mesoporous Silicates Material. J Hazard Mater 186: 76-83.

114. Zhang J, Shen Z, Mei Z, Li S, Wang W (2011) Removal of Phosphate by Fe-coordinated Amino-functionalized 3D Mesoporous Silicates Hybrid Materials. J Environ Sci 23: 199-205.

115. Long F, Gong JL, Zeng GM, Chen L, Wang XY, et al. (2011) Removal of Phosphate from Aqueous Solution by Magnetic Fe-Zr Binary Oxide. Chem Eng J 171: 448-455.

116. Dai J, Yang H, Yan H, Shangguan Y, Zheng Q, et al. (2011) Phosphate Adsorption from Aqueous Solutions by Disused Adsorbents: Chitosan Hydrogel Beads after the Removal of Copper(II). Chem Eng J 166: 970-977.

117. McConnell EL, Fadda HM, Basit AW (2008) Gut Instincts: Explorations in Intestinal Physiology and Drug Delivery. Int J Pharm 364: 213-226.

118. Karageorgiou K, Paschalis M, Anastassakis GN (2007) Removal of Phosphate Species from Solution by Adsorption onto Calcite Used as Natural Adsorbent. J Hazard Mater 139: 447-452.

119. Yokoi T, Tatsumi T, Yoshitake H (2004) Fe3+ Cordinated to Amino-functionalized MCM-41: An Adsorbent for the Toxic Oxyanions with High Capacity, Resistibility to Inhibiting Anions, and Reusability after a Simple Treatment. J Colloid Interface Sci 274: 451-457.

120. Bhardwaj RK, Glaeser H, Becquemont L, Klotz U, Gupta SK, et al. (2002) Piperine, a major constituent of black pepper, inhibits human P-glycoprotein and CYP3A4. J Pharmacol Exp Ther 302: 645-650.

121. Agency for Toxic Substances and Disease Registry (1999) Toxicological Profile for Mercury. Atlanta, GA.

122. US Food and Frug Administration (2000) Guidance for Industry: Action Levels for Poisonous or Deleterious Substances in Human Food and Animal Feed. College Park, MD.

123. Berntssen MH, Hylland K, Lundebye AK, Julshamn K (2004) Higher faecal excretion and lower tissue accumulation of mercury in Wistar rats from

contaminated fish than from methylmercury chloride added to fish. Food Chem Toxicol 42: 1359-1366.

124. Yoshitake H, Yokoi T, Tatsumi T (2002) Adsorption of Chromate and Arsenate by Amino-Functionalized MCM-41 and SBA-1. Chem Mater 14: 4603-4610.

125. Smedley PL, Kinniburgh DG (2002) A review of the source, behaviour and distribution of arsenic in natural waters. Appl Geochem 17: 517-568.

126. Tandon RK, Crisp PT, Ellis J, Baker RS (1984) Effect of pH on chromium(VI) species in solution. Talanta 31: 227-228.

APPENDIX

Stabilization Studies of Lyophilized Antibody Conjugated Mesoporous Silica Nanoparticle with Cationic polymer for siRNA Delivery

Thanapon Sangvanich, Worapol Ngamcherdtrakul, Moataz Reda, Shenda Gu, Wassana Yantasee

Key words: Oligonucleotide delivery, nanoparticles, lyophilization, formulation, cancer, polymers, mesoporous silica, antibody

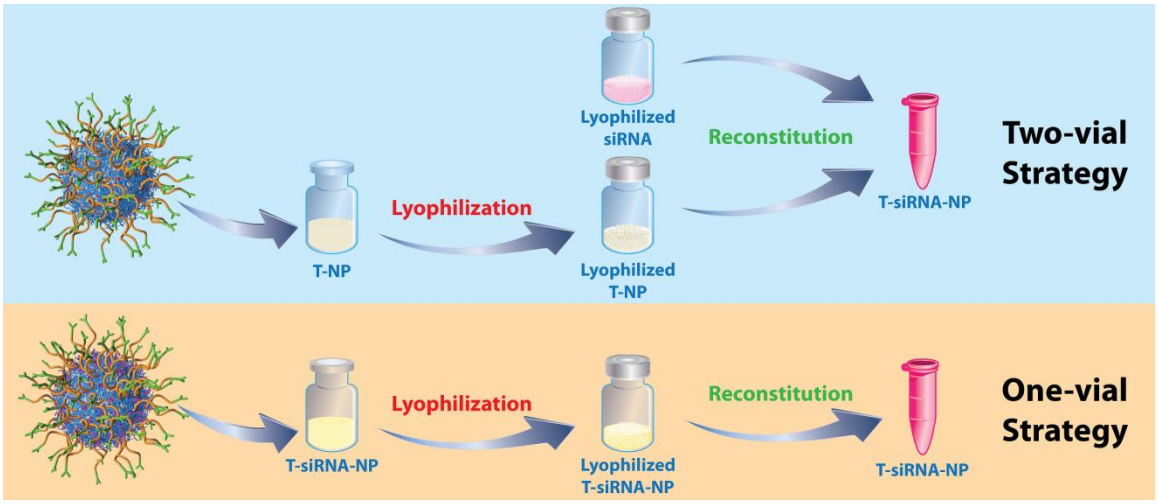

Abstract

Long-term stability of therapeutic candidates is necessary toward their clinical applications. For most nanoparticle systems formulated in aqueous solutions, lyophilization or freeze-drying is a common method to ensure long-term stability. Lyophilization of complex nanoparticle systems can be challenging with respect to preserving physicochemical properties as well as the biological activities of the materials. While lyophilization of lipid, polymeric, or inorganic nanoparticles have been studied, studies on hybrid polymeric-inorganic nanoparticles containing biomolecules are non-existent. We recently reported an effective siRNA carrier for treating drug-resistant HER2+ breast cancer and skin fibrosis in preclinical studies. The nanoparticle system consists of 50-nm mesoporous silica nanoparticles decorated with a co-polymer, antibody, and siRNA. Herein, we studied the stabilization of the material following lyophilization in which we varied buffers, lyoprotectant agents (LPA), reconstitution, time and temperature of freezing and drying steps. We then evaluated the lyophilized materials in terms of easy reconstitution, hydrodynamic size, charge, siRNA loading, gene silencing, cancer cell killing, and shelf-life under various temperatures. We also compared the stability between nanoparticles lyophilized with and without siRNA. The material was best formulated in Tris HCl buffer with 5 w/w% trehalose. The lyophilized material can be stored for at least 6 months at -20 °C.

Introduction

In the past decade, nanoparticles have been widely developed as carriers for delivery of antibodies, oligonucleotides, and drugs. Nanoparticles protect cargos against enzymatic degradation, prevent rapid clearance of small compounds by the kidneys, and prolong blood circulation half-life of the cargos. Typically, nanoparticles are formulated in solutions as colloidal systems, which cannot be stored long-term due to physical instability (aggregation) and chemical instability (hydrolysis of chemical compositions) [1]. In order to facilitate long term storage, all traces of water must be removed by a process of freeze-drying or lyophilization [2,3]. However, lyophilization of nanoparticles is more challenging than traditional chemical compounds since the process may affect both the physical (e.g., size) and chemical properties of the nanoparticles. This is especially true when the nanoparticles consist of many components. Therefore, optimization of the lyophilization process is clearly needed.

We have recently developed cationic polymer modified mesoporous silica nanoparticles (MSNPs) as a promising siRNA carrier for breast cancer treatment [4]. The MSNP of 50 nm in size was surface-modified with positively charged polyethylenimine (PEI) and polyethyleneglycol (PEG). PEI modification allows the nanoparticles to carry negatively charged small interfering RNA (siRNA) and promotes endosomal escape, while PEG modification provides a stealth effect to avoid recognition and elimination by the phagocytosis system [5,6]. The PEI was cross-linked to increase buffering capacity and enhance endosomal escape of siRNA by proton sponge effect principle [7]. The modified nanoparticles (PEG-PEI-NP) are then conjugated with antibodies for targeting the cancer cells of interest. Specifically, Trastuzumab (Herceptin, Genentech), a

humanized monoclonal HER2 antibody, was used as a homing agent for HER2 positive cancer. The material has shown to overcome drug resistance in two HER2 positive cancer mouse models [4,8]. Making the material stable over a long period is needed for its clinical evaluation.

Lyophilization of polymeric nanoparticles systems, such as poly(lactic-co-glycolic acid) (PLGA) [9,10], polycaprolactone (PCL) [11] or polyethylenimine (PEI) [12], and lipid nanoparticle systems [13-15], have been explored. Likewise, lyophilization of inorganic nanoparticle systems, such as silica [16] or gold [17] nanoparticles, have also been attempted. However, little has been reported on lyophilization conditions of hybrid nanoparticle systems which include both polymer and inorganic particles, let alone antibody. Amine-modified silica nanoparticles were successfully lyophilized in the present of trehalose as a lyoprotectant (LPA) [16], which was shown to produce cake-like powder that is easy-to-reconstitute. However, the long lyophilization time of over 6 days is not highly economical.

Our aim was to achieve a stable long-term storage of the antibody (trastuzumab) conjugated PEI-PEG-MSNP for siRNA delivery. Ideally, the material should be kept stable for at least 6 months without requiring an expensive -80 °C freezer. It must be easily reconstituted and preserve the properties and performance of the material for siRNA delivery. Trastuzumab has been lyophilized with trehalose to sustain protein structure and activity during long-term storage [18], but its lyophilization when combined with nanoparticles has not been reported. Lastly, we also compared the stability of the lyophilized materials from one vial strategy (siRNA was loaded on the nanoparticles

prior to lyophilization) and two vial strategy (nanoparticles and siRNA were lyophilized separately).

Experimental

Chemicals and Reagents

Tetraethyl orthosilicate (TEOS), cetyltrimethylammonium chloride (CTAC), sodium phosphate mono basic ($NaH_2PO_4 \cdot H_2O$), sodium phosphate dibasic (Na_2HPO_4), triethanolamine (TEA) and trehalose dehydrate were purchased from Sigma Aldrich (St. Louis, MO). Branched-PEI (10 kDa) was purchased from Alfa Aesar (Ward Hill, MA). Maleimide-PEG(5kDa)-NHS was purchased from JenKem Technology USA (Plano, TX). Trastuzumab (Herceptin®, Genentech) was obtained from the OHSU pharmacy. PBS (pH 7.2) was obtained from Life Technologies (Carlsbad, CA). Desalting columns (MW 40 kDa), RNase free water, Traut's reagent, dithiobis(succinimidyl propionate) (DSP), Zeba spin column – MW-40,000, ethanol, HCl, sodium hydroxide and DharmaFECT#1 were purchased from Thermo Fisher Scientific (Waltham, MA). Tris-HCl buffer was purchased from Boston BioProducts (Ashland, MA). All reagents are of the highest purity grade available. RPMI-1640 cell media, fetal bovine serum (FBS) and penicillin/streptomycin (P/S) were purchased from Life Technologies (Carlsbad, CA).

siHER2 (sense: 5' CACGUUUGAGUCCAUGCCCAAUU 3', antisense: 5' UUGGGCA-UGGACUCAAACGUGUU 3'), siSCR (sense: 5' UGGUUUACAUGUCG-ACUAA 3', anti-sense: 5' UUAGUCGACAUGUAAACCA 3') and DyLight677-siSCR were custom synthesized (in vivo HPLC grade) by Dharmacon, Thermo Scientific (Lafayette, CO). siLUC (sense: 5' CGGAUUACCAGGGAUUUCAtt 3', antisense: 5'

UGAAAUCCCUGGUAAUCCGtt 3') was custom synthesized by Life Technologies (Carlsbad, CA).

Nanoparticle synthesis

Nanoparticles were synthesized following our recently published protocol [4]. Briefly, CTAC surfactant (0.15 M) was mixed with TEA (350 µL) in 125 mL of water at 95 °C. TEOS (3 mL) was then slowly added to the mixture under vigorous stirring for 1 h. The nanoparticles were then recovered by centrifugation at 30,250×g and 18 °C for 1 h, washed twice with ethanol and dried overnight. The dried nanoparticles were re-suspended and refluxed in acidic methanol (0.6 M HCl), recovered, washed with ethanol and dried in a desiccator to obtain mesoporous silica nanoparticles (MSNPs). Ten milligrams of dry MSNPs with the size of 50 nm were then mixed with branched-PEI in absolute ethanol at a mass ratio of 4 part MSNP and 1 part PEI. The mixture was shaken continuously for 3 hours at room temperature, centrifuged at 21,130×g for 30 min and resuspended in the ethanol solution containing free PEI and 0.2 mg DSP as a crosslinker. The mixture was shaken for 40 min, then washed twice to remove excess PEI and DSP. Maleimide-PEG(5kDa)-NHS was conjugated to MSNP-PEI at a ratio of 5 to 1 (mal-PEG-NHS to PEI-MSNP) in PBS pH 7.2 under stirred condition for 20 hours. The MSNP-PEI-PEG was washed twice with the PBS, resuspended and kept in PBS until use.

Antibody, trastuzumab (T), was conjugated to MSNP-PEI-PEG via a thiol-maleimide reaction following our published recipe [4]. First, trastuzumab was thiolated with Traut's reagent in phosphate buffer pH 8.0 with 50-fold molar excess of reagent for 2 h and purified by Zeba spin column. Thiolated trastuzumab was mixed with MSNP-

PEI-PEG at a ratio of 1:1 overnight at 4 °C under continuous stirring. The conjugated MSNP-PEI-PEG (denoted T-NP) was washed with copious amount of PBS to remove excess antibody. T-NP was then stored in PBS pH 7.2 until use.

The loading of siRNA was achieved by mixing T-NP and siRNA (at nanoparticle/siRNA mass ratio of 25 or 50) in PBS solution under rigorous shaking of 250 rpm for 30 min at room temperature.

Freeze thaw of nanoparticle (T-NP)

Nanoparticles at 10 mg/mL in 100 mM Tris HCl buffer (pH 7.4) or PBS with 0 – 10% trehalose (%w/w of trehalose per nanoparticle) as a lyoprotectant (LPA) were slowly frozen at -1 °C/min from room temperature to -80 °C overnight. The frozen materials were slowly thawed to room temperature.

Lyophilization of nanoparticle (T-NP)

Nanoparticle was formulated at 10 mg/mL in 100 mM Tris HCl buffer pH 7.4 or PBS with 0 – 25% trehalose (%w/w) as the lyoprotectant (LPA). Then 500 µL of each nanoparticle formula was lyophilized in a 2-mL glass vial in a BenchTop Freeze Dryer (SP Scientific VirTis AdVantage 2.0, Warminster, PA). The "Initial" lyophilization conditions were adapted from the work by Sameti et al on amine-modified silica nanoparticle [16]. Specifically, the formulation was slowly frozen at a shelf temperature of -55 °C for 6 h. Primary drying was performed at the shelf temperature of -55 °C and pressure of 100 µBar for 24 h. The shelf temperature was then gradually increased to -40 °C and the pressure was reduced 20 µBar for secondary drying. After completion, vials

were capped under vacuum with a built-in stoppering function. To reduce total lyophilization time, the conditions have been further optimized as follows: reducing the freezing time from 6 to 3 h (still at -55 °C), increasing the primary drying temperature to -40 °C (100 µBar), and increasing the secondary temperature to 20 °C (20 µBar) while shortening the time to 12 h. Thermocouples were inserted into representative vials to monitor product temperature throughout the lyophilization process.

Storage, Reconstitution, and siRNA loading

Lyophilized nanoparticles were used immediately or stored at 4 different temperatures, -20 °C, 4 °C, 20 °C and 37 °C, for a specified period of time (up to 6 months) prior to characterization and performance evaluation. Prior to use, the lyophilized material was reconstituted with 500 µL of RNase free water to 10 mg/mL. The suspension was sonicated for 1 min. Size and charge were measured as described. For siRNA loading, the reconstituted nanoparticles were mixed with (Dy677)siSCR in PBS to achieve a NP/siRNA mass ratio of 50. The mixture was shaken at 250 rpm and room temperature before being centrifuged at 21,130×g for 30 min. To ensure complete siRNA loading onto the nanoparticle, fluorescent signal of (Dy677)siSCR was measured to be negligible in the supernatant by Tecan Infinite M200. The size and charge of the nanoconstruct (post siRNA binding) were then measured.

Characterization of size and zeta potential by DLS

Hydrodynamic diameter and zeta potential (charge) evaluations were performed on a Zetasizer Nano ZS (Malvern Instruments, Westborough, MA). For size

measurement, the 100 µg/mL of the material in 100 mM Tris-HCl buffer or PBS was used. The charge was measured in 10 mM NaCl using the same suspension conditions. The samples were loaded in appropriate cuvettes/capillary cells, equilibrated to 25 °C before a minimum of 3 measurements were made.

Luciferase knockdown

The LM2-4luc+/H2N (over-expressing luciferase and HER2) cell line, a gift from Prof. Robert Kerbel (University of Toronto), was used for the initial gene silencing efficacy assessment of the nanoparticles as previously reported.[4] Cells were cultured in RPMI-1640 supplemented with 5% FBS and 1X P/S at 37 °C in 5% CO_2 atmosphere. Cells were seeded at 3,500 cells/well in a 96-well plate under cell medium without antibiotic for 24 hours prior to treatment. Nanoparticles loaded with siLUC or siSCR at NP/siRNA mass ratio of 50 were applied to each well at a fixed dose of 30 nM siRNA. After overnight incubation (~20 h), cells were washed once and replenished with complete media containing antibiotics. At 48 h post treatment, cells were lysed and analyzed for luciferase activity by the Luciferase Glow Assay Kit (Thermo Fisher Scientific) and protein concentration by BCA protein assay kit (Thermo Fisher Scientific), following the manufacturer's protocols. Luciferase activity of the lysate was normalized with the corresponding protein concentration in the same well.

Cancer cell death

HER2+ human breast cancer cells, BT474, were obtained from ATCC. Cells were cultured in RPMI-1640 supplemented with 10% FBS and 1X P/S. Cells were maintained

at 37 °C in 5% CO_2 air atmosphere and were passaged weekly by trypsinization. Cells were plated in a 96-well plate with cell medium without antibiotic. One day after seeding, cells were treated with nanoparticles loaded with siHER2 at NP/siRNA of 50. siRNA dose was 60 nM. The media was switched to complete media after overnight incubation. Five days after treatment with T-siHER2-NP, cells were analyzed for viability using CellTiter-Glo® Luminescent Assay (Promega, Madison, WI). The value was reported against scrambled siRNA counterpart (T-siSCR-NP).

Lyophilization of the nanoconstruct post siRNA loading (T-siRNA-NP)

In addition to nanoparticle lyophilization, we also investigate lyophilization of the nanoconstruct after siRNA loading. Briefly, 10 mg/mL nanoparticles (T-NP) were mixed with siLUC at a NP/siRNA mass ratio of 25 in 100 mM Tris HCl buffer containing 0.5 mg/mL trehalose. Five-hundred microliters of T-siLUC-NP suspension was aliquoted to 2-mL glass vials and underwent the same lyophilization conditions as described. The lyophilized nanoconstructs were stored at -20 °C for a specified period of time prior to use.

Results and discussion

Buffer selection

In order to stabilize the pH, drugs or nanoparticles are prepared in physiological buffer systems such as phosphate buffered saline (PBS) or Tris HCl buffer. PBS was evaluated since our nanoparticle was synthesized, bound with siRNA, and initially kept in this buffer. Tris HCl was another buffer we evaluated as it was shown to be suitable

buffer in silica nanoparticle lyophilization [16] and not affected by pH change from temperature [19], unlike PBS was in previous reports [19-21]. We investigated the effect of both buffers on freeze-thawed and freeze-dried nanoparticles. The nanoparticles were suspended at 10 mg/mL with a trehalose content of 0 and 10% (w/w of nanoparticles) in either 1X PBS or 100 mM Tris HCl (pH 7.4). The formulae were then frozen slowly at the rate of -1 °C/min overnight. For the freeze-thaw study, the materials were thawed slowly back to room temperature. For the freeze-dry study, the materials underwent 2 drying steps as described in experimental section. After reconstitution, hydrodynamic sizes of all freeze-thawed materials remained similar to that of the freshly made material as shown in **Figure 1A**. The freeze-thawed materials did not aggregate in PBS nor Tris HCl buffer even without trehalose as lyoprotectant. The lyophilized materials in PBS, however, aggregated even in the presence of trehalose (**Figure 1B**). The sizes increased to 1.5-fold over that of freshly made counterpart. When lyophilized in Tris HCl buffer, the particles did not aggregate and retained the original size when in the presence of 10% trehalose (**Figure 1B**). Furthermore, it was the only formulation that retained the size of the nanoconstruct once loaded with siRNA to that of freshly made counterpart (**Figure 1B**). Although a previous report [22] suggests that PBS may affect the freezing step (e.g., drastic pH change due to decrease in PBS solubility as temperature decreases) leading to unwanted particle aggregation, our data indicate that it was the drying step that caused our particle aggregation in the PBS system. On the other hand, low concentration of Tris HCl buffer, which did not cause drastic pH change during the freezing step [19,23]. appeared to protect the nanoparticle better in the drying step too. Tris HCl was selected as lyophilization buffer in all subsequent experiments.

Lyoprotectant selection and optimization

Lyoprotectant (LPA) is a vital component in lyophilized nanoparticle formula. It protects nanoparticles stresses generated during the freezing and drying step of lyophilization [3]. These stresses along with concentration changes encountered during the freezing step could cause particle aggregation, irreversible fusion or destabilization [24]. The most common LPAs used are sugars and other polyol compounds, such as trehalose, sucrose, glucose, sorbitol and glycerol. We screened for the best LPAs by performing a freeze-thaw experiment on our nanoparticles using all five LPAs and found trehalose and sucrose to be the best at preserving the size and charge of our nanoparticles (not shown). However, since our nanoparticles are developed as siRNA carriers for cancer therapeutics, we chose trehalose over sucrose since there is evidence that sucrose can accelerate tumor growth in tumor bearing mice [25]. Trehalose was also previously reported as an effective LPA for silica nanoparticles [16] and trastuzumab antibody [18].

Next we investigated the concentration of trehalose (TL) required for lyophilization of our nanoparticles. The nanoparticle suspension at 10 mg/mL in 100 mM Tris HCl with a trehalose content of 0 – 25% were lyophilized under the aforementioned conditions. All lyophilized T-NP with trehalose content of 5 – 25% (w/w% of T-NP) retained the average size and charge of the freshly made material after 1 min of sonication as shown in **Figure 2A**. However, with 25% trehalose, the finished product had partially collapsed cake, while lower trehalose contents produced perfect cakes (**Supplemental Figure 1**). It is possible that high amount of trehalose caused a drop in collapse temperature of the mixture (i.e., -30 °C for trehalose-water binary mixture [26]).

When the product temperature during primary drying exceeds the collapse temperature, it will cause a loss of cake structure [27]. Therefore, we rejected the 25% trehalose condition. We also rejected the 0% trehalose condition, since without it, the material increased in both size (**Figure 2A**) and size distribution (data not shown).

In addition to size and charge, luciferase knockdown and cancer cell killing were used to test performance of the lyophilized materials upon loading with siLUC and siHER2, respectively. When delivering siLUC, the lyophilized materials yielded comparable luciferase knockdown efficacy with freshly made material counterparts (from the same batch), but 5% trehelose condition yielded the closet outcomes (**Figure 2B**). When delivering siHER2, they also yielded comparable cell viability of BT474 cells with freshly made materials (**Figure 2C**). Some exception was found with 0% trehalose condition, which yielded the material that was more toxic to cells than freshly made material (e.g., greater non-specific cell death with T-siSCR-NP). The bigger size (see **Figure 2A**) may contribute to higher toxicity due to higher cell uptake. Based on the particle size and efficacy, the 5 – 10% trehalose possessed similar characteristics as the freshly made counterpart. However, the lower amount of additive is more desirable for human applications, thus 5% trehalose was selected for subsequent lyophilization processes and long-term storage study.

Reconstitution

The working drug formula must be reconstituted easily in clinics. We tested the reconstitution of the optimal lyophilized T-NP (with 5% trehalose). Five-hundred microliters of RNase-free water were added slowly to the lyophilized cake. The

suspension was vortexed for a given time and subjected to hydrodynamic size measurement. After 30 second of vortexing, the size was about 6 times of that of freshly made material and only reduced to about 3 times after a prolonged period of 10 min (**Supplemental Figure 2A**). On the other hand, after only 1 min of sonication, the size and size distribution (**Supplemental Figures 2A and B**) were the same with those of the freshly made material. We concluded that 1 min of sonication was best at reconstitution of lyophilized T-NP and was used throughout the studies.

Time and temperature optimization

The initial lyophilization employed -55 °C for 6 h during the freezing step, followed by 2 drying steps at -55 °C for 24 h and -40 °C for 54 h. The entire lyophilization process took almost 4 days. We proceeded to optimize the freezing time and drying temperature in order to shorten the entire process while preserving characteristics and performance of the lyophilized materials. We started with the formulation of 10 mg/mL T-NP in 0.1 M Tris HCl with 5 %w/w trehalose. Freezing time was reduced to from 6 h to 3 h. During the primary drying, product temperature must be above the collapse temperature to avoid collapsing of lyophilized cake [3]. Primary drying temperature was increased to -40 °C with chamber pressure of 100 µBar. At this condition, the product temperature, monitored with thermocouple, was stabilized at -20 °C for at least 10 h (overnight) before the primary drying was stopped to ensure complete ice sublimation. The total primary drying time was 24 h. Trastuzumab antibody was shown to preserve protein structure after undergoing lyophilization with the secondary drying temperature of 20 °C [18]. Thus, we elevated the secondary drying temperature of

our material (containing trastuzumab) from -40 °C to 20 °C under the chamber pressure of 20 µBar, which allowed us to shorten the drying time to 12 h. The lyophilized product under the "optimized" conditions demonstrated non-collapse cake-like structure similar to **Supplemental Figure 1** (with 5% trehalose). At these new conditions, size, luciferase silencing and cancer cell killing of the lyophilized T-NP were preserved (similar to those from the original conditions and to those of freshly made materials (**Figure 3**), while the total time was reduced from 88 h to 42 h. Hence, these optimized lyophilization conditions were used in the subsequent shelf-life study.

Long-term storage of lyophilized nanoparticles (T-NP)

To optimize the storage condition, the nanoparticles lyophilized under the aforementioned conditions were stored at 4 different temperatures; -20 °C, 4 °C, 20 °C, and 37 °C. The lyophilized products were evaluated bi-monthly for physical appearance, size, charge, siRNA loading, luciferase silencing efficacy and cancer cell killing efficacy. All materials (stored at 4 temperatures) retained the same cake appearance to the freshly lyophilized product. The materials were reconstituted and measured for hydrodynamic size (relative to freshly made material) as shown in **Figure 4A**. The material stored at 20 °C started to aggregate at 6 weeks and the one stored at 37 °C started to aggregate as soon as 2 weeks (i.e., not fully reconstituted even after 7 min of sonication) (**Figure 4A**). The lyophilized products stored at -20 °C and 4 °C for up to 8 weeks were reconstituted effectively within 1 min of sonication to achieve same size and size distribution of freshly made material (**Figure 4B**). At week 12, the material stored at 4 °C had larger size distribution (**Figure 4C**) and the size was increased by 150% by week 16 of storage

(**Figure 4A**). On the contrary, the material stored at -20 °C continued to retain both size and size distribution for at least 6 months (longer term was not monitored).

Based on size, the best two storage temperatures were -20 °C and 4 °C. Next, we evaluated charge (zeta potential), siRNA loading, luciferase silencing efficacy and the cancer cell killing efficacy of lyophilized materials stored at both temperatures. The charge (**Figure 5A**) and siRNA loading (**Figure 5B**) of both materials remained similar to the freshly made nanoparticle. Luciferase silencing efficacy (**Figure 5C**, with siLUC) and cancer cell killing efficacy (reported as viability of BT474 cells, **Figure 5D**, with siHER2) of both materials were also comparable to the freshly made materials for up to 8 weeks, while the one stored at 4 °C started to deviate from the performance of freshly made materials at 12 weeks. This was in agreement with the larger size and size distribution of the material (**Figure 4C**). Larger particle sizes lead to higher silencing efficacy and BT474 cell killing, but are not desirable for in vivo use. On the other hand, the material stored at -20 °C retained comparable size (**Figure 4A**) and efficacies to those of freshly made materials (**Figure 5C & 5D**). We conclude that -20 °C is the most suitable temperature for long-term storage of the nanoparticles.

Long-term storage of lyophilized siRNA loaded nanoparticles (T-siRNA-NP)

The data so far were collected with lyophilized nanoparticles that were loaded with siRNA after lyophilization. Next, we investigated the shelf-life of lyophilized nanoconstruct (i.e., nanoparticles were loaded with siRNA before being lyophilized). This one vial strategy is more convenient to administer in clinics than the two vial strategy (requiring no mixing, just reconstituted in saline and use). Freshly made

nanoparticles at the concentration of 10 mg/mL were mixed with siRNA (siLUC) with the NP/siRNA mass ratio of 25 in 100 mM Tris HCl buffer (pH 7.4) and 5% trehalose. The suspension underwent lyophilization with the aforementioned conditions and stored at -20 °C. The lyophilized material was characterized weekly for hydrodynamic size, charge and luciferase silencing efficacy as shown in **Figures 4A-C**, respectively. Although the lyophilized material retained the charge and silencing efficacy of the freshly made material counterpart for up to 8 weeks (longer term was not monitored), it started to aggregate by week 4 (**Figure 6A**, size increased to 1.3 times of freshly made material). Therefore, we conclude that for long term storage, having nanoparticle and siRNA in separate vials prior to lyophilization will yield a better outcome. This is also preferable in personalized medicine setting since it allows interchangeable siRNAs (for targeting different genes) using the same nanoparticle formulation. This is especially true for nanoparticle systems like ours, which allow easy loading of siRNA (with 30 min simple mixing at room temperature) that can be done in clinics.

Conclusions

In summary, we successfully developed the lyophilization process for a hybrid polymer-inorganic nanoparticle system. The antibody conjugated PEI-PEG-silica nanoparticles were lyophilized in Tris buffer with 5% trehalose as the lyoprotectant. The optimized conditions produced lyophilized material with cake-like structure and retained hydrodynamic size, charge (zeta potential), siRNA loading ability, silencing efficacy, and cancer cell killing efficacy of the freshly made material. The freeze-dried nanoparticles can be stored at -20 °C for at least 6 months. The lyophilization conditions, storage

conditions, and material evaluation should be applicable to other similar nanoparticle systems consisting of inorganic nanoparticle cores that are surface modified with cationic polymers and PEG and conjugated with biomolecules like antibodies.

Acknowledgements

This work was supported by NCI/SBIR (Contract No. HHSN261201300078C), the Prospect Creek Foundation, and OHSU's VPR fund. The authors are grateful to Dr. Robert Kerbel of University of Toronto for breast cancer cell lines, Samuel Mihelic and Brandon Beckman for his contribution in material synthesis and tissue culture work. OHSU, W.N., and W.Y. have a significant financial interest in PDX Pharmaceuticals, LLC, a company that may have a commercial interest in the results of this research and technology. This potential personal and institutional conflict of interest has been reviewed and managed by OHSU. The authors are grateful to Dr. Leslie Muldoon for her independent review of the data in this paper as required by OHSU conflict of interest guidelines.

Reference

1. Chacón M, Molpeceres J, Berges L, Guzmán M, Aberturas MR (1999) Stability and freeze-drying of cyclosporine loaded poly(D,L-lactide-glycolide) carriers. Eur. J. Pharm. Sci. 8: 99-107.
2. Franks F (1998) Freeze-drying of bioproducts: Putting principles into practice. Eur. J. Pharm. Biopharm. 45: 221-229.
3. Abdelwahed W, Degobert G, Stainmesse S, Fessi H (2006) Freeze-drying of nanoparticles: Formulation, process and storage considerations. Adv. Drug Deliv. Rev. 58: 1688-1713.
4. Ngamcherdtrakul W, Morry J, Gu S, Castro DJ, Goodyear SM, et al. (2015) Cationic Polymer Modified Mesoporous Silica Nanoparticles for Targeted siRNA Delivery to HER2+ Breast Cancer. Adv. Func. Mater. 25: 2646-2659.
5. Gref R, Luck M, Quellec P, Marchand M, Dellacherie E, et al. (2000) 'Stealth' corona-core nanoparticles surface modified by polyethylene glycol (PEG): influences of the corona (PEG chain length and surface density) and of the core composition on phagocytic uptake and plasma protein adsorption. Colloids Surf. B Biointerfaces 18: 301-313.
6. Zhang Z, Berns AE, Willbold S, Buitenhuis J (2007) Synthesis of poly(ethylene glycol) (PEG)-grafted colloidal silica particles with improved stability in aqueous solvents. J. Colloid Interface Sci. 310: 446-455.
7. Eliyahu H, Barenholz Y, Domb AJ (2005) Polymers for DNA delivery. Molecules 10: 34-64.

8. Gu S, Hu Z, Ngamcherdtrakul W, Castro DJ, Morry J, et al. (2016) Therapeutic siRNA for drug-resistant HER2-positive breast cancer. Oncotarget 7: 14727-14741.
9. Holzer M, Vogel V, Mantele W, Schwartz D, Haase W, et al. (2009) Physico-chemical characterisation of PLGA nanoparticles after freeze-drying and storage. Eur. J. Pharm. Biopharm. 72: 428-437.
10. Fonte P, Araujo F, Seabra V, Reis S, van de Weert M, et al. (2015) Co-encapsulation of lyoprotectants improves the stability of protein-loaded PLGA nanoparticles upon lyophilization. Int. J. Pharm. 496: 850-862.
11. Saez A, Guzman M, Molpeceres J, Aberturas MR (2000) Freeze-drying of polycaprolactone and poly(D,L-lactic-glycolic) nanoparticles induce minor particle size changes affecting the oral pharmacokinetics of loaded drugs. Eur. J. Pharm. Biopharm. 50: 379-387.
12. Brus C, Kleemann E, Aigner A, Czubayko F, Kissel T (2004) Stabilization of oligonucleotide-polyethylenimine complexes by freeze-drying: physicochemical and biological characterization. J. Control Release 95: 119-131.
13. Yadava P, Gibbs M, Castro C, Hughes JA (2008) Effect of lyophilization and freeze-thawing on the stability of siRNA-liposome complexes. AAPS PharmSciTech 9: 335-341.
14. Maitani Y, Aso Y, Yamada A, Yoshioka S (2008) Effect of sugars on storage stability of lyophilized liposome/DNA complexes with high transfection efficiency. Int. J. Pharm. 356: 69-75.
15. Kundu AK, Chandra PK, Hazari S, Ledet G, Pramar YV, et al. (2012) Stability of lyophilized siRNA nanosome formulations. Int. J. Pharm. 423: 525-534.

16. Sameti M, Bohr G, Ravi Kumar MN, Kneuer C, Bakowsky U, et al. (2003) Stabilisation by freeze-drying of cationically modified silica nanoparticles for gene delivery. Int. J. Pharm. 266: 51-60.
17. Alkilany AM, Abulateefeh SR, Mills KK, Yaseen AI, Hamaly MA, et al. (2014) Colloidal stability of citrate and mercaptoacetic acid capped gold nanoparticles upon lyophilization: effect of capping ligand attachment and type of cryoprotectants. Langmuir 30: 13799-13808.
18. Cleland JL, Lam X, Kendrick B, Yang J, Yang TH, et al. (2001) A specific molar ratio of stabilizer to protein is required for storage stability of a lyophilized monoclonal antibody. J. Pharm. Sci. 90: 310-321.
19. Kolhe P, Amend E, Singh SK (2010) Impact of freezing on pH of buffered solutions and consequences for monoclonal antibody aggregation. Biotechnol. Prog. 26: 727-733.
20. Pikal-Cleland KA, Carpenter JF (2001) Lyophilization-induced protein denaturation in phosphate buffer systems: monomeric and tetrameric beta-galactosidase. J. Pharm. Sci. 90: 1255-1268.
21. Croyle MA, Cheng X, Wilson JM (2001) Development of formulations that enhance physical stability of viral vectors for gene therapy. Gene Ther 8: 1281-1290.
22. Pikal-Cleland KA, Rodriguez-Hornedo N, Amidon GL, Carpenter JF (2000) Protein denaturation during freezing and thawing in phosphate buffer systems: monomeric and tetrameric beta-galactosidase. Arch. Biochem. Biophys. 384: 398-406.
23. Carpenter JF, Pikal MJ, Chang BS, Randolph TW (1997) Rational design of stable lyophilized protein formulations: some practical advice. Pharm. Res. 14: 969-975.

24. Abdelwahed W, Degobert G, Fessi H (2006) A pilot study of freeze drying of poly(epsilon-caprolactone) nanocapsules stabilized by poly(vinyl alcohol): formulation and process optimization. Int. J. Pharm. 309: 178-188.
25. Kimura Y, Sumiyoshi M (2007) High-fat, high-sucrose, and high-cholesterol diets accelerate tumor growth and metastasis in tumor-bearing mice. Nutr. Cancer 59: 207-216.
26. Yang G, Gilstrap K, Zhang A, Xu LX, He X (2010) Collapse temperature of solutions important for lyopreservation of living cells at ambient temperature. Biotechnol. Bioeng. 106: 247-259.
27. Patel SM, Doen T, Pikal MJ (2010) Determination of end point of primary drying in freeze-drying process control. AAPS PharmSciTech 11: 73-84.

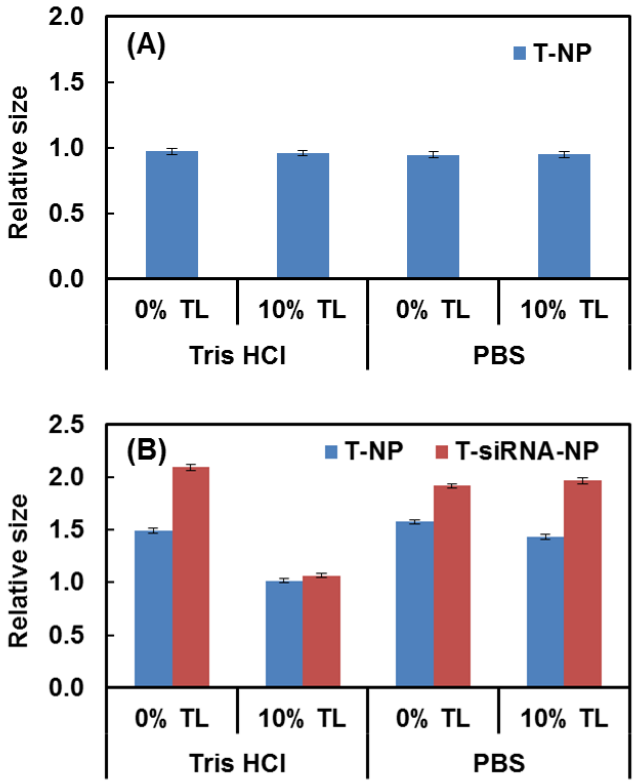

Figure 1. Hydrodynamic size evaluation of (A) freeze-thawed or (B) lyophilized nanoparticles. All values were normalized against those of freshly made material from the same batch. The nanoparticles underwent freeze-thaw or freeze-dry process at 10 mg/mL with 0 and 10% trehalose (TL) in 0.1 M Tris HCl pH 7.4 or PBS. The reconstituted nanoparticles were sonicated for 1 min before measurement. The lyophilized nanoparticles were loaded with siHER2 at NP/siRNA mass ratio of 50.

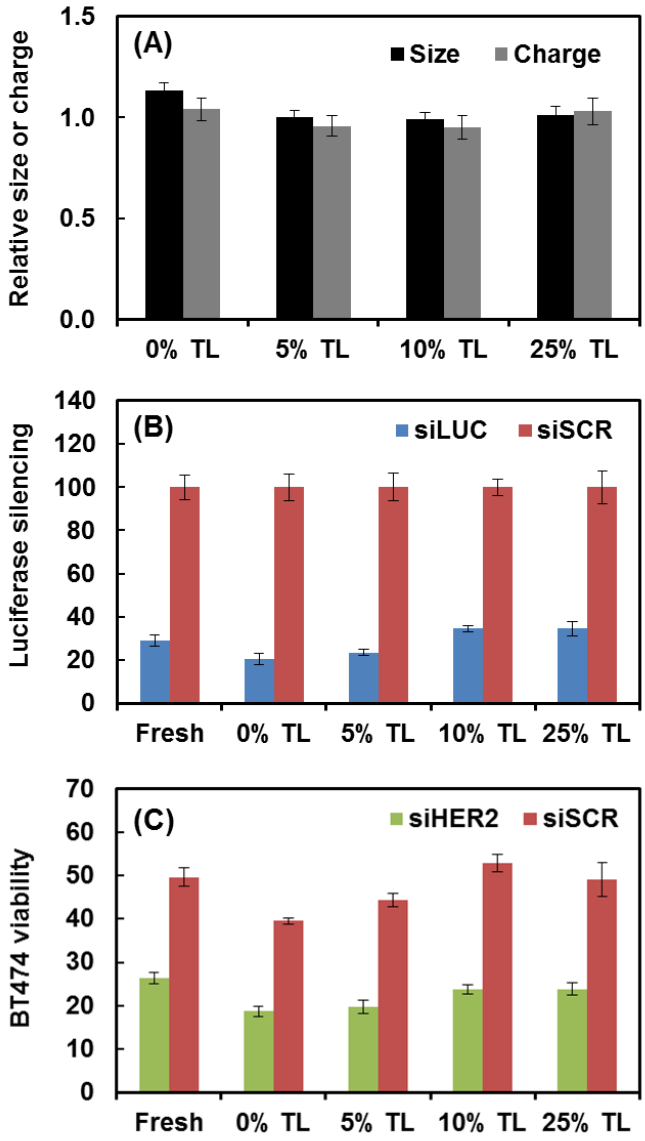

Figure 2. Lyoprotectant optimization. Silica nanoparticles (T-NP) were lyophilized at 10 mg/mL in 10 mM Tris HCl with 0 – 25 % trehalose (TL) as lyoprotectant. (A) Size and charge evaluation of lyophilized T-NP. Values were normalized against those of freshly made materials. (B) Silencing of luciferase in LM2-4luc+/H2N (high HER2, high luciferase) upon treatment with 30 nM siLUC loaded on lyophilized T-NP, at 48 h post transfection. (C) BT474 cell viability following treatment with 60 nM siHER2 loaded on lyophilized T-NP, at 5 days post transfection. All were benchmarked against scrambled siRNA (siSCR).

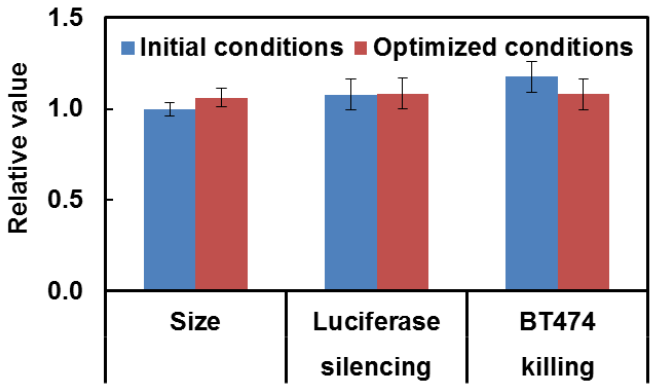

Figure 3. Comparison of lyophilized materials from two lyophilization conditions (with varying time and temperature). T-NPs were lyophilized at 10 mg/mL in 100 mM Tris HCl with 5% TL. In original conditions, samples were slowly frozen at -55 °C for 6 h and followed by primary drying at -55 °C for 24 h and secondary drying at -40 °C for 54 h. In optimized conditions, freezing step time was reduced to 3 h while primary drying step was performed at -40 °C for 24 h and secondary drying step at 20 °C for 12 h.

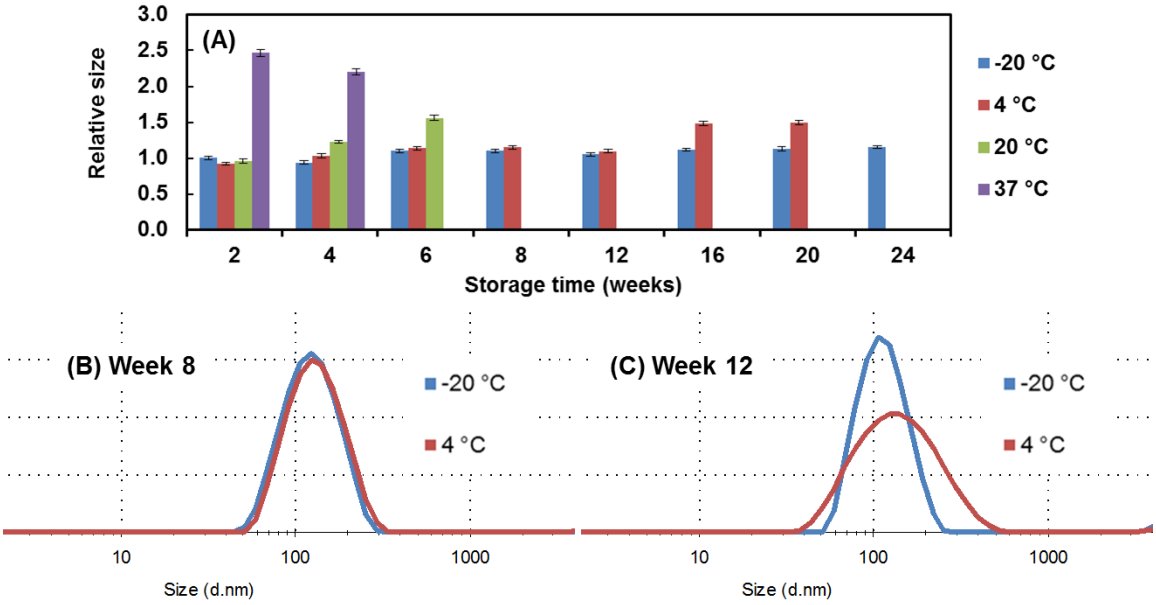

Figure 4. Hydrodynamic size of lyophilized nanoparticles stored at various time and temperature. All values were normalized against those of freshly made material from the same batch. The nanoparticles (T-NP) were lyophilized at 10 mg/mL in the presence of 5% w/w TL and 0.1 M Tris buffer pH 7.4. The materials were then stored at -20, 4, 20 and 37 °C. The reconstituted nanoparticles were sonicated for 1 min before binding with siRNA at the NP/siRNA mass ratio of 50. (A) Hydrodynamic diameter of siRNA-nanoconstructs (T-siRNA-NP). (B, C) Size distribution of lyophilized T-NPs stored at -20 °C and 4 °C at week 8 (B) and week 12 (C).

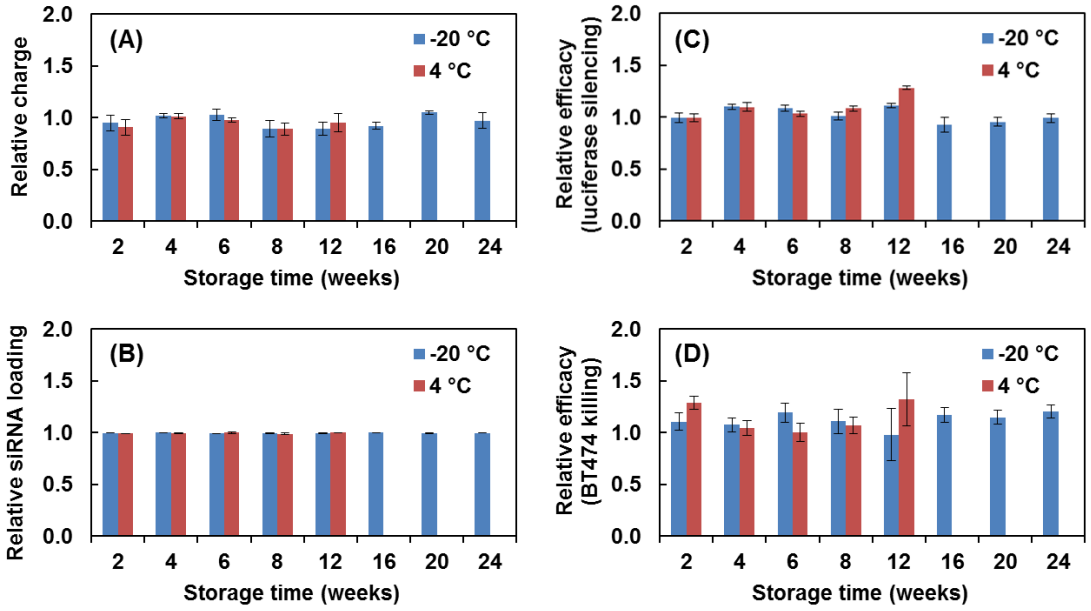

Figure 5. Charge, siRNA loading, luciferase silencing efficacy, and cancer cell killing of lyophilized nanoparticles stored at various time and temperature. All values were normalized against those of freshly made material from the same batch. All conditions were the same as in **Figure 4** except storage temperature was -20 °C or 4 °C. (A) Charge of siRNA-nanoconstruct (T-siRNA-NP) measured in 10 mM NaCl. (B) siRNA loading of lyophilized nanoparticles; all loaded at NP/siRNA mass ratio of 50. (C) Silencing of luciferase in LM2-4luc+/H2N upon treatment with 30 nM siLUC loaded on lyophilized T-NP, at 48 h post transfection. (D) BT474 cell viability following treatment with 60 nM siHER2 loaded on lyophilized T-NP, at 5 days post transfection. All were benchmarked against scrambled siRNA (siSCR) and normalized to values from freshly made material.

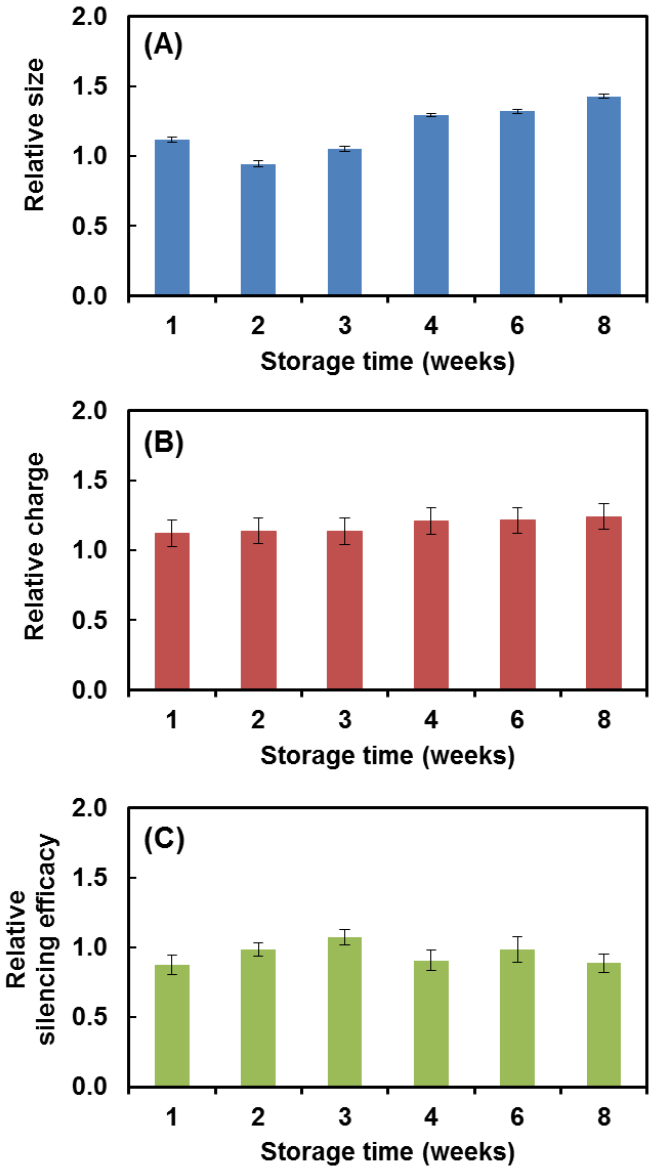

Figure 6. Lyophilized nanoconstruct (T-siRNA-NP) evaluation as a function of time. All values were normalized against those of freshly made material from the same batch. The nanoparticles were loaded with siLUC at the NP/siRNA mass ratio of 25 before being lyophilized at 10 mg/mL NP in the present of 5% w/w TL and 0.1 M Tris buffer (pH 7.4). The lyophilized nanoconstructs were stored at -20 °C and reconstituted by sonication for 1 min. (A) Hydrodynamic size, (B) zeta potential (charge) measurement in 10 mM NaCl and (C) Silencing of luciferase in LM2-4luc+/H2N (high HER2, high luciferase) upon treatment with 60 nM siLUC loaded on lyophilized T-NP, at 48 h post transfection.